To all members of my family

ProQuest LLC.
789 East Eisenhower Parkway
P.O. Box 1346
Ann Arbor, MI 48106 – 1346

T-2247

LIQUID-VAPOR AND LIQUID-LIQUID-VAPOR PHASE EQUILIBRIA IN THE NITROGEN + ETHYLENE SYSTEM FROM 120 to 200 K

by

Khaled A. Massoud Gasem

T-2247

A Thesis submitted to the Faculty and the Board of Trustees of the Colorado School of Mines in partial fulfillment of the requirements for the degree of Master of Science in Chemical and Petroleum - Refining Engineering.

Signed: KHALED A. ASEERY
Student

Golden, Colorado
Date: 12/17, 1979

Approved: J. F. Kelsey
Thesis Advisor

J. F. Kelsey for P. E. Parker
Head of Department

Golden, Colorado
Date: 12/17, 1979

ABSTRACT

Liquid-vapor equilibrium compositions have been measured for the N_2 + C_2H_4 system between 120 K and 200 K and pressures up to 93 bars. At lower temperatures, the system exhibits a liquid-phase separation similar to that observed in the N_2 + C_2H_6 system. Data generated at 200 K were compared with existing data and showed good agreement. Semi-empirical equations were developed for the prediction of the separation pressure at a given temperature and the solubility of N_2 in the bottom liquid layer.

In addition, phase behavior comparisons were made on the N_2 + light hydrocarbon systems where different critical locus behavior was observed depending on the degree of miscibility of N_2 in the hydrocarbon.

TABLE OF CONTENTS

LIST OF FIGURES

Page

LIST OF TABLES

ACKNOWLEDGEMENTS

My sincere thanks and deep appreciation to my advisors: A. J. Kidney and M. J. Hiza for their continuous guidance and encouragement throughout this study.

This work was performed at the National Bureau of Standards (NBS) in Boulder. The author would like to express his deep gratitude to NBS for the use of their fine facilities.

Last, but not least, I am in debt to the Libyan people for their support throughout the years.

CHAPTER 1

INTRODUCTION

Liquid-vapor phase equilibria measurements, or fluid phase equilibria in general, continue to be a major aspect of thermodynamic studies, not only for their direct industrial use in process design, but also for their importance in the testing and extension of current molecular theories of fluid mixtures.

Recently, the rapid increase in the petrochemical industries itensified the interest in high purity C_2H_4. It is estimated that the rate of production of C_2H_4 will reach 29 billion pounds by the end of the year 1979, making it the fifth largest chemical industry in the United States (C&E News, 1979). This great demand for C_2H_4, especially in the plastic sector of the industry (66 percent of total production rate) coupled with the predicted shortages in the early 1980's, made the diversification of the feed stock used in the production of C_2H_4 imperative. This in-turn, leads to greater demand for phase equilibria data for systems containing C_2H_4, The purpose of this work is to study the N_2 + C_2H_4 system, especially at low temperatures where the liquid separation phenomena is expected to occur and three phases coexist (liquid (C_2H_4 rich)-liquid (N_2 rich) - vapor (N_2 rich).

This system, N_2 + C_2H_4, is very important from an academic point of view also, due to the relatively simple molecular structure of its components and the expected nonideal behavior exhibited by the partial liquid immiscibility at low temperatures.

Systems such as N_2 + C_2H_4, N_2 + C_2H_6, or N_2 + light hydrocarbon in general, containing relatively simple molecules (molecules which have low intermolecular forces and low stearic effects) lend themselves more easily to theoretical treatment and are very helpful in understanding the observed macroscopic behavior of liquid solutions (C.A. Eckert and J.M. Prausnitz, 1965). Of all the possible binary combinations of nitrogen and light hydrocarbon, only CH_4 and C_2H_6 have been studied in a wide range of conditions.

Normally, systems with partial liquid immiscibility are studied using a visual equilibrium cell however, in our case a different experimental procedure was developed using the phase rule behavior as a guideline. In order to predict the liquid separation properties of this system at any given temperature, equations were developed based on theory, but containing many simplifying assumptions.

CHAPTER 2

PREVIOUS EXPERIMENTAL WORK

2.1 $N_2 + C_2H_4$

To our knowledge, no experimental work has been done on this system except that of Grausø, et al. (1977). Grausø's work includes two isotherms at higher temperature, specifically at 200 K and 260 K, which are removed from the liquid phase separation temperature range and consequently no reference to this phenomena was made by Grausø et al.

2.2 $N_2 + C_2H_6$

A number of investigators have studied the separation phenomena in this system:

R.T. Ellington, et al. (1959)

S.D. Chang, et al. (1967)

P. Yu, et al. (1969)

A complete listing of the data available is given in a bibliography by Hiza, Kidnay, and Miller (1975).

CHAPTER 3

THE EXPERIMENTAL PROCEDURE

The measurements in this study were made in a closed loop vapor recirculation system. The general flow diagram is given in figure (1) and the cryostat schematic is shown in figure (2). The detailed description of the cryostat and the recirculation pump are given elsewhere (Hiza and Duncan, 1969), (Duncan and Hiza, 1970). Therefore, only a general description of the equipment will be given here along with the experimental procedure.

Due to the phase split exhibited by the system at lower temperatures coupled with flat phase envelopes, different experimental procedures were developed for the different regions of study.

3.1 The Liquid-Vapor Measurements

The experimental procedure followed in the liquid-vapor measurements was to evacuate the system very thoroughly for at least 30 minutes. While the evacuation process was going on the system was cooled down to the desired temperature using liquid nitrogen. The system was then purged with C_2H_4 and 4 to 10 cc of C_2H_4 were condensed in the equilibrium cell. The recirculation pump was turned on to equilibrate the liquid C_2H_4 with its vapor, and then the vapor pressure of C_2H_4 was measured

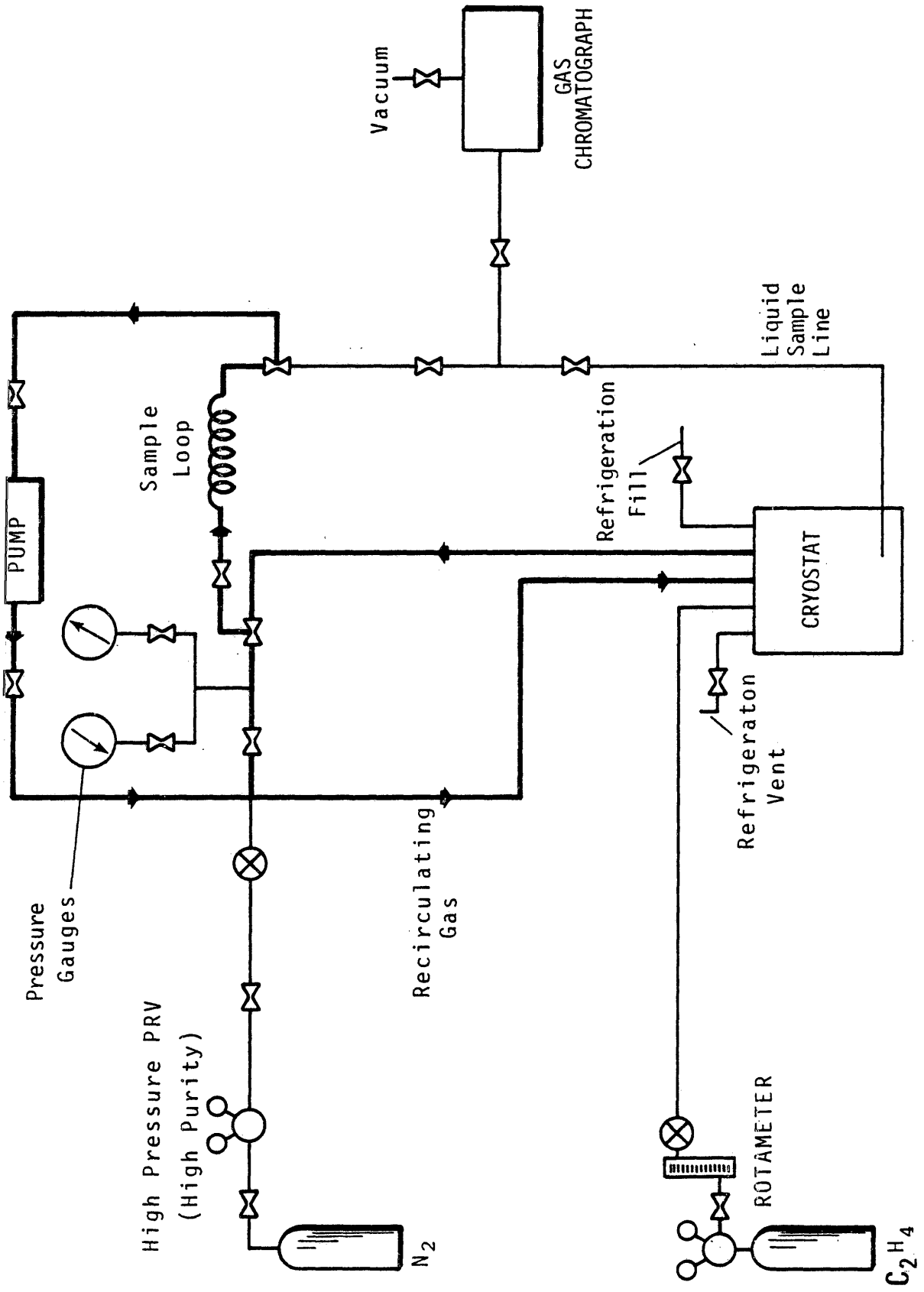

Figure 1. Flow Diagram of Experimental Apparatus.

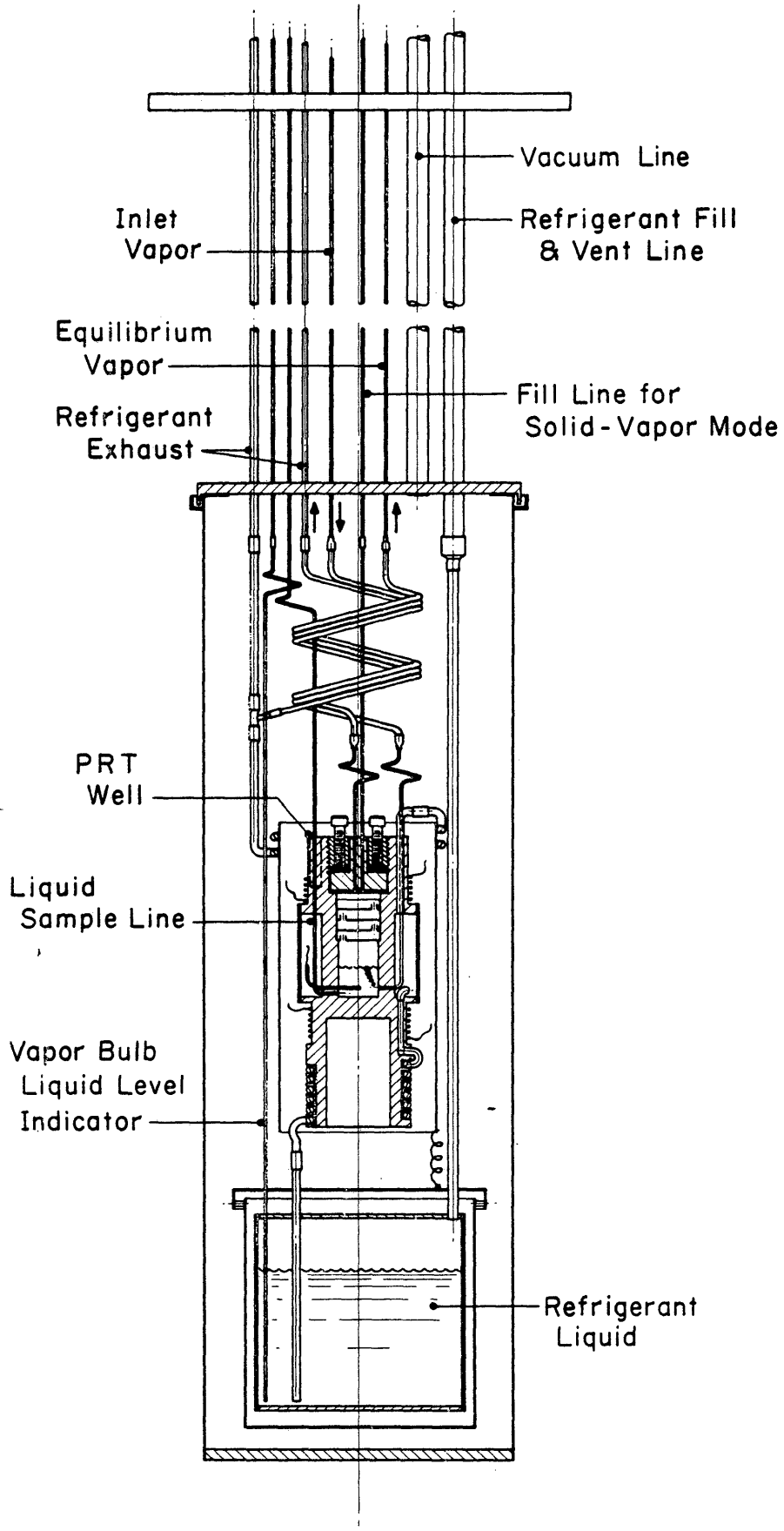

Figure 2. Cryostat Plan.

using a Fused Quartz Precision Pressure gauge. This was done to ensure that the temperature control and the system as a whole were functioning properly. Once that was done, the system was pressurized to the desired pressure with nitrogen gas and left to equilibrate.

When equilibrium was established in the system, as determined by the constancy of the temperature and pressure measurements, the recirculation pump was stopped. The liquid sample lines were purged, and the liquid sample was withdrawn and collected in a 500 cc bomb for thorough mixing. The mixing process was aided by using a heating lamp. Once the liquid sample was withdrawn, the vapor sample was immediately isolated in the sample loop, withdrawn, and analyzed in the gas chromatograph. Upon completion of the vapor analysis the vaporized liquid sample was analyzed in the same manner.

3.2 Separation Region Measurement (liquid-liquid-vapor measurements)

The isotherms obtained in the separation region were determined in three different steps:

(1) The liquid-vapor measurements were obtained in the same manner described above for the higher temperature isotherms.

(2) For the separation locus measurements C_2H_4 was condensed and N_2 was added in small increments until the appearance of the second liquid phase was detected by noting the point at which pressure remains constant with further addition of N_2. To check for the consistency of this unvariant pressure value

the pressure was reduced by venting and was observed to go back to the same value. After separation pressure was established, sufficient N_2 was added to form several cc's of the second liquid layer and then the recirculation pump was turned on for at least 15 minutes to allow for good mixing. Once equilibrium was established, the pump was turned off, the two liquids were allowed to settle, and the composition of the lower liquid layer and the vapor phase were analyzed as described earlier.

(3) For the liquid-vapor measurements between the LV critical point and the separation pressure only 1/8 of the normal amount of C_2H_4 ($\leq$ 1 cc) was condensed in the equilibrium cell. This amount was chosen after many trials with different values. Also, special care was taken as not to over pressurize the cell with N_2 which proved to give meaningless results.

To determine the upper liquid layer composition, the liquid-vapor curve obtained above the separation pressure was extended to lower pressures till it intersects with the separation pressure line (the horizontal line shown in the separation isotherms). The point of intersection of the two lines represents the upper layer liquid composition.

3.3 Temperature Measurement and Control:

The temperature of the system was controlled and measured with an estimated accuracy of $\pm$.02 K using a calibrated (IPTS-68) platinum resistance thermometer connected to a universal poten-

iometer (type K-3) which in turn connected to a Keithley nanovolt null detector. Passing a 1.0 ma current through the thermometer and measuring the voltage drop with the potentiometer for a zero reading on the null detector gave an equivalent thermometer resistance which could then be related to the temperature with an uncertainty of about ±.02 K. The temperature control was maintained using a 100 ohm heater powered by a proportional-integral controller to balance the refrigeration obtained by evaporating liquid nitrogen.

3.4 Pressure Measurement

The pressure measurements were made with two Bourdon tube gauges which had ranges of 0-50 bars and 0-200 atmospheres. In the range of 0-50 bars the accuracy of the pressure measurements was ±.05 bar while in the region above 50 bars the accuracy was ±0.2 atm.

For the vapor pressure measurements, a Texas Instruments Fused Quartz Precision Pressure guage was used with an estimated accuracy of ± 0.015 psia.

3.5. The Analysis System

A Beckman GC-2A Chromatograph equipped with a thermal conductivity detector was used to analyze all the samples. A five-foot Porapak R, 800/100 mesh, column with 1 cm^3 sample loop, and helium as the carrier gas was used. The temperature (83°C) and other chromatographic settings were selected so as to obtain

sharp peaks. Gas pressures especially for the purpose of calibration were measured using the TI gauge mentioned earlier. For more details see the appendix.

3.6 Calibration of the Gas Chromatograph

Calibration of the gas chromatograph was done by preparing several N_2 + C_2H_4 gas mixtures of different compositions. The amount of each component in the calibration mixtures was accurately determined gravimetrically using a Voland 25 kg equal arm balance which, has a standard deviation of weighings of $\pm$.7 mg. The mole faction of each component was calculated by:

$$X_i = \frac{M_i/W_i}{\sum M_i/W_i}$$

where M_i = the mass of the component and W_i = the molecular weight of the component. The injection pressure of each calibration run was measured by the TI gauge. By multiplying the mole fraction (X_i) by the total pressure (P) the partial pressure was obtained for each component. The area (A_i) corresponding to each partial pressure was obtained from the electronic integrator.

After all the points on the calibration curves for both components were obtained, a least-squares fit analysis was made to produce an equation for each component which relates A_i to P_i (a calibration equation). Normally the equations have been of the form:

$$y = mx$$

where: y = partial pressure

x = integrator area

$$m = \frac{\sum X_i Y_i}{\sum X_i^2}$$

However, in this investigation it was found that a better fit was obtained with a fit of the form:

$$y = mx + b.$$

For more details refer to the appendix.

Normalization of Raw Mole Fractions

One of the well-established facts in gas chromatography is that the sensitivity of the analytical system varies with time due to many factors. In the present work, however, the problem of introducing a correction factor to the calculated mole fraction (X_i) was avoided due to inherent normalization present in the calculation procedure for X_i. The validity of this statement can be easily proven.

Assuming that the sensitivity of the system is different from its sensitivity at the time of the calibration, then a correction factor (CF) must be introduced to the partial pressure (P_i) calculated from the calibration curve equation for each component. Let this corrected partial pressure be CP_i.

Then $CP_{N_2} = P_{N_2}(CF)$

Similarly $CP_{C_2H_4} = P_{C_2H_4}(CF)$

The corrected (normalized) mole fraction (X_i) is then calculated as

$$X_{N_2} = \frac{P_{N_2}(CF)}{P_{N_2}(CF) + P_{C_2H_4}(CF)}$$

$$X_{N_2} = \frac{P_{N_2}}{P_{N_2} + P_{C_2H_4}}$$

Since the correction factor (CF) cancels out from both the numerator and the denominator as shown in the above equations then it may be concluded that the reported expermental mole fractions are actually the normalized mole fractions and that the variations of the sensitivity are taken care of.

CHAPTER 4

EXPERIMENTAL RESULTS

4.1 The separation Phenomena in N_2+C_2H_6 Binary

Since visual aid was lacking in the apparatus used in this work, the procedure used to study the liquid phase separation needed verification. To provide verification, a similar system to the one under investigation (N_2+C_2H_4) and with the same character of partial liquid miscibility and which had been studied previously (with a visual cell) was needed. The N_2+ C_2H_6 binary mixture is such a system. The system is ideal due to the fact that C_2H_6, has a close boiling point to that of C_2H_4, has the same number of carbon atoms and best of all, has been studied by at least three different investigators.

Phase rule behavior studies made on the separation locus of N_2 + C_2H_6 where three phases (liquid-liquid-vapor) coexist using the procedure outlined earlier (the results of which are shown in table 4-1) gave excellent agreement with the separation locus reported by Ellington, et al. (1959) as can been seen in Figure (3). Also excellent agreement was observed with the results obtained by Yu, et al. (1969), especially at T > 125 K. At lower temperatures, Yu's data exhibit scatter, which may be attributed to poor temperature control.

The above mentioned investigators reported that the separation phenomena occurs in a temperature range from 133.3 K as

Table 4-1

Separation Pressure of the N_2 + C_2H_6

@ Different Temperatures

T(K)	P(bar)
105	10.35
110	13.85
115	18.10
120	23.38
125	29.38
130	36.55
135	44.20

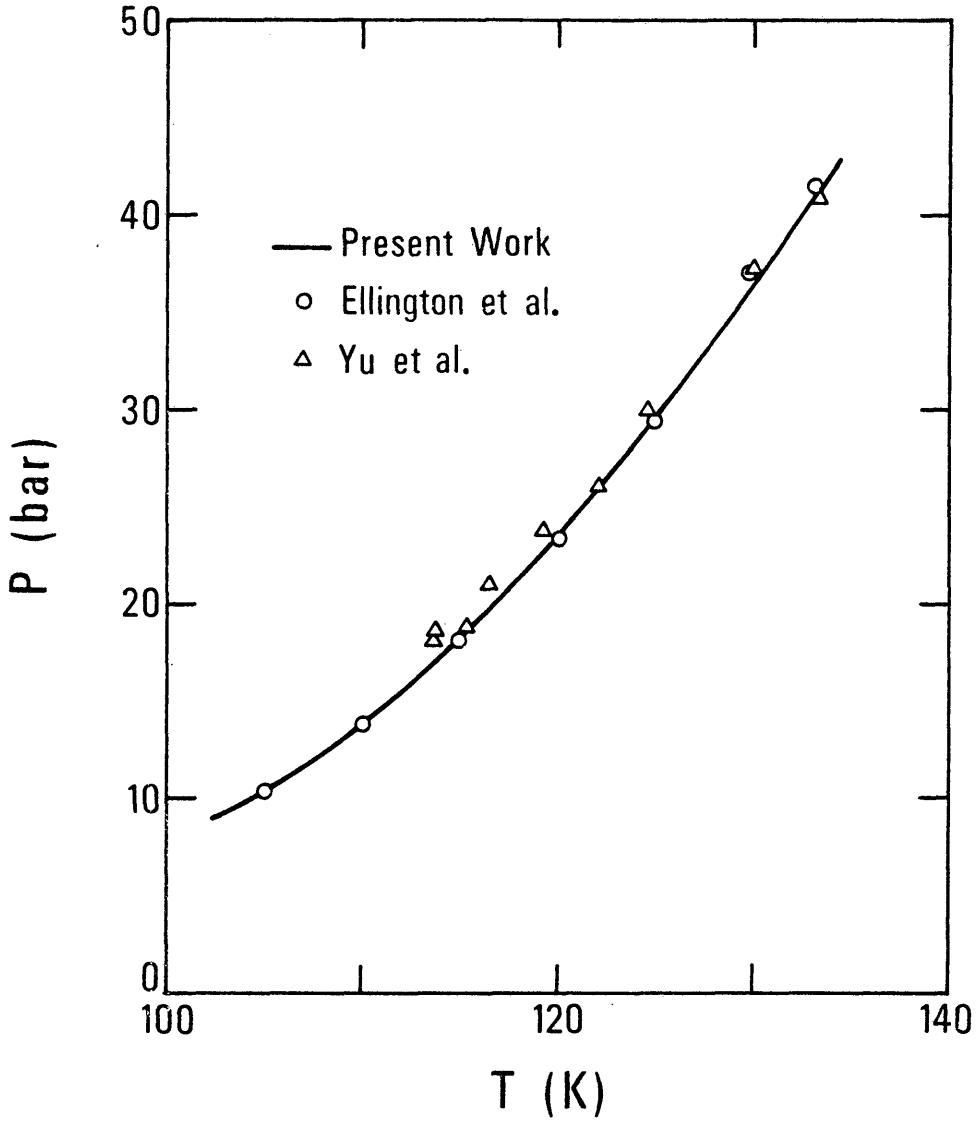

Figure 3. N_2 + C_2H_6 Separation Locus

the upper observable separation temperature down to 88.4 K the quadruple point reported by Ellington (1959). In this work, however, the univariant temperature-pressure measurements show similar behavior up to 139 K. The cause of this observed behavior can be attributed to one of two possible reasons: (1) that the separation actually occurs up to 139 K or (2) that the phase envelope of the isotherms generated above the reported upper separation temperature (UST) are very flat, and thus the composition has little dependence on pressure. This latter explanation seems more likely since the (N_2+C_2H_4) system produced very flat isotherms. M. Simon, et al. (1972) reported similar behavior for the CH_4+CF_4 system which exhibits the same type of partial miscibility.

It would have been very desirable to finalize the conclusions on this observed behavior, however, limitations in the apparatus used (especially the lack of a visual cell) made this task unattainable. Several other conclusions have been made for the region above the last observable separation point and the formation of miscible isotherms. Ellington, et al. (1959) using a dew point-bubble point visual apparatus concluded that the region is "a double retrograde condensation region" and that very high pressures are reached by the phase envelope. Yu, et al. (1969), however, concluded the liquid-vapor critical temperature will be reached before the upper critical solution temperature. One of our objectives in the following sections is to shed more light on behavior in this region by studying the N_2+C_2H_4 system since it showed the same type of partial miscibility behavior.

4.2 $N_2+C_2H_4$ System

The data obtained in this investigation are presented both graphically and in tabular form for each isotherm in the following sections. A table showing normalized mole fractions, K factors, and enhancement factor is presented. Plots of the liquid-vapor equilibrium data and an expanded-scale plot of the liquid phase lower region, and Henry's Law region, are also given.

One of the major problems encountered in phase equilibrium studies has been the verification of the thermodynamic consistency of the data obtained. Although many techniques have been developed over the years, some more complicated than others (especially now with aid of the computer), a number of the simpler methods still give reliable conclusions about the consistency of the data obtained experimentally. Our aim here is to use some of those simpler tests.

Two types of consistency tests must be performed before the data can be assumed to have a good chance of being thermodynamically consistent:

(1) The external consistency tests which are used to check the consistency (accuracy) of the apparatus used. These include:

(a) Measurements of the vapor pressure of the less valatile component (C_2H_4 in our case) to ensure proper temperature and pressure measurement and control.

(b) Comparison of results obtained using the apparatus at hand to those of other investigators at the same conditions of operation.

(c) A plot of Henry's law constant versus T (or $\ln H_{21}$ vs 1/T) for all the data available on the system for the sake of comparison between the data of the other investigators and that obtained with the apparatus used. This is a good test when the data are collected at differenct conditions.

(2) The internal consistency tests which are used to check consistency of the data collected on the same apparatus at different experimental conditions. These include:

(a) A plot of $(P-P^0_{C_2H_4})$ versus X_{N_2}, which must extrapolate smoothly to the origin as $X_{N_2} \longrightarrow 0$ if the lower pressure liquid compositions are consistent. Furthermore, for small values of X_{N_2}, Henry's Law holds indicating a linear relation according to

$$\lim_{X_{N_2} \longrightarrow 0} \frac{P_{N_2}}{X_{N_2}} = H_{N_2,C_2H_4}$$

(b) To check for the vapor phase consistency the enhancement factor,

$$\frac{Y_{C_2H_4} P}{P^0_{C_2H_4}}$$

is plotted versus $(P-P^{\circ}_{C_2H_4})$. This plot should produce a smooth curve extrapolating to a value of 1.0.

(c) A plot of $(P-P^{\circ}_{C_2H_4})$ versus $K_{C_2H_4}P$ is used to check for the combined consistency of the liquid and vapor compositions at lower pressures. This also should produce a smooth curve extrapolating to the vapor pressure of C_2H_4 at the temperature of interest.

(d) The critical locus (along with separation locus in the lower temperature region) for all the data available should produce a smooth curve. This test may also be considered an external consistency test when the results obtained are compared to other investigators' work on the system (if available).

4.2.1 External Consistency of the $N_2 + C_2H_4$ System

Representative values of C_2H_4 vapor pressure obtained with the apparatus at different temperatures are tabulated below showing the range obtained for these values at different times. Shown below also, are the values obtained by other investigators at the same temperatures. The slight difference exhibited may be attributed to the difference of purity of materials used in each investigation.

Table 4-2

Vapor Pressure of C_2H_4 at Different Temperatures

Date	T(K)	$P^{o}_{C_2H_4}$ (bar) Present Work	$P^{o}_{C_2H_4}$ (bar) Goodwin Fit*	$\Delta P^{o}_{C_2H_4}$ (bar)
4/19	120.00	0.0104	0.01365	3.25×10^{-3}
4/30		0.0137		-5.00×10^{-5}
5/19	125.28	0.0268	0.02550	-1.30×10^{-3}
5/10	134.00	0.0689	0.06556	-3.34×10^{-3}
4/18	140.00	0.1180	0.11820	2.00×10^{-4}
6/13	144.92	0.1819	0.18138	-5.20×10^{-4}
6/12		0.1824		-1.02×10^{-3}
6/18	150.00	0.2732	0.27300	-2.00×10^{-3}
6/16		0.2741		-1.10×10^{-3}
6/7	160.00	0.5630	0.56868	5.68×10^{-3}
3/15	200.00	4.5550	4.54467	-1.03×10^{-2}

* Goodwin, 1979

Grausø, et al. (1977) studied the same system (N_2 + C_2H_4) at 200 K and 260 K using a similar apparatus. To check for consistency, data at 200 K were collected (Table 4-2). Upon comparison excellent agreement between the two data sets was obtained, as shown in figure (4). Similarly, excellent agreement was observed in all the consistency tests performed as shown in figures (5), (6), and (7) as well as in the K-factor plots for C_2H_4 and N_2 shown in figure (8). This coupled with the good vapor pressure measurements cited above leads to the conclusion that a very good chance for thermodynamically consistent data exists for the system under investigation. In the following sections, the data obtained are divided into separate sections, each including a number of isotherms with similar phenomenological

4-2.2 Separation Region Isotherms (120, 125.28, 134 and 140 K)

There are no previous measurements of the N_2 + C_2H_4 system in this low temperature region. Tables (4-3) through (4-6) show the normalized mole fractions and the K-factors for the system. The lack of scatter in the liquid-vapor equilibrium data as shown in figures (9), (10), (11), and (12) indicates the mechanical consistency of the apparatus used.

Excellent results in terms of the smoothness of the curves and the linearity (when applicable) in $(P - P^0_{C_2H_4})$ versus X_{N_2} plots indicate a good degree of consistency for the liquid phase

Table 4-3

N_2 + C_2H_4 System @ 200.00 K

Date	P(bar)	$P-P^{o}_{C_2H_4}$	X_{N_2}	Y_{N_2}	$X_{C_2H_4}$	$Y_{C_2H_4}$	$Y_{C_2H_4} P/P^{o}_{C_2H_4}$	K_{N_2}	$K_{C_2H_4}$	$K_{C_2H_4} P$
3/29	4.56	0.00	0.00	0.00	1.00	1.00	-	-	1.00	4.56
3/29	8.37	3.81	0.0132	0.4166	0.9868	0.5834	1.0708	31.561	0.592	4.9550
3/29	13.20	8.64	0.0236	0.6035	0.9764	0.3965	1.1478	25.572	0.406	5.3592
3/15	15.76	11.20	0.0351	-	0.9649	-	-	-	-	-
3/15	17.60	13.04	0.0394	0.6860	0.9606	0.3140	1.2119	17.411	0.327	5.7552
4/13	26.37	21.81	0.0648	0.7642	0.9352	0.2358	1.3636	11.793	0.252	6.6452
4/13	37.97	33.41	0.1021	0.8093	0.8979	0.1907	1.5879	7.927	0.212	8.0496
4/13	47.30	42.74	0.1332	0.8248	0.8668	0.1752	1.8173	6.192	0.202	9.5546
3/15	12.27	7.71	-	0.580	-	0.4200	1.1301	-	-	-
3/15	13.88	9.32	-	0.6186	-	0.3814	1.1605	-	-	-

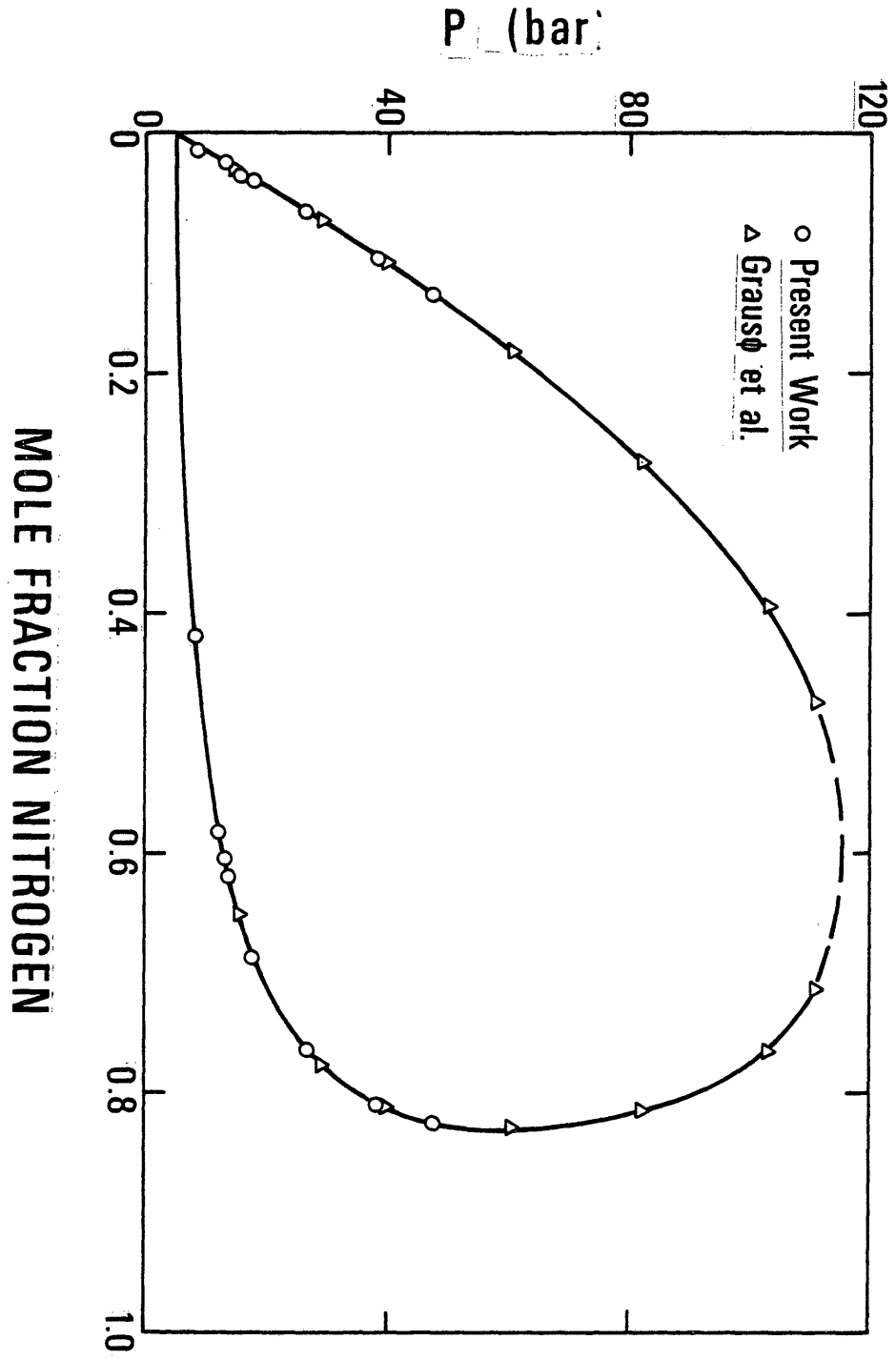

Figure 4. $N_2 + C_2H_4$ @ 200.00 K

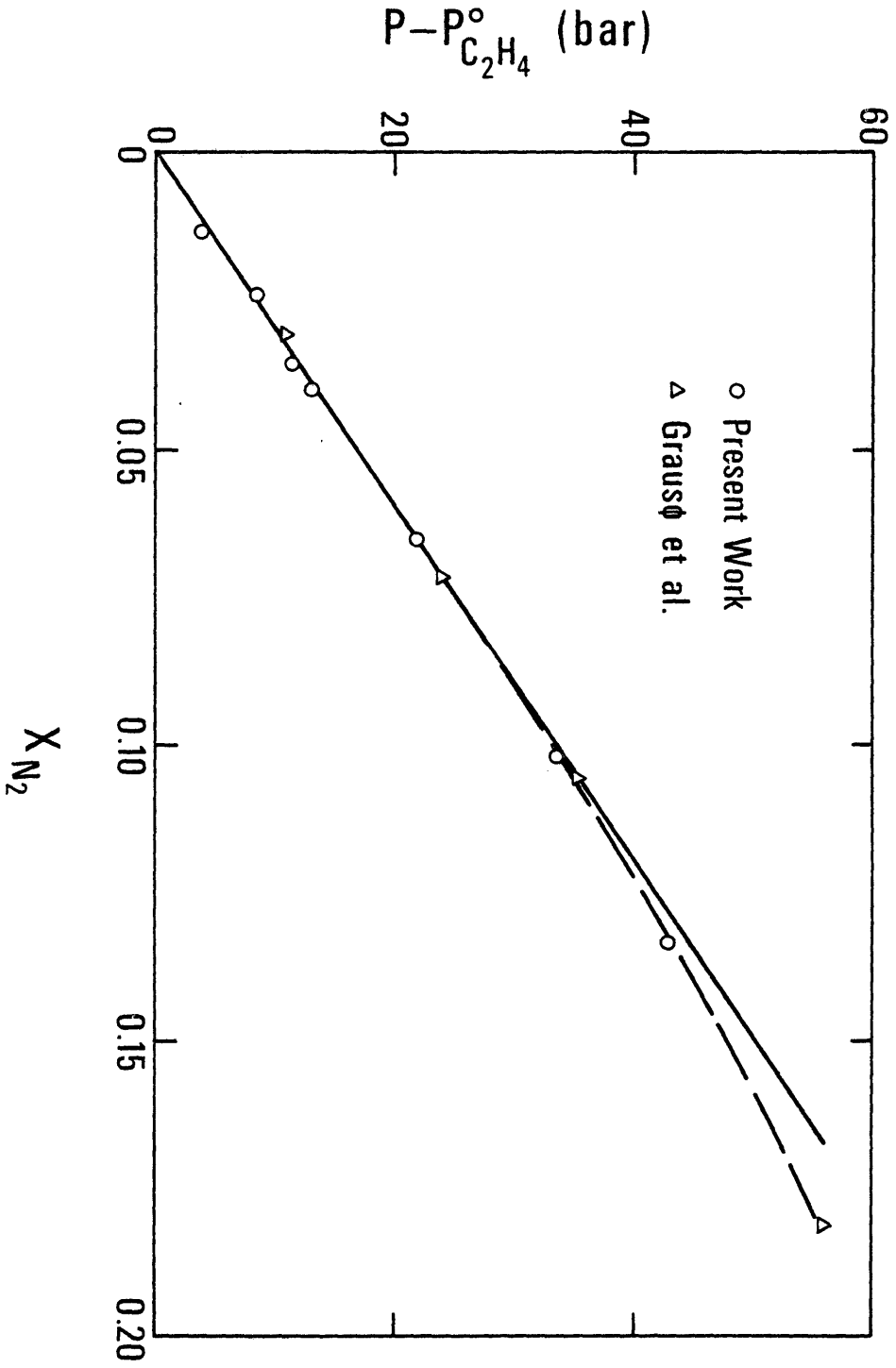

Figure 5. $N_2 + C_2H_4$ @ 200.00 K

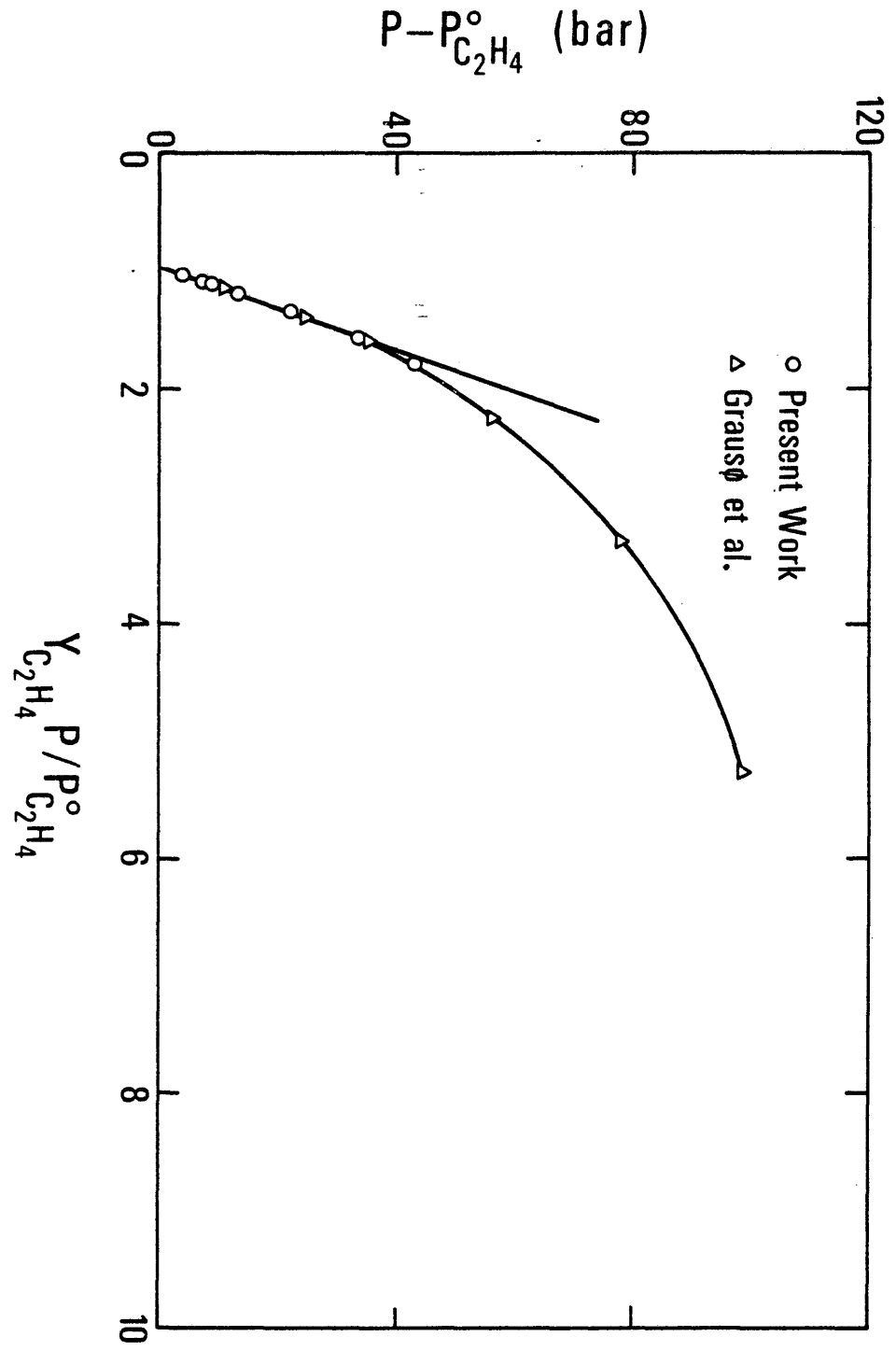

Figure 6. Enhancement Factor for N_2 + C_2H_4 System @ 200.00 K

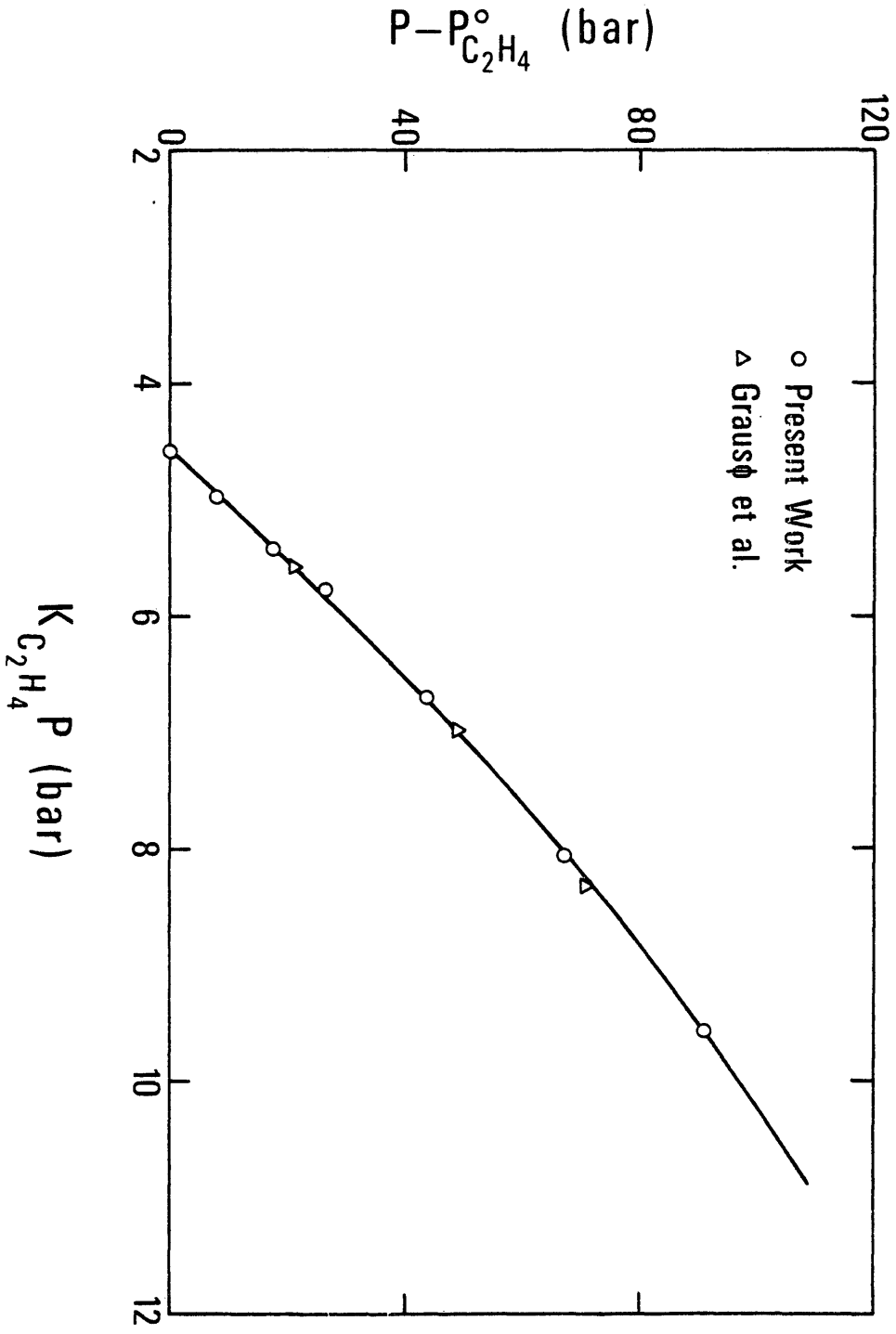

Figure 7. N_2 + C_2H_4 System @ 200.00 K

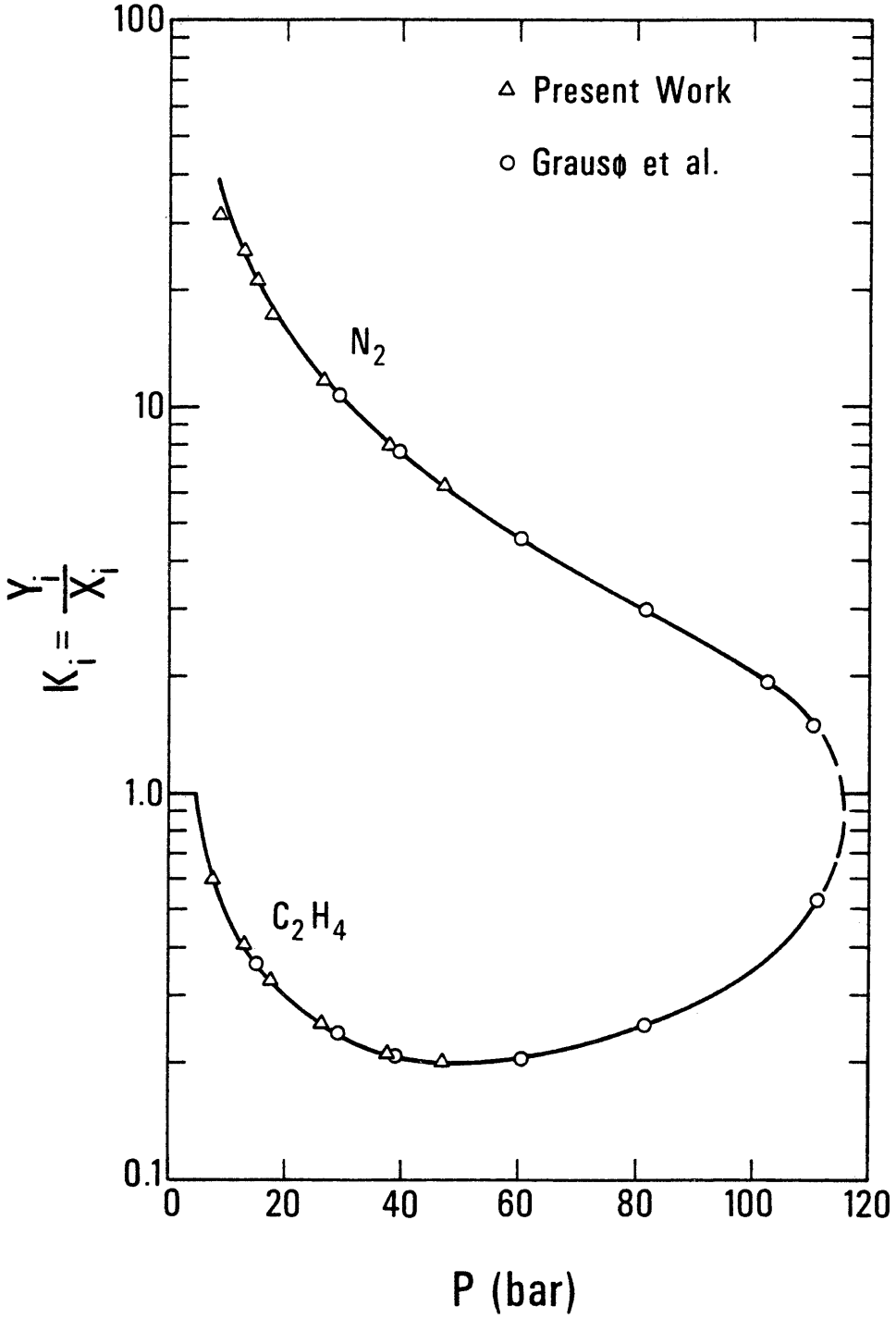

Figure 8. K Factor for N_2 + C_2H_4 System @ 200.00 K

Table 4-4

N_2 + C_2H_4 System @ 120.00 K

Date	P(bar)	$P-P^{o}_{C_2H_4}$	X_{N_2}	Y_{N_2}	$X_{C_2H_4}$	$Y_{C_2H_4}$	K_{N_2}	$K_{C_2H_4}$
4/20	0.01	0.00	0.00	0.00	1.00	1.00	--	1.00
4/20	6.44	6.43	0.0451	1.00	0.9549	0.00	22.17	-
4/20	10.35	10.34	0.0719	1.00	0.9281	0.00	13.91	-
4/20	15.03	15.02	0.1083	1.00	0.8917	0.00	9.23	-
4/25	20.86	20.85	0.1666	1.00	0.8334	0.00	6.00	-
4/25	22.805	22.89	0.2024	1.00	0.7976	0.00	4.94	-

Table 4-5

N_2 + C_2H_4 System @ 125.28 K

Date	P(bar)	$P-P^{\circ}_{C_2H_4}$	X_{N_2}	Y_{N_2}	$X_{C_2H_4}$	$Y_{C_2H_4}$	K_{N_2}	$K_{C_2H_4}$
5/9	00.024	0.00	0.00	0.00	1.00	1.00	--	1.00
5/9	4.96	4.936	0.0286	0.997	0.9704	0.0030	34.86	0.0031
5/9	10.06	10.036	0.0601	0.9994	0.9399	0.0006	16.63	0.0004
5/9	15.07	15.046	0.0953	1.00	0.9047	0.00	10.49	0.00
5/8	18.18	18.156	0.1129	1.00	0.8871	0.00	8.86	0.00
5/8	21.50	21.476	0.1414	1.00	0.8586	0.00	7.07	0.00
5/8	26.35	26.321	0.1954	0.9994	0.8046	0.0006	5.11	0.0007
5/9	28.80	28.476	0.2282	0.9981	0.7718	0.0019	4.37	0.0025
6/22	29.10	29.076	--	0.9996	--	0.0004	--	--
6/22	30.31	30.286	0.9188	--	0.0812	--	--	--

TABLE 4-6

N_2 + C_2H_4 System @ 134.00 K

Date	P(bar)	$P-P^{o}_{C_2H_4}$	X_{N_2}	Y_{N_2}	$X_{C_2H_4}$	$Y_{C_2H_4}$	$Y_{C_2H_4}P/P^{o}_{C_2H_4}$	K_{N_2}	$K_{C_2H_4}$	$K_{C_2H_4}P$
5/10	0.069	0.00	0.00	0.00	1.00	1.00	--	--	1.00	--
5/14	6.71	6.641	0.0338	0.9906	0.9662	0.0094	0.914	29.31	0.0097	0.0651
5/14	16.66	16.591	0.0851	0.9965	0.9149	0.0035	0.845	11.71	0.0038	0.0633
5/14	26.46	26.391	0.1517	0.9966	0.8483	0.0034	1.304	6.57	0.0040	0.1477
5/10	36.92	36.851	0.2302	0.9918	0.7698	0.0082	4.388	4.31	0.0107	0.3950
5/10	40.33	40.261	0.2516	0.9880	0.7484	0.0120	7.014	3.93	0.0160	0.6453

$N_2 + C_2H_4$ System @ 140.00 K

Date	P(bar)	$P-P^{O}_{C_2H_4}$	X_{N_2}	Y_{N_2}	$X_{C_2H_4}$	$Y_{C_2H_4}$	$Y_{C_2H_4}P/P^{O}_{C_2H_4}$	K_{N_2}	$K_{C_2H_4}$	$K_{C_2H_4}P$
4/18	0.118	0.00	0.00	0.00	1.00	1.00	--	--	1.00	0.118
4/19	6.06	5.942	--	0.9787	--	0.0213	1.0939		--	--
4/18	10.47	10.332	0.0469	0.9878	0.9531	0.0122	1.0825	21.474	0.0128	0.1340
4/18	16.0	15.882	0.0736	0.9917	0.9264	0.0083	1.1254	14.331	0.00896	0.1434
4/18	21.93	21.812	0.1038	0.9931	0.8962	0.0069	1.2823	9.567	0.0077	0.1689
4/18	28.75	28.632	0.1424	0.9925	0.8576	0.0075	1.8273	6.969	0.0087	0.2501
4/19	35.985	35.867	0.1947	0.9902	0.8053	0.0098	2.9886	5.086	0.0122	0.4390
4/19	42.985	42.867	0.2373	0.9855	0.7627	0.0145	5.2821	4.153	0.0190	0.8167
4/19	47.875	47.757	0.2792		0.7208	--	--	--	--	--
4/19	49.03	48.91	--	0.9731	--	0.0269	11.1772	--	--	--
4/19	50.26	50.14	0.3019	0.9646	0.6981	0.0354	15.0780	3.1951	0.0507	2.5482
6/21	50.45	50.33	--	0.9714	--	0.0286				
6/21	51.27	51.15	0.9316	0.9737	0.0684	0.0263				
6/21	52.60	50.54	--	0.9682	--	0.0318				
6/21	53.60	53.48	0.9481	0.9690	0.0519	0.0310				
6/21	54.10	53.98	0.9658	0.9717	0.0342	0.0283				

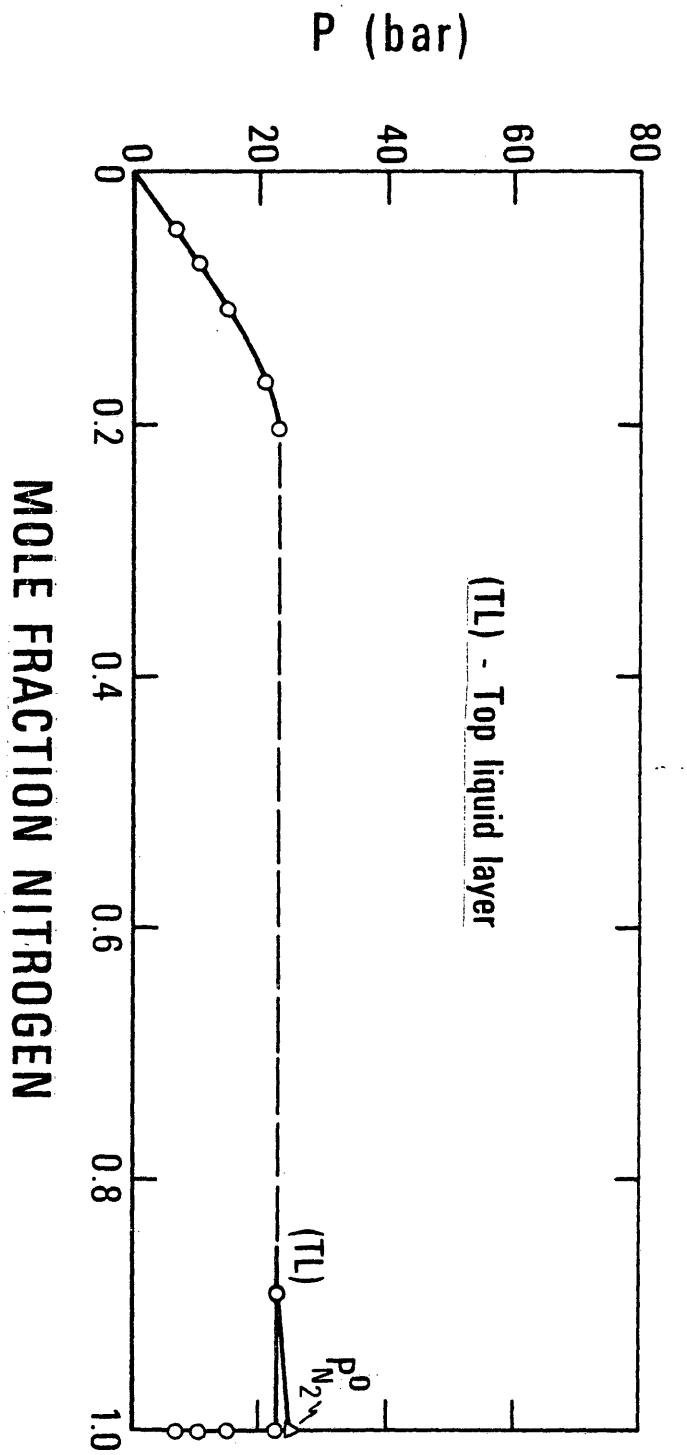

Figure 9. N_2 + C_2H_4 System @ 120.00 K

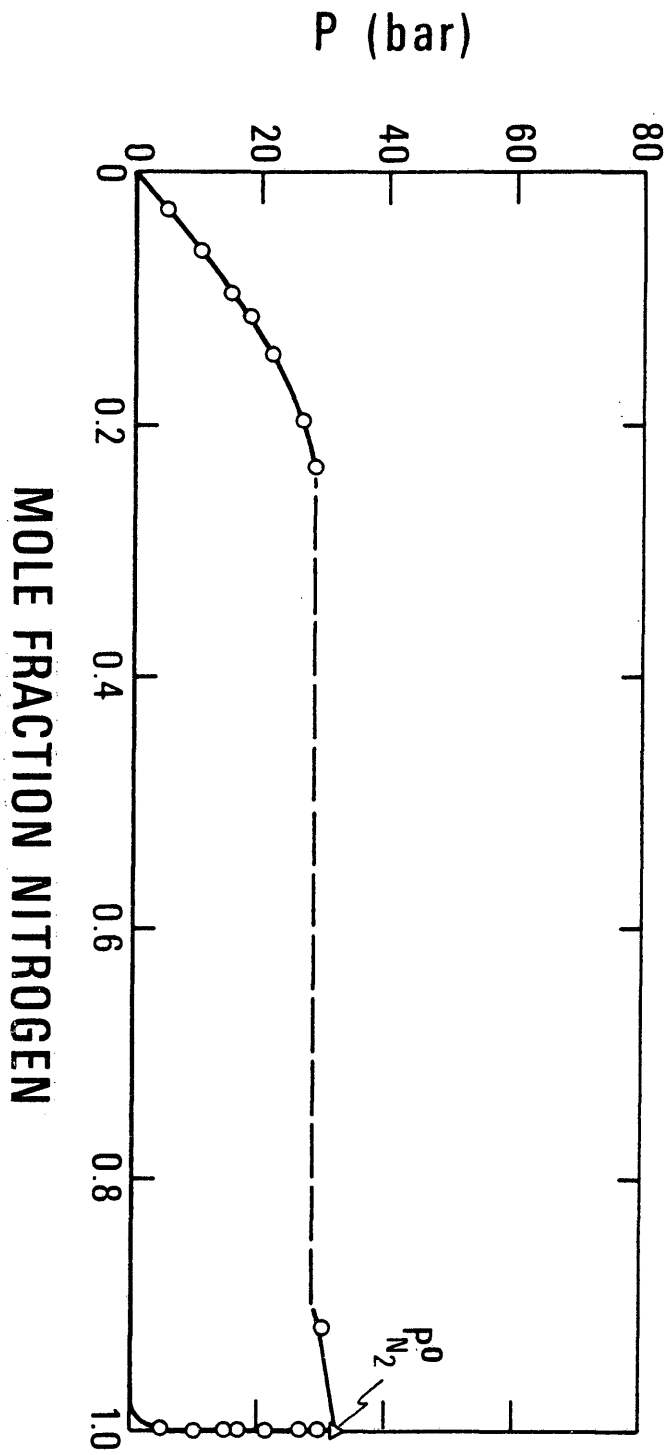

Figure 10. N_2 + C_2H_4 System @ 125.28 K

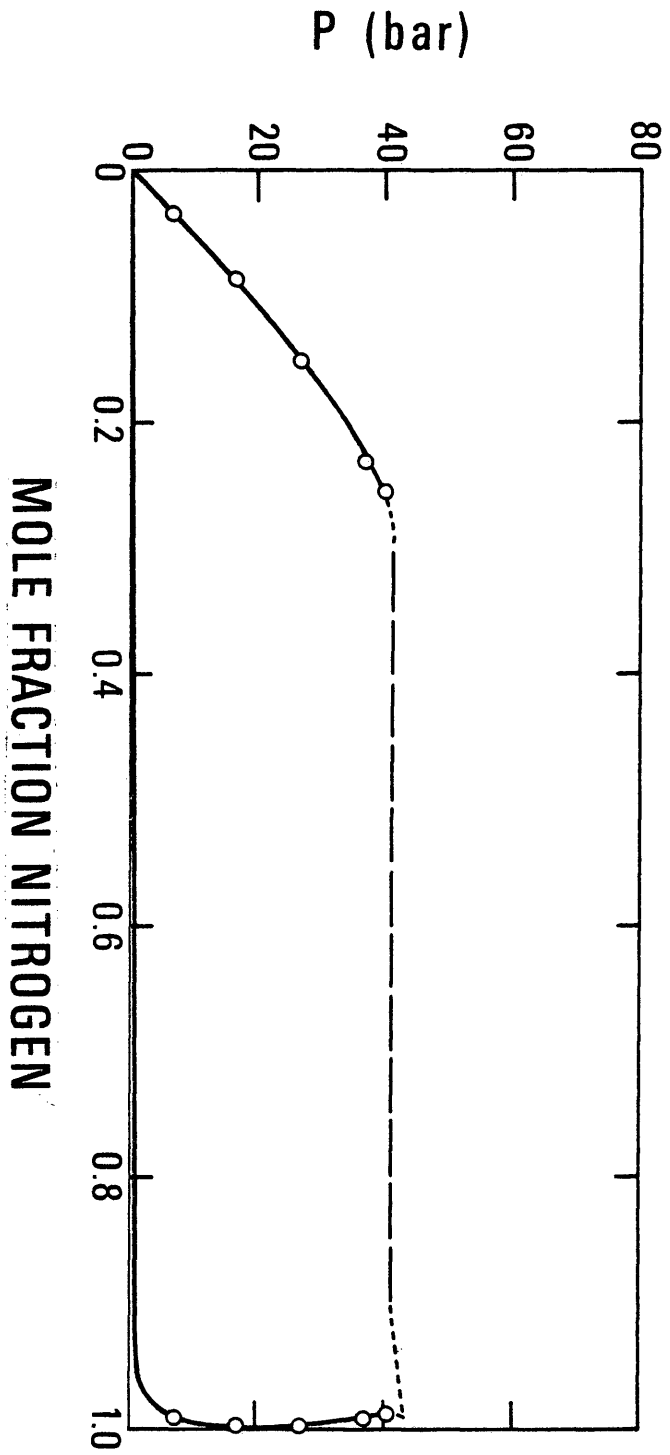

Figure 11. $N_2 + C_2H_4$ @ 134.00 K

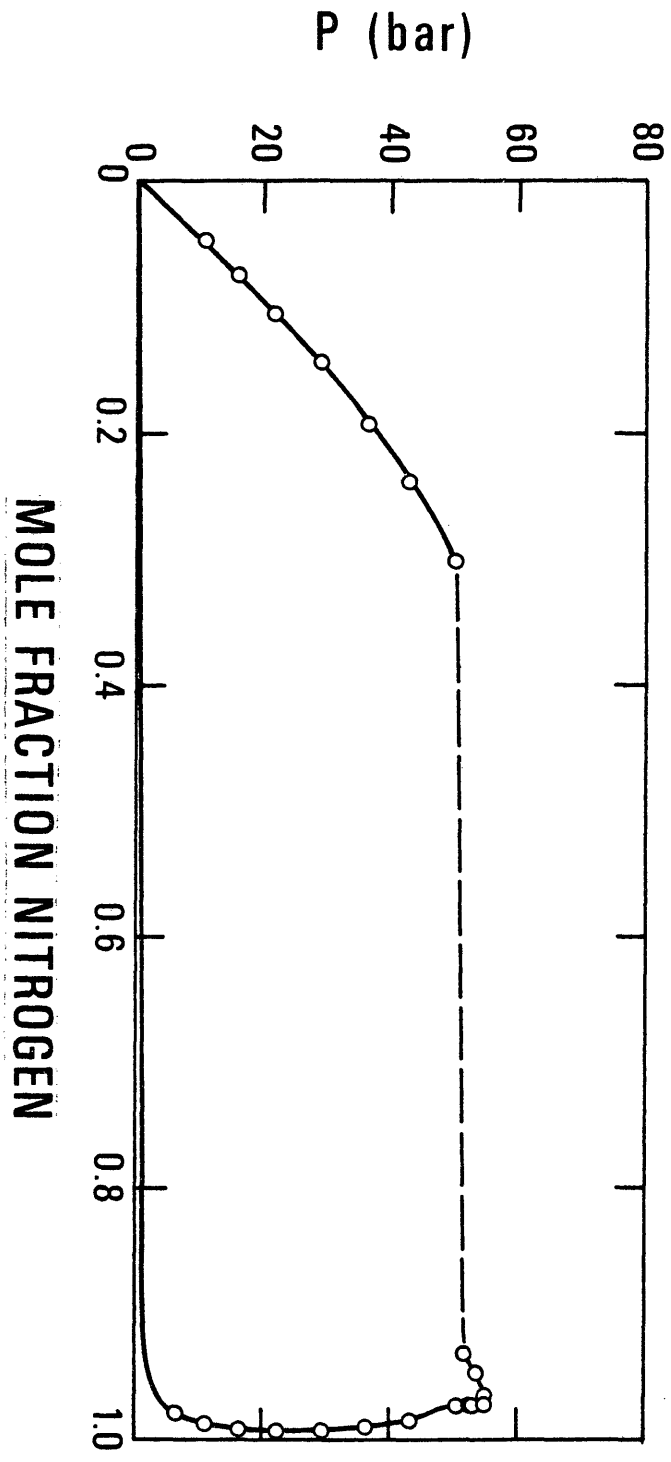

Figure 12. N_2 + C_2H_4 System @ 140.00 K

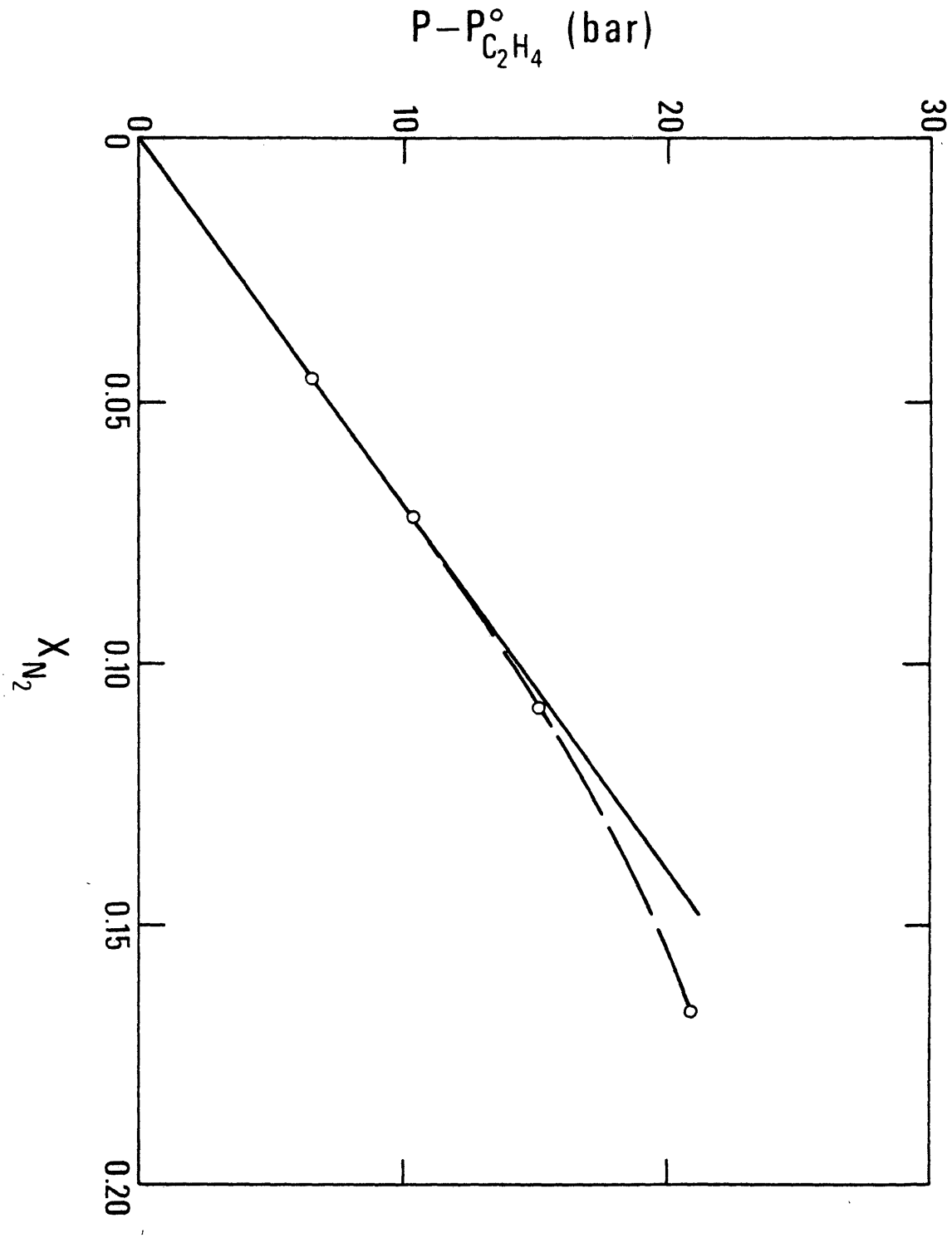

Figure 13. N_2+C_2H_4 System @ 120.00 K.

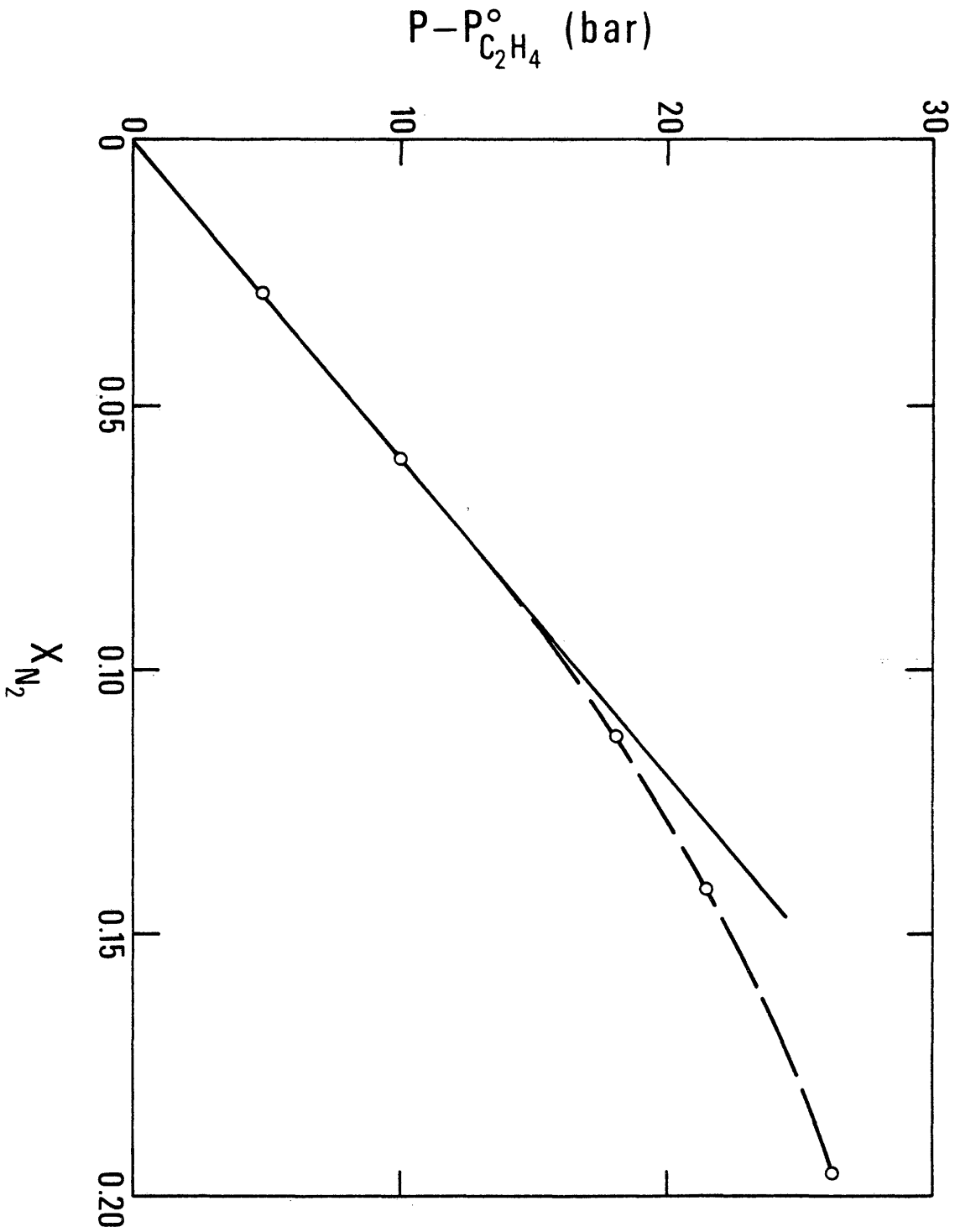

Figure 14. N_2+C_2H_4 System @ 125.28 K

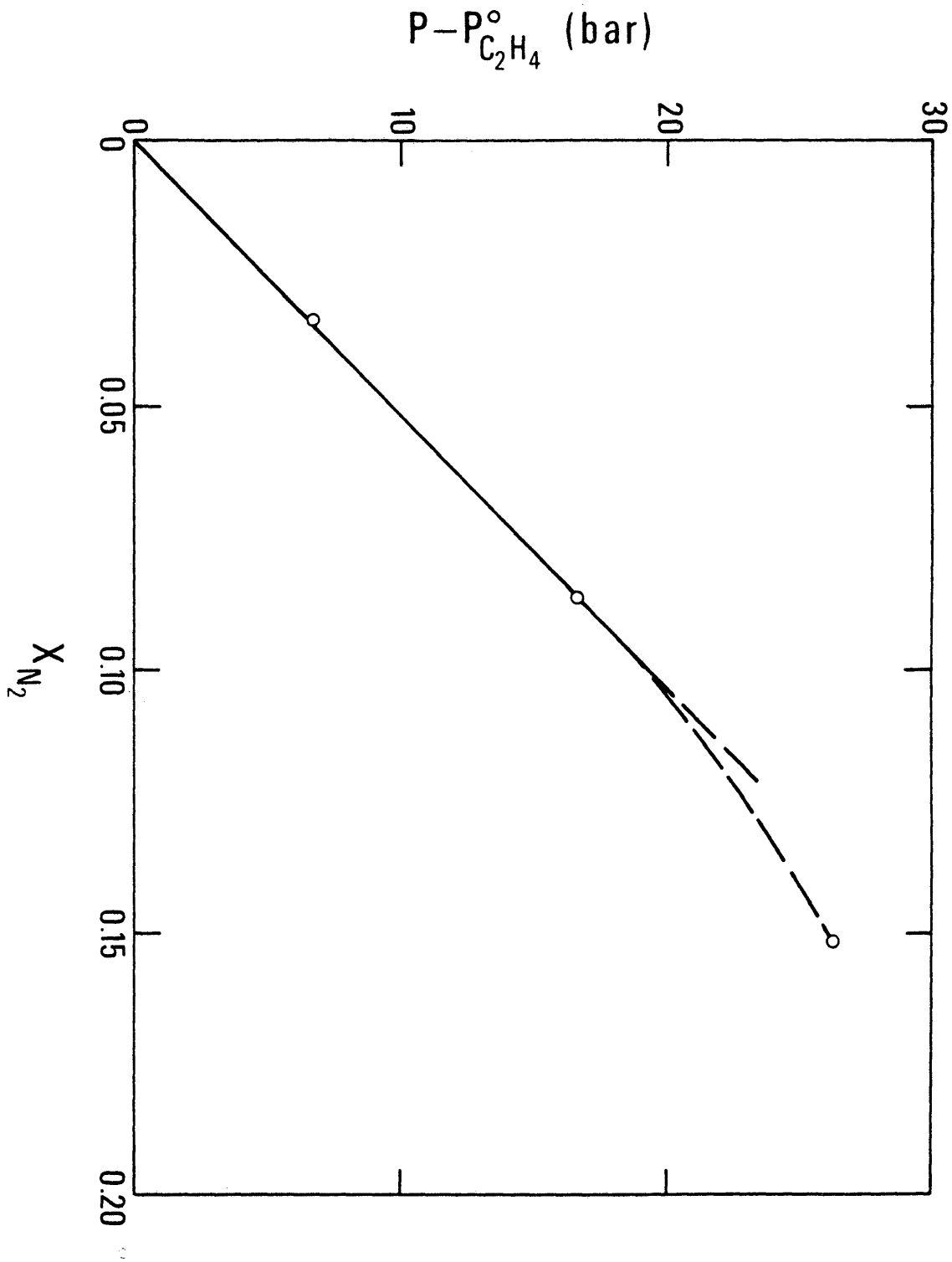

Figure 15. N_2 + C_2H_4 System @ 134.00 K

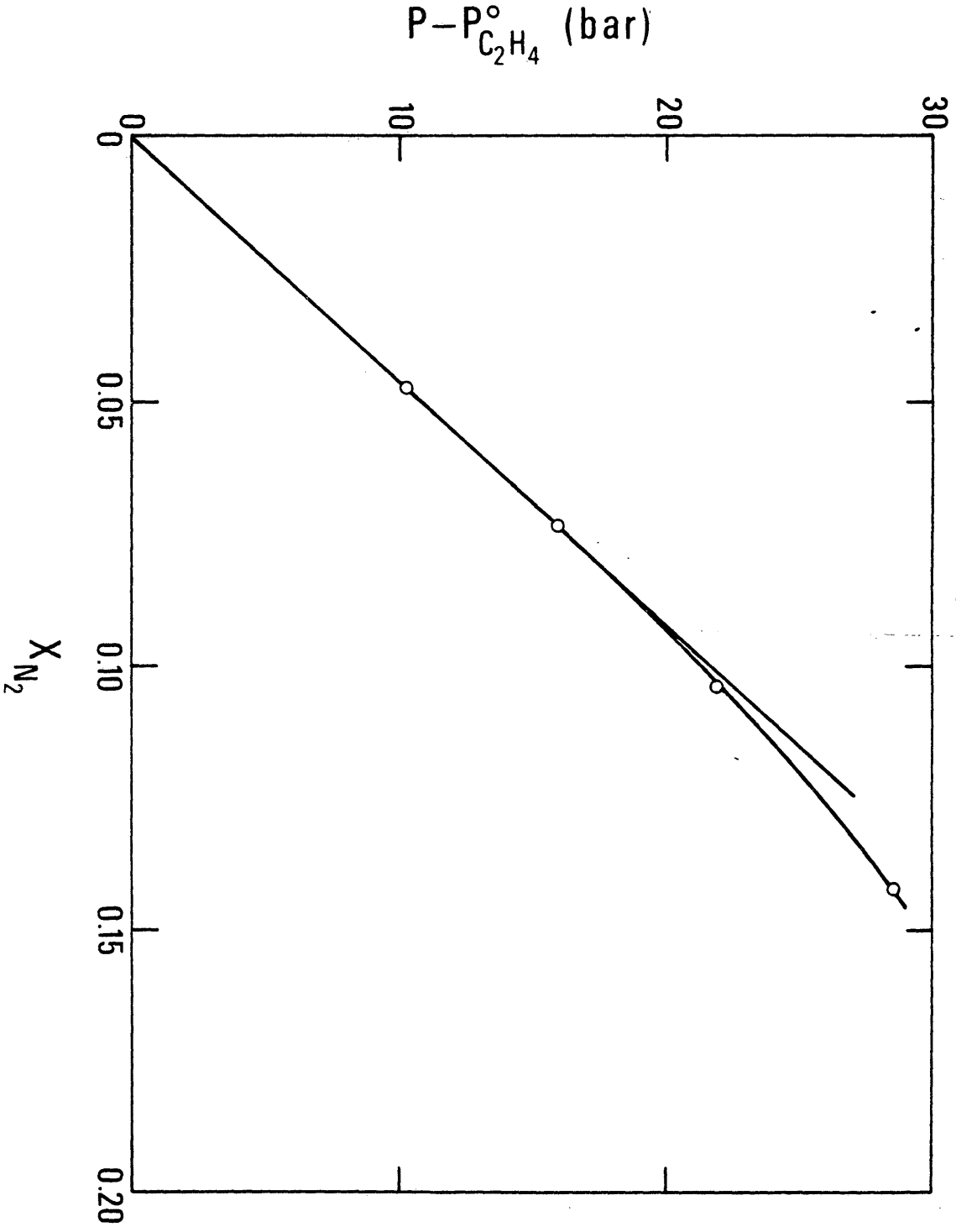

Figure 16. N_2+C_2H_4 System @ 140.00 K

compositions. It may be noted no vapor consistency tests (enhancement factor test) or liquid-vapor test ($K_{C_2H_4}P$) are given for temperatures $\leq$134 K. This is due to the fact that the vapor phase composition is almost pure N_2 and no meaningful results can be obtained from such plots.

Figures (17) and (18) show the above mentioned tests for the 140 K data. Good consistency is indicated by the smoothness of the curves obtained and the accuracy of the values obtained at the extrapolation points.

In order to determine the location of the two liquid phase region, measurements of top liquid layer composition and some other measurements in the region between the separation pressure and the normal liquid-vapor critical were needed. Although this was a very difficult task with the apparatus used in this investigation, some data were obtained for the 120, 125.28, and 140 K isotherms and the two liquid phase region was (partially) established as shown in the isotherms of figure (34) and the coexistence curve in figure (19). As can be seen from the coexistence curve data shown in Table (4-7), the lower liquid layer composition is always richer in C_2H_4 than that of the top liquid layer which is almost pure N_2 (similar to the vapor phase composition).

One of the difficulties involved in the measurements mentioned above was the sensitivity of the results obtained to the amount of C_2H_4 introduced into the equilibrium cell. This can be easily understood since the liquid-vapor envelopes of this region are very flat, as shown in figures (9) through (12).

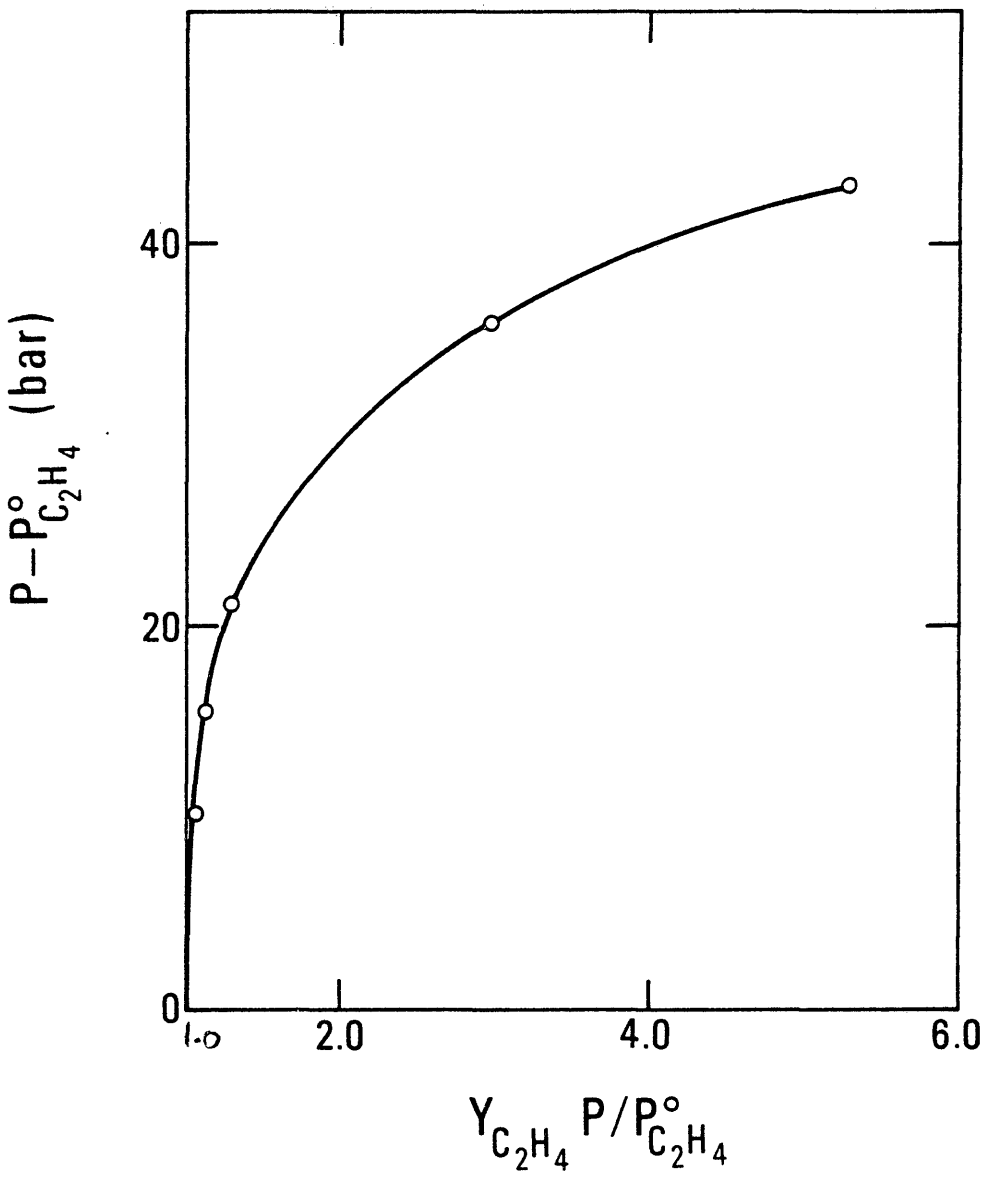

Figure 17. Enhancement Factor for N_2+C_2H_4 System @ 140.00 K.

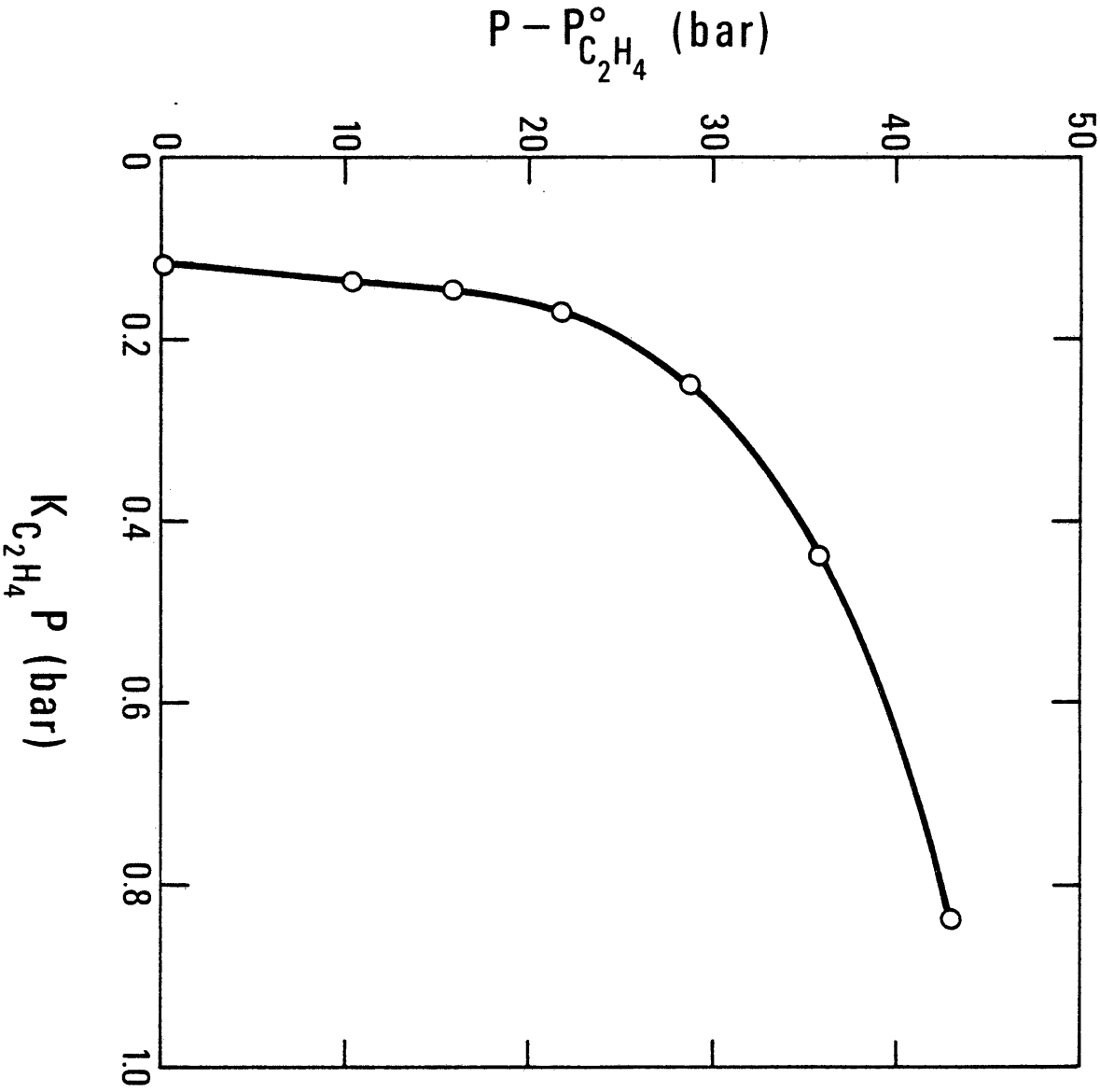

Figure 18. N_2+C_2H_4 System @ 140.00 K.

TABLE 4-8

Coexistence $T-P-X_{N_2}$ for the $N_2 + C_2H_4$ System

T(K)	P(bar)	$X^{I}_{N_2}$ (BL)	$X^{II}_{N_2}$ (TL)	Y_{N_2}
105.00	10.25			
110.00	13.71			
115.00	17.90			
120.00	22.85	0.2024	0.890	1.000
125.28	28.80	0.2282	0.900*	0.9981
130.00	35.10	0.2501	-	0.9935
134.00	41.10	0.2710	0.900*	0.9900
135.00	42.10	0.2761	-	0.9836
140.00	50.26	0.3019	0.925 *	0.9646

* Upper liquid layer compositions obtained from the intersection of the liquid-vapor curve above the separation pressure and the separation line.

e.g.

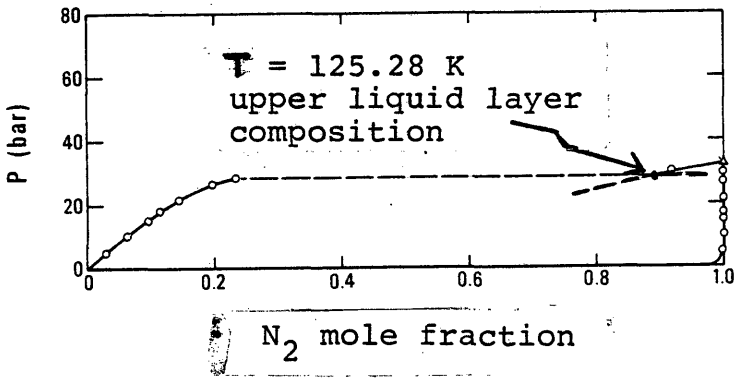

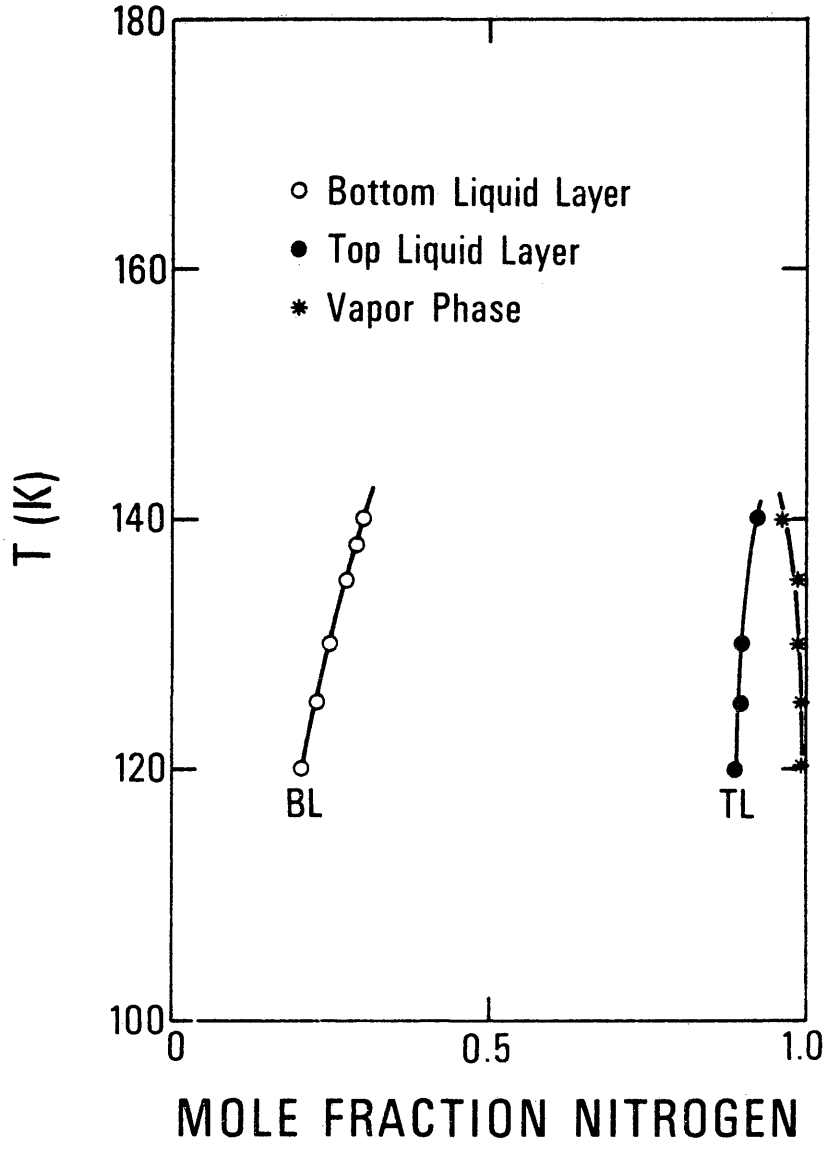

Figure 19. The Coexistence Curve for N_2 + C_2H_4

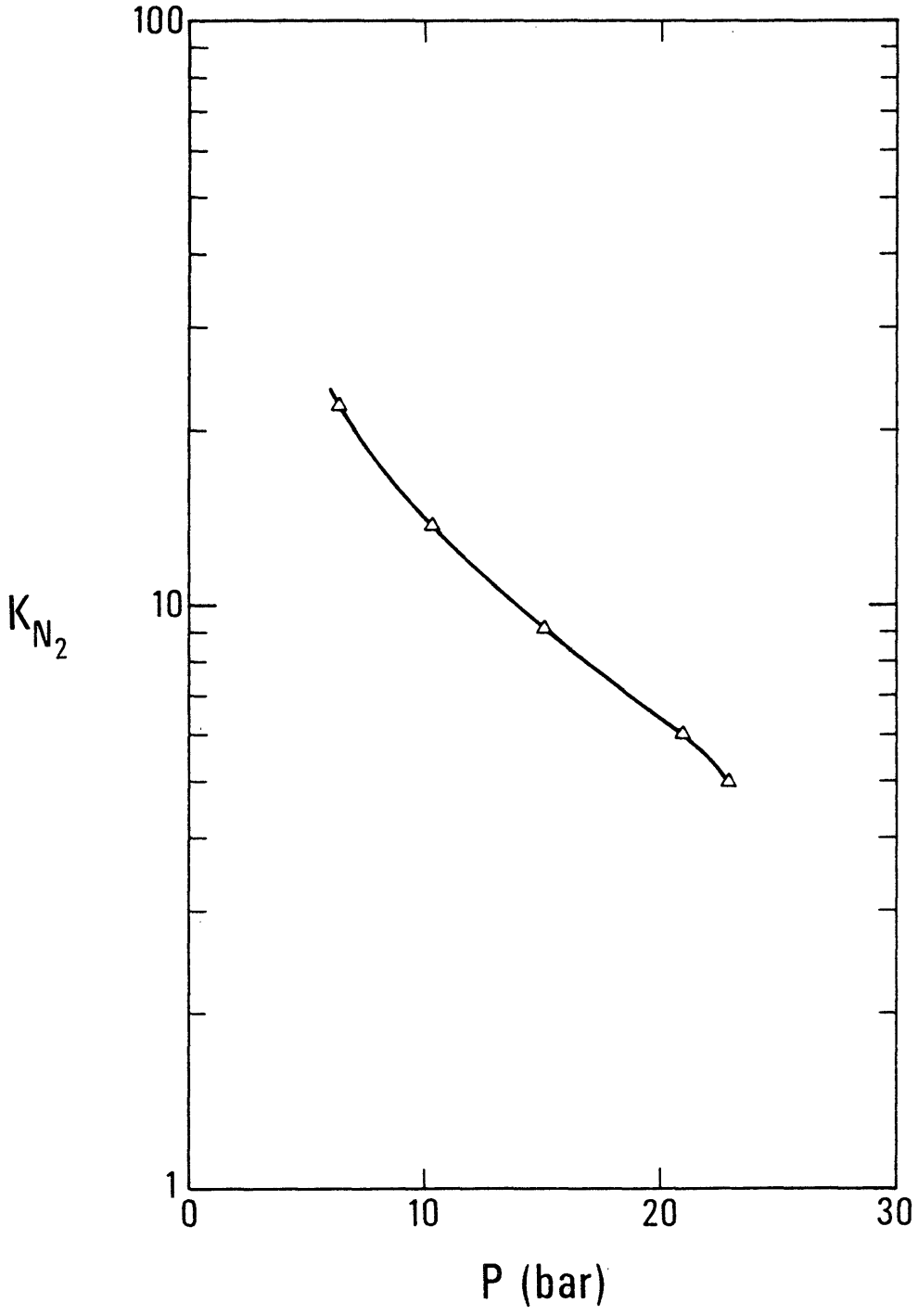

Figure 20. K Factor for N_2+C_2H_4 System @ 120.00 K.

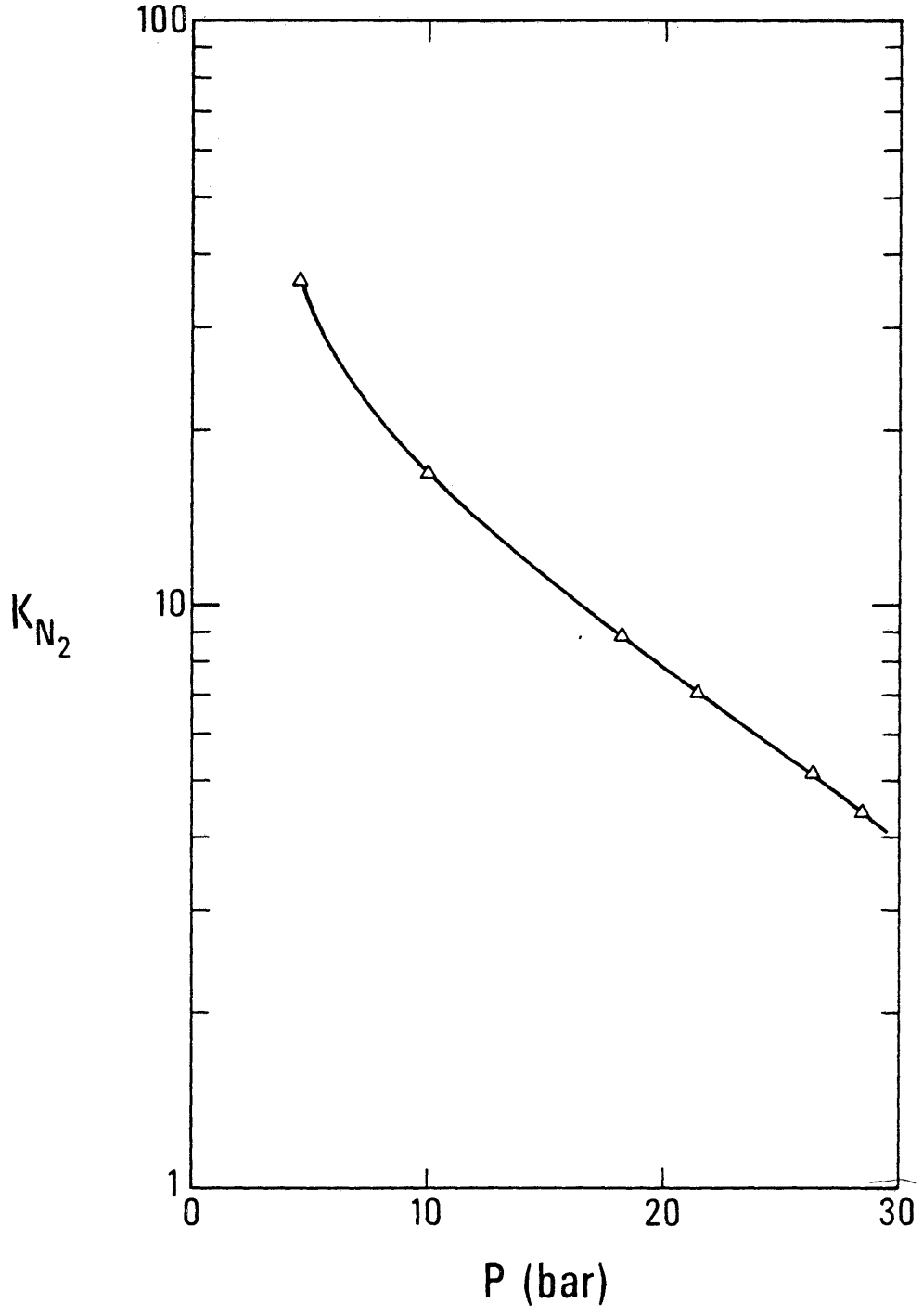

Figure 21. K Factor for N_2+C_2H_4 System @ 125.28 K.

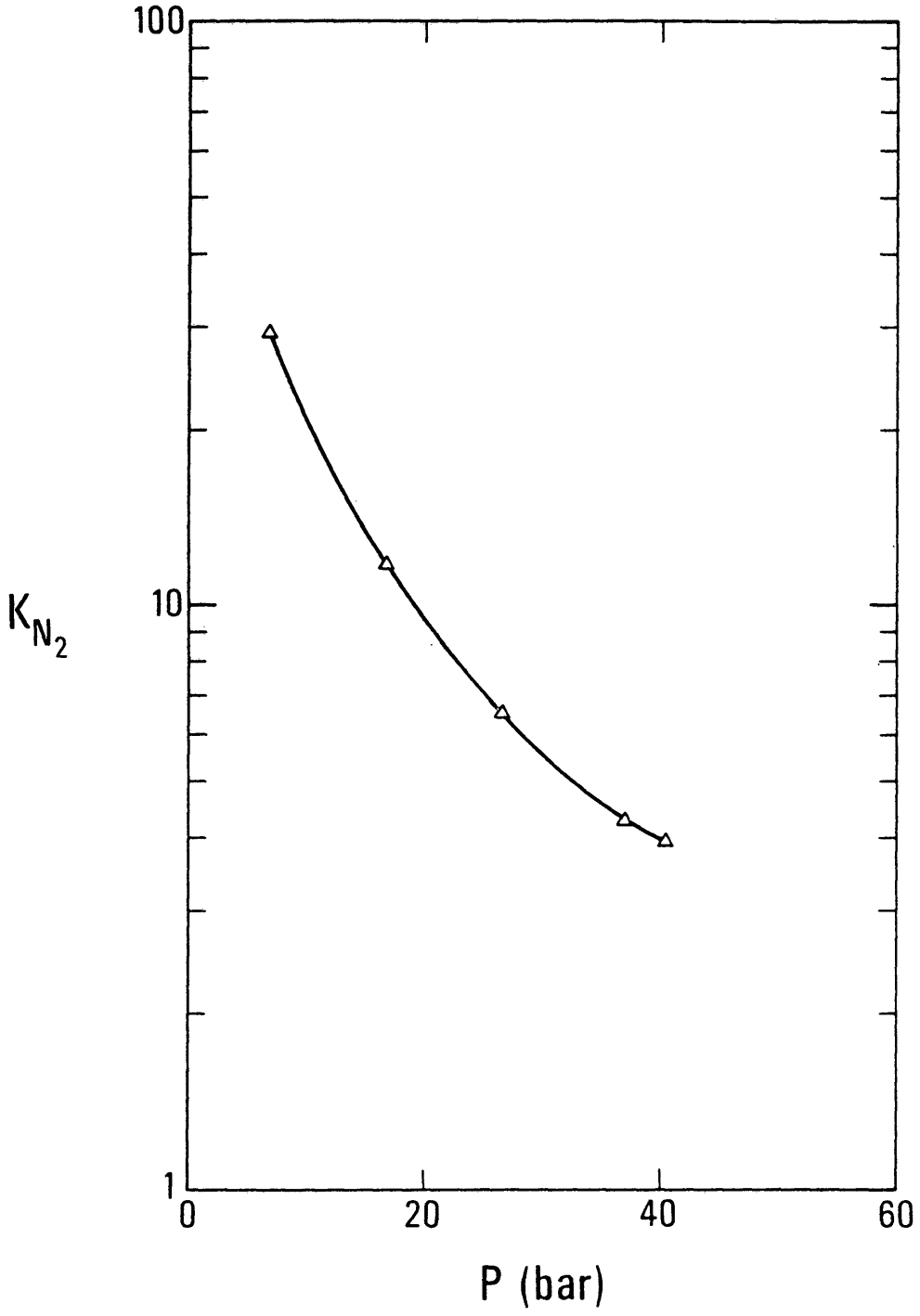

Figure 22. K Factor for N_2+C_2H_4 System @ 134.00 K.

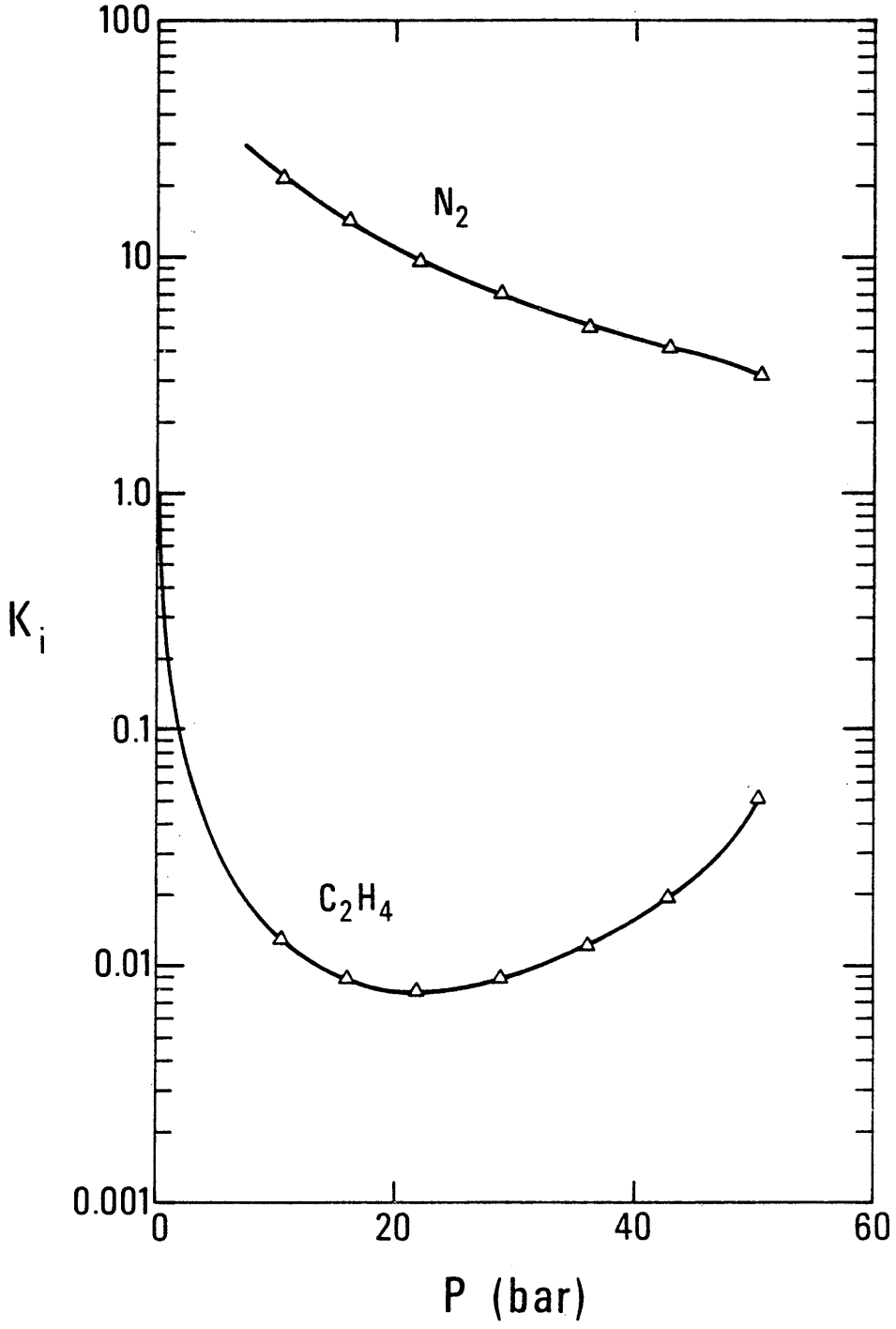

Figure 23. K Factor for N_2+C_2H_4 System @ 140.00 K.

In the isotherms obtained in this region some curvature (hook-like) near the critical points is observed. This type of behavior was reported for other systems such as the methane-propane system and methane-ethane system (I. Wichterle, et al., 1971).

Figures (20) through (23) show the plot of K-factors versus temperature. Good consistency is exhibited by the gradual and smooth transitions observed with temperature.

4-2.3 144.92 K Isotherm

Figure (24) shows the vapor-liquid data obtained at 144.92 K. This isotherm has special importance since it represents the transition region, the region between the normal vapor-liquid isotherms and the isotherms involving liquid phase separation. Consistency tests in the lower pressure regions all show good internal consistency as can be seen in figures (25) and (26).

Figure (27) shows a plot of $(Y-X)^2_{N_2}$ versus pressure which is another consistency test used to check for the vapor and the liquid composition near the critical region. This test was not applied to the other isotherm in the separation region due to sudden shift in composition at the separation pressure. Internally consistent data should produce a smooth curve extrapolating to the critical pressure. Figure (27) shows such behavior which should mean good internal consistency. However, due to the lack of a windowed equilibrium cell, no absolute assertion can be given for

TABLE 4-9

N_2 + C_2H_4 System @ 144.92 K

Date	P(bar)	$P-P^{o}_{C_2H_4}$	X_{N_2}	Y_{N_2}	$X_{C_2H_4}$	$Y_{C_2H_4}$	$Y_{C_2H_4}P/P^{o}_{C_2H_4}$	K_{N_2}	$K_{C_2H_4}$	$K_{C_2H_4}P$
6/12	0.1824	0.00	0.00	0.00	1.00	1.00	1.00	--	1.00	0.1824
6/12	16.02	15.84	0.0716	0.9864	0.9284	0.0136	1.1945	13.777	0.0146	0.2347
6/12	30.97	30.84	0.1502	0.9882	0.8498	0.0118	2.0035	6.579	0.0139	0.4300
6/13	45.36	45.18	0.2357	0.9826	0.7643	0.0174	4.3271	4.169	0.0228	1.0327
6/29	51.10	50.92	0.2776	0.9776	0.7224	0.0224	6.2754	3.522	0.0310	1.5845
6/29	55.93	55.75	0.3070	0.9658	0.6930	0.0342	10.4869	3.146	0.0494	2.7602
6/29	59.28	59.10	0.3502	0.9508	0.6498	0.0492	15.9900	2.715	0.0757	4,4884
6/12	59.78	59.60	0.3326	0.9508	0.6674	0.0492	16.1250	2.859	0.0737	4.4069
6/29	60.08	59.90	0.6123	0.9570	0.3877	0.0430	14.1636	1.563	0.1109	6.6635
6/27	63.53	63.35	0.7838	0.9574	0.2162	0.0426	14.8376	1.221	0.1970	12.5179
6/29	63.60	63.42	0.6376	--	0.3624	--	--	--	--	--
6/28	64.44	64.26	0.8004	0.9507	0.1196	0.0493	17.4172	1.188	0.4122	26.5626

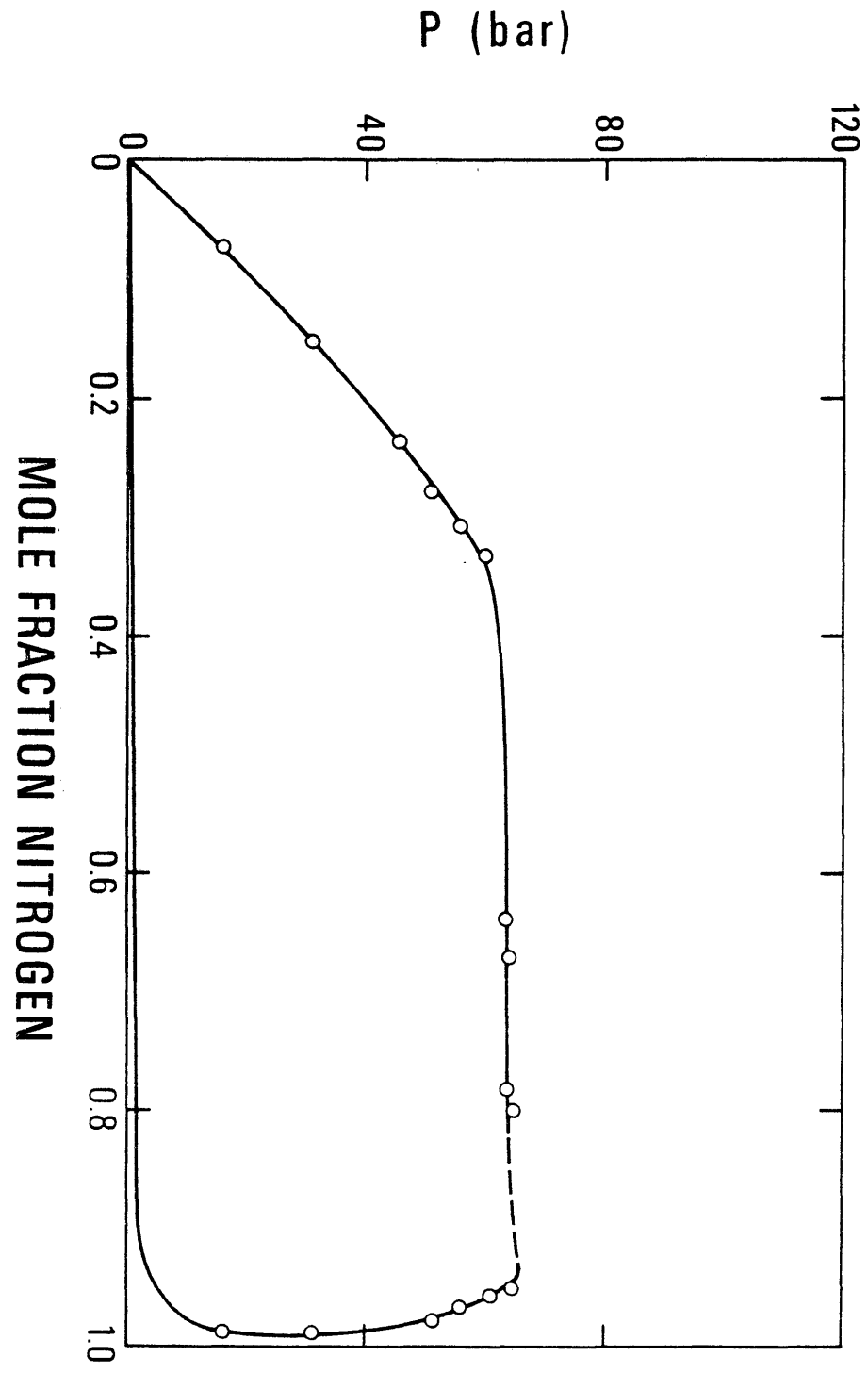

Figure 24. $N_2 + C_2H_4$ @ 144.92 K

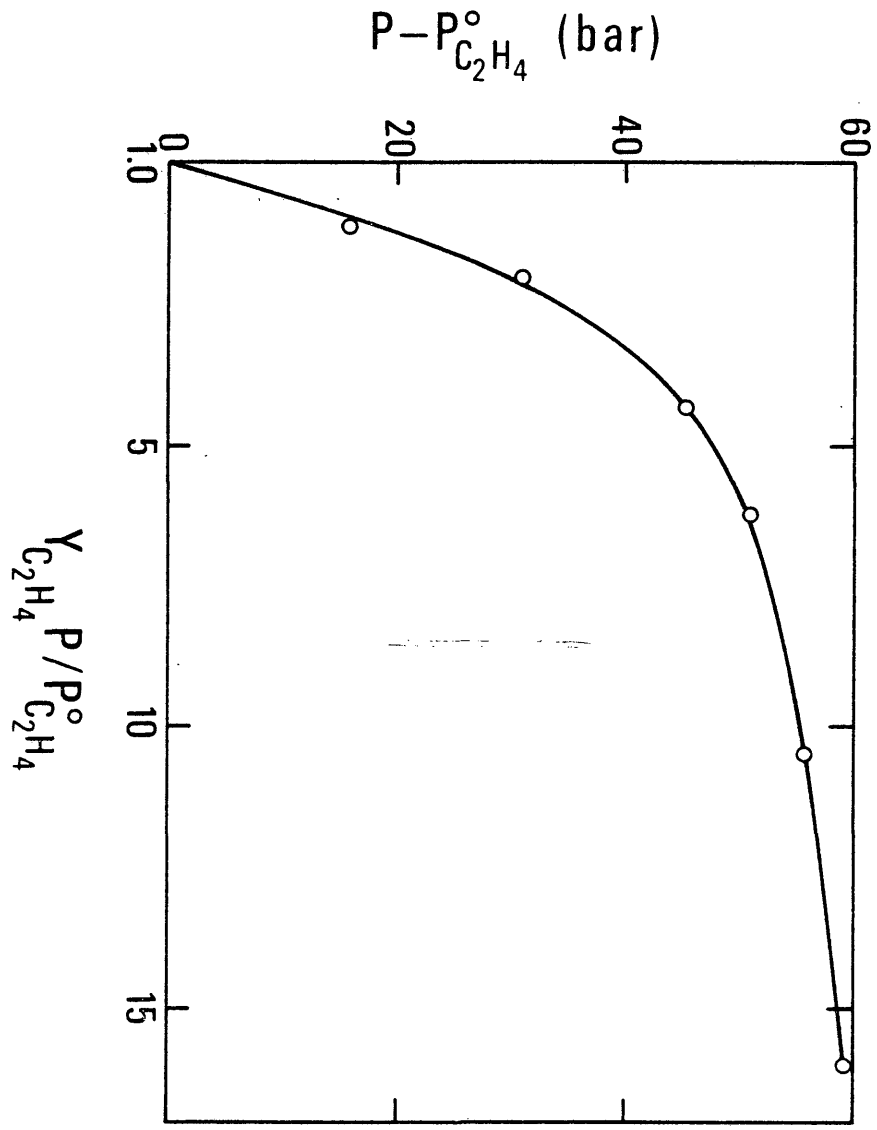

Figure 25. Enhancement Factor for N_2+C_2H_4 System @ 144.92 K.

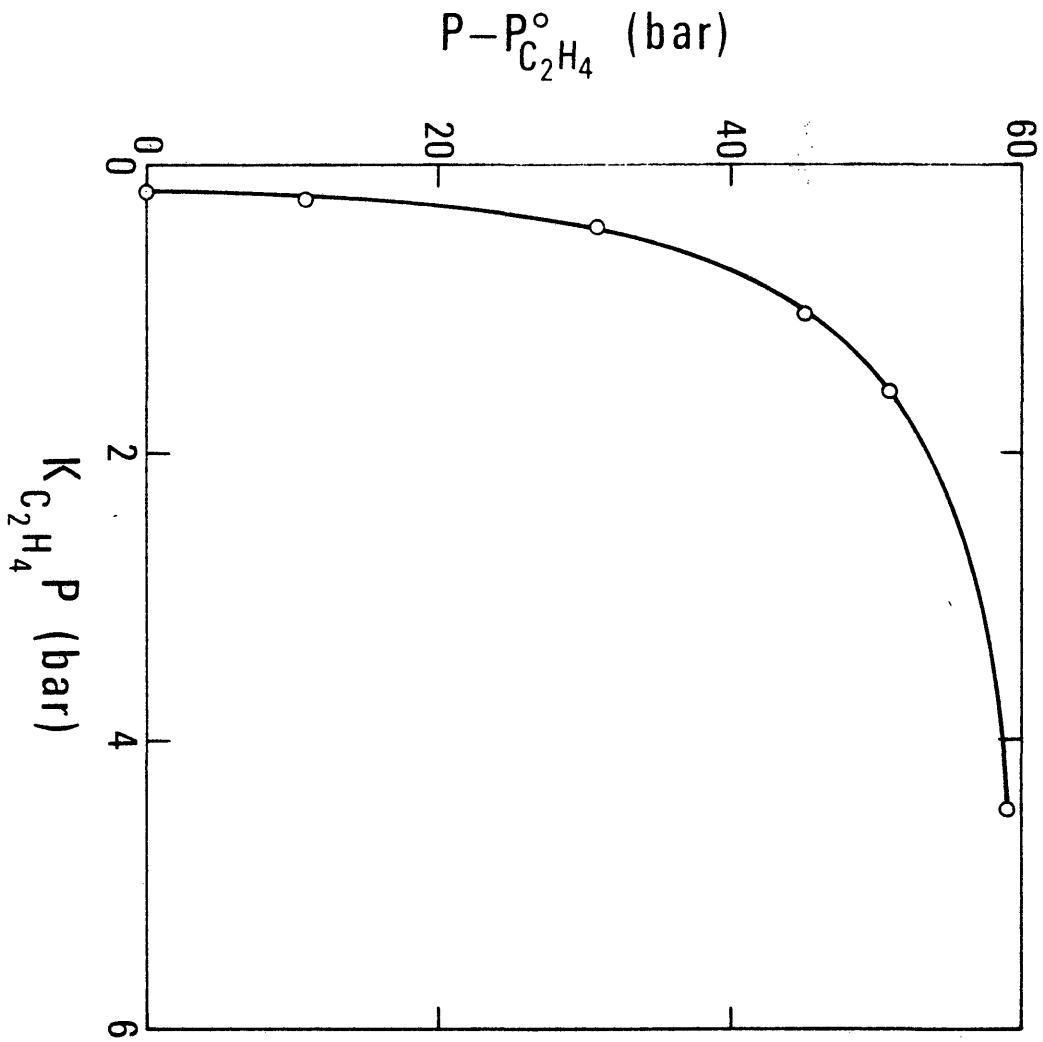

Figure 26. N_2+C_2H_4 System @ 144.92 K.

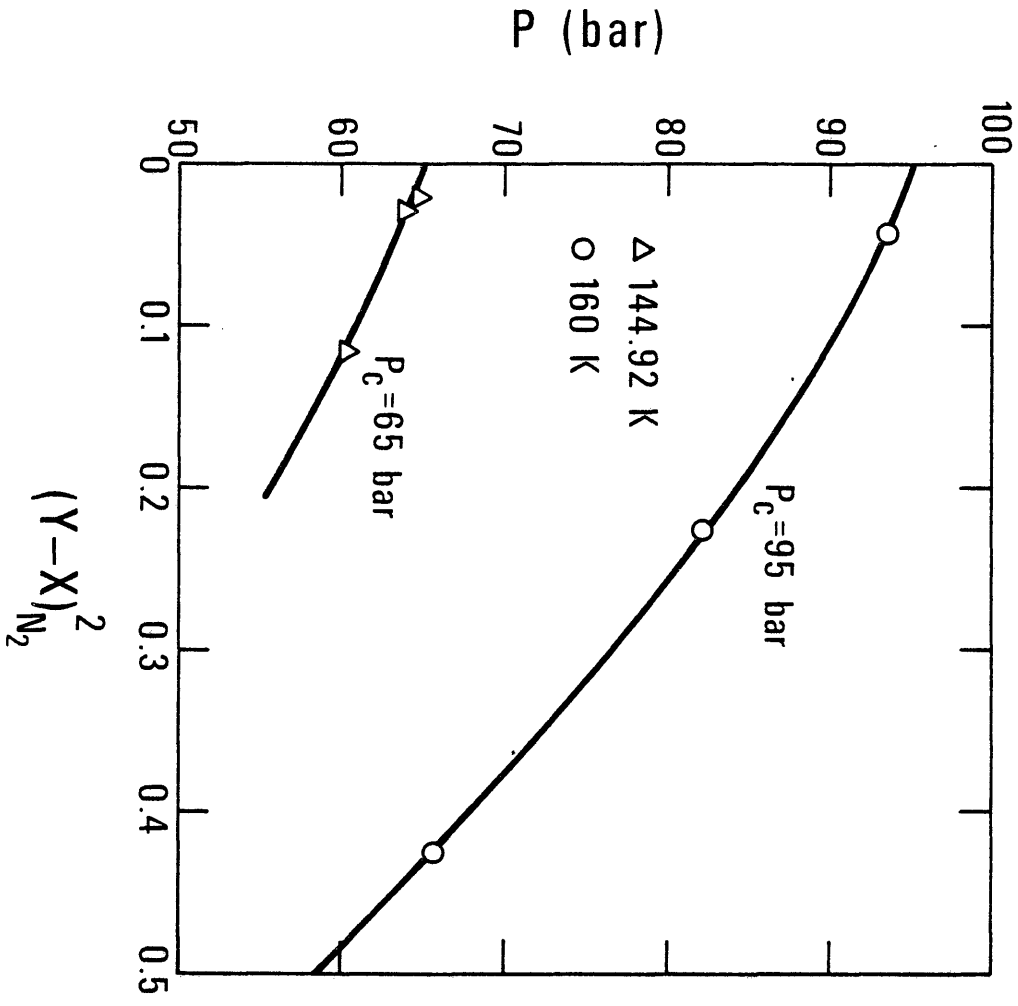

Figure 27. N_2 + C_2H_4 System @ 144.92 K

$$K_i = \frac{Y_i}{X_i}$$

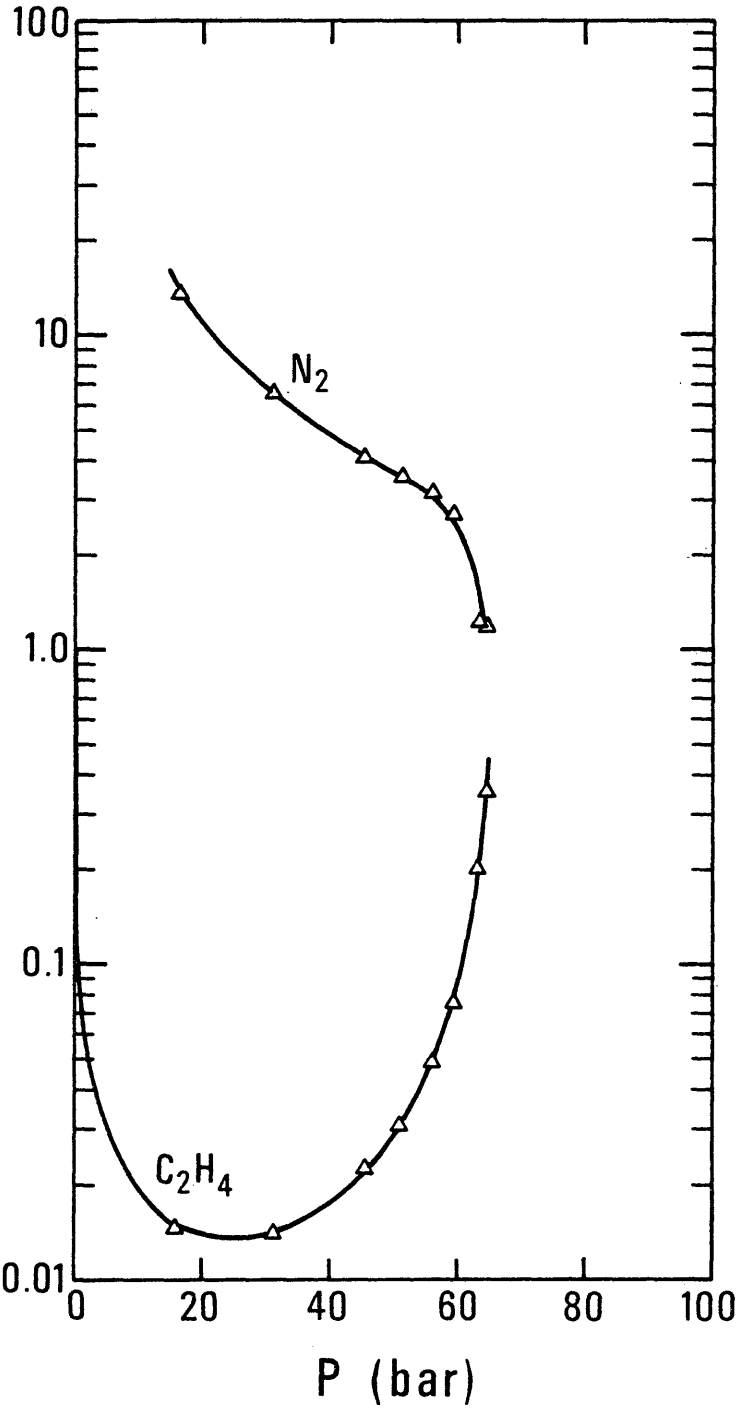

Figure 28. K Factor for N_2+C_2H_4 @ 144.92 K.

the quality of the data obtained, especially since the consistency test mentioned above is not rigorous.

Although the shapes of the vapor-liquid envelopes obtained in this range of temperatures are not commonly obtained several systems with partial miscibility exhibit the same type of P-T-X_{N_2} diagrams (W. Street, 1965, and M. Simon, et al., 1972).

4-2.4 160 K Isotherm

This isotherm shown in Figure (29) exhibits the characteristics of the normally miscible system, although the relatively flat region near the critical point may be indicative of some immiscibility effects. Figure (30), (31), (32), and (33) show the results of the consistency tests. Generally the data (Table 4-10) show excellent consistency except for the lower pressure (below 8 bars) liquid compositions which maybe attributed to the limitations in the sampling mechanism. The $(Y-X)^2_{N_2}$ versus pressure test was applied as shown in Figure (27). The smooth curvature of the graph indicates good internal consistency at higher pressures.

4.3 Overall View on N_2 + C_2H_4 Binary

Figure (34) shows all the data collected for this system with the two phase boundaries drawn by the dashed line. A P(T)-projection of the vapor-liquid critical locus of all the isotherms available for the system, including other investigator's work (Grausø, et al. (1977)), is shown in figure (35). The separation locus, characteristic of the lower temperature region, is also given.

Date	P(bar)	$P-P^{o}_{C_2H_4}$	X_{N_2}	Y_{N_2}	$X_{C_2H_4}$	$Y_{C_2H_4}$	$Y_{C_2H_4}P/P^{o}_{C_2H_4}$	K_{N_2}	$K_{C_2H_4}$	$K_{C_2H_4}P$
3/30	0.563	0.00	0.00	0.00	1.00	1.00	-	-	1.00	0.563
3/30	4.30	3.74	0.0167	0.8587	0.9833	0.1413	1.079	51.42	0.144	0.6192
3/30	5.80	5.24	0.0219	0.8927	0.9781	0.1073	1.105	40.76	0.1097	0.6363
4/15	7.20	6.64	0.0247	0.9113	0.9753	0.0887	1.134	36.89	0.091	0.6548
4/15	8.17	7.61	0.0285	0.9210	0.9715	0.0790	1.146	32.32	0.0813	0.6643
4/15	8.97	8.41	0.0310	0.9267	0.9690	0.0733	1.168	29.76	0.0756	0.6785
4/10	11.20	10.64	0.0398	0.9391	0.9602	0.0609	1.212	23.60	0.063	0.7056
4/19	11.52	10.96	0.0406	0.9402	0.9594	0.0599	1.226	23.16	0.062	0.7142
4/16	14.70	14.14	0.0525	0.9511	0.9475	0.0489	1.277	18.12	0.052	0.7644
4/16	18.09	17.53	0.0663	0.9567	0.9337	0.0433	1.391	14.43	0.046	0.8321
4/16	21.50	20.94	0.0797	0.9618	0.9203	0.0382	1.459	12.07	0.042	0.9030
4/17	27.95	27.39	0.1062	0.9660	0.8938	0.0340	1.688	9.10	0.038	1.0620
4/17	34.97	34.41	0.1350	0.9676	0.8650	0.0324	2.012	7.17	0.0375	1.3113
4/17	40.80	40.24	0.1615	0.9670	0.8383	0.0330	2.391	5.99	0.039	1.5912
4/17	48.30	47.74	0.2023	0.9631	0.7977	0.0369	3.166	4.76	0.046	2.2218
6/7	65.58	65.02	0.2923	0.9473	0.7077	0.0527	6.139	3.241	0.074	4.8529
6/11	82.00	81.44	0.4315	0.9079	0.5685	0.0921	13.414	2.104	0.1620	13.2840
6/11	93.42	92.86	0.6538	0.8631	0.3462	0.1369	22.716	1.320	0.3954	36.9383

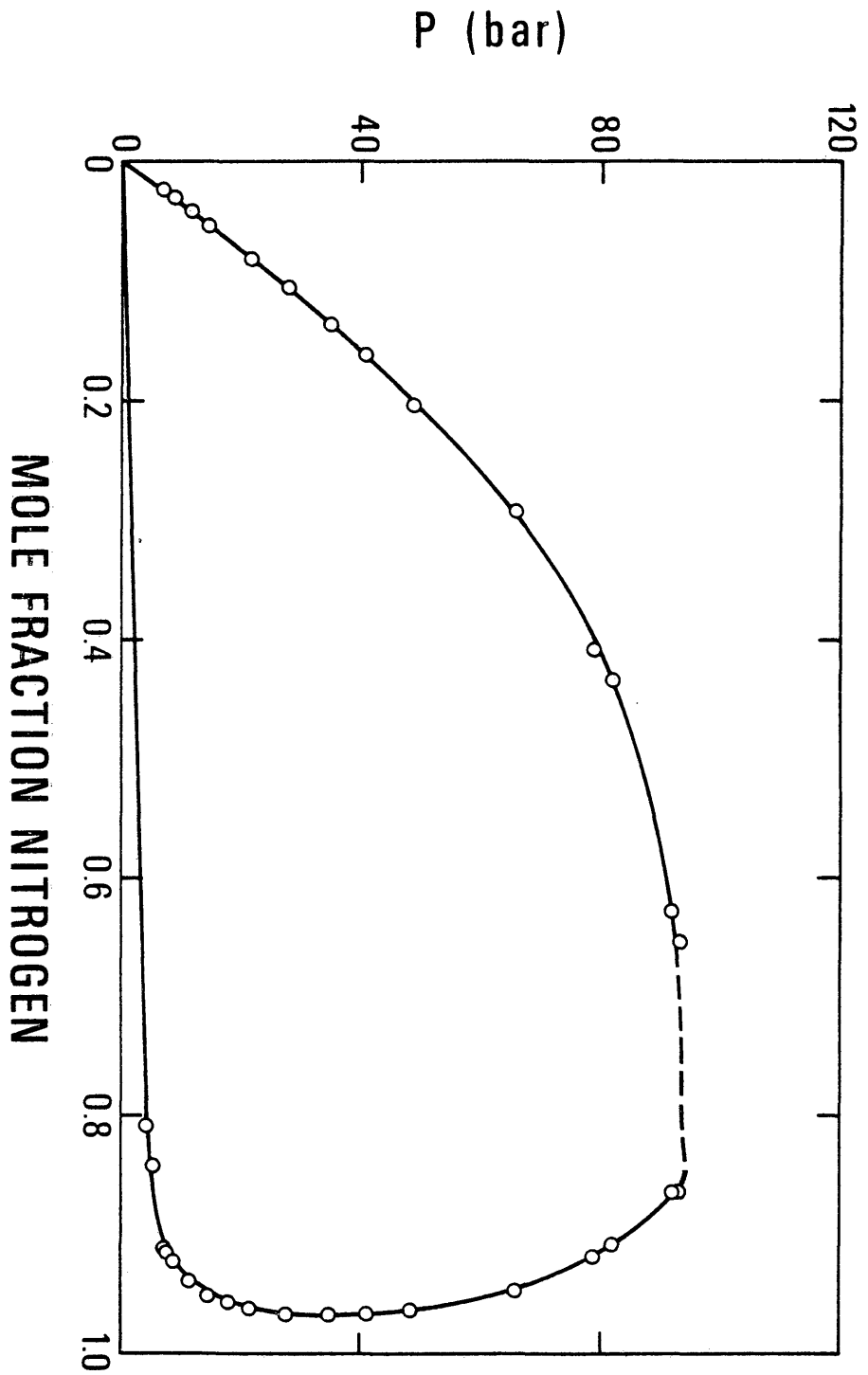

Figure 29. N_2 + C_2H_4 @ 160.00 K

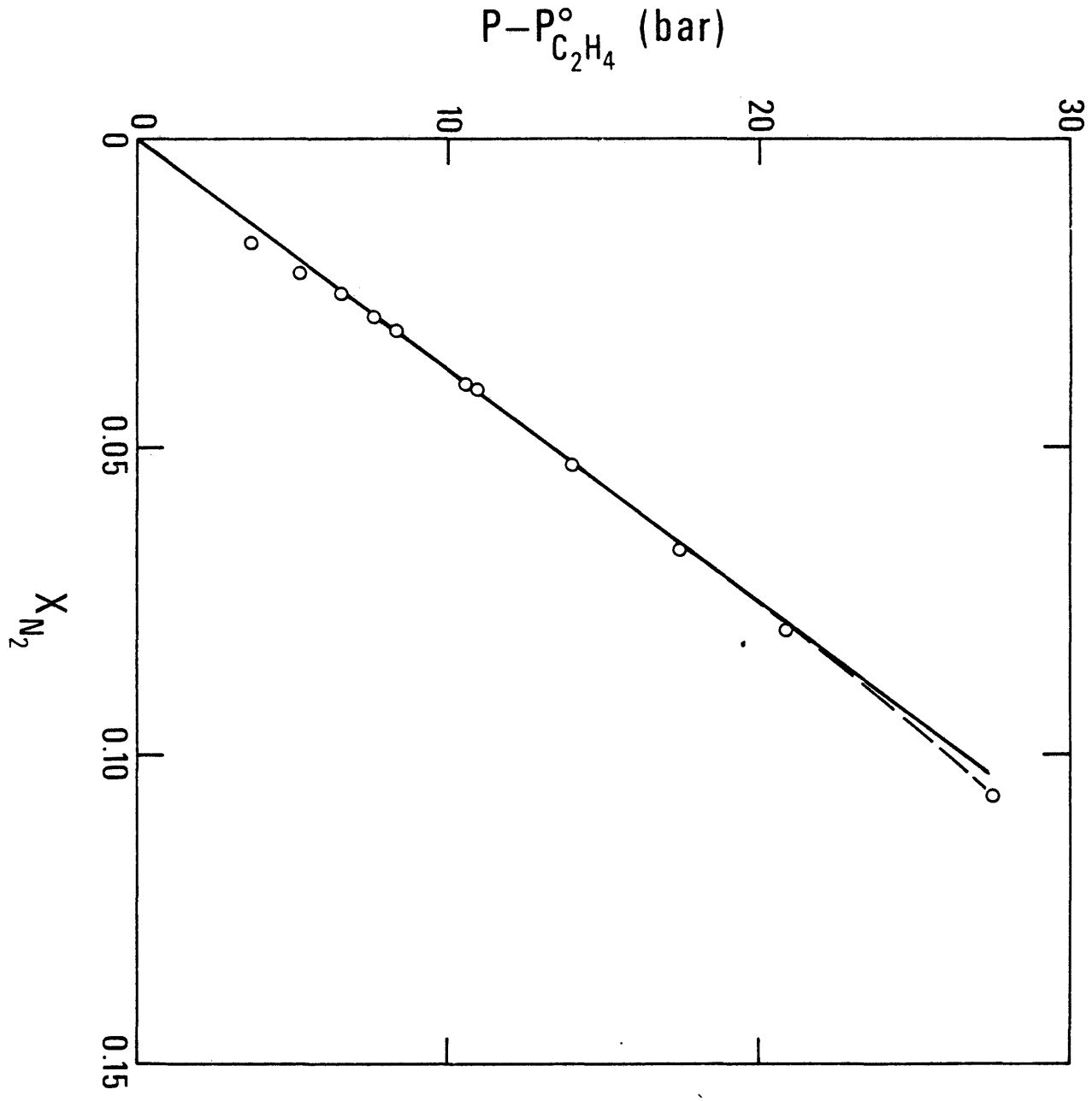

Figure 30. N_2+C_2H_4 System @ 160.00 K.

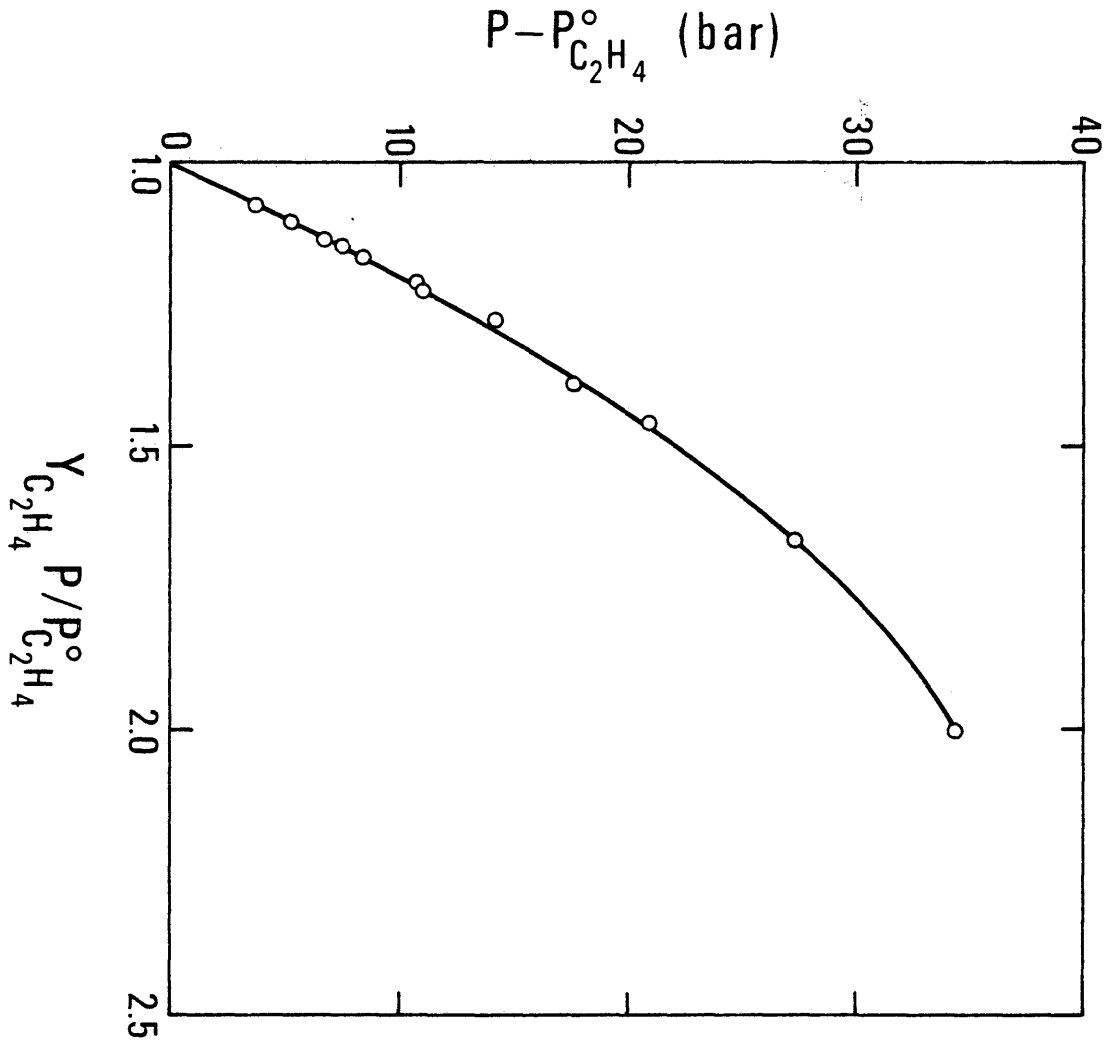

Figure 31. Enhancement Factor for N_2+C_2H_4 System @ 160.00 K.

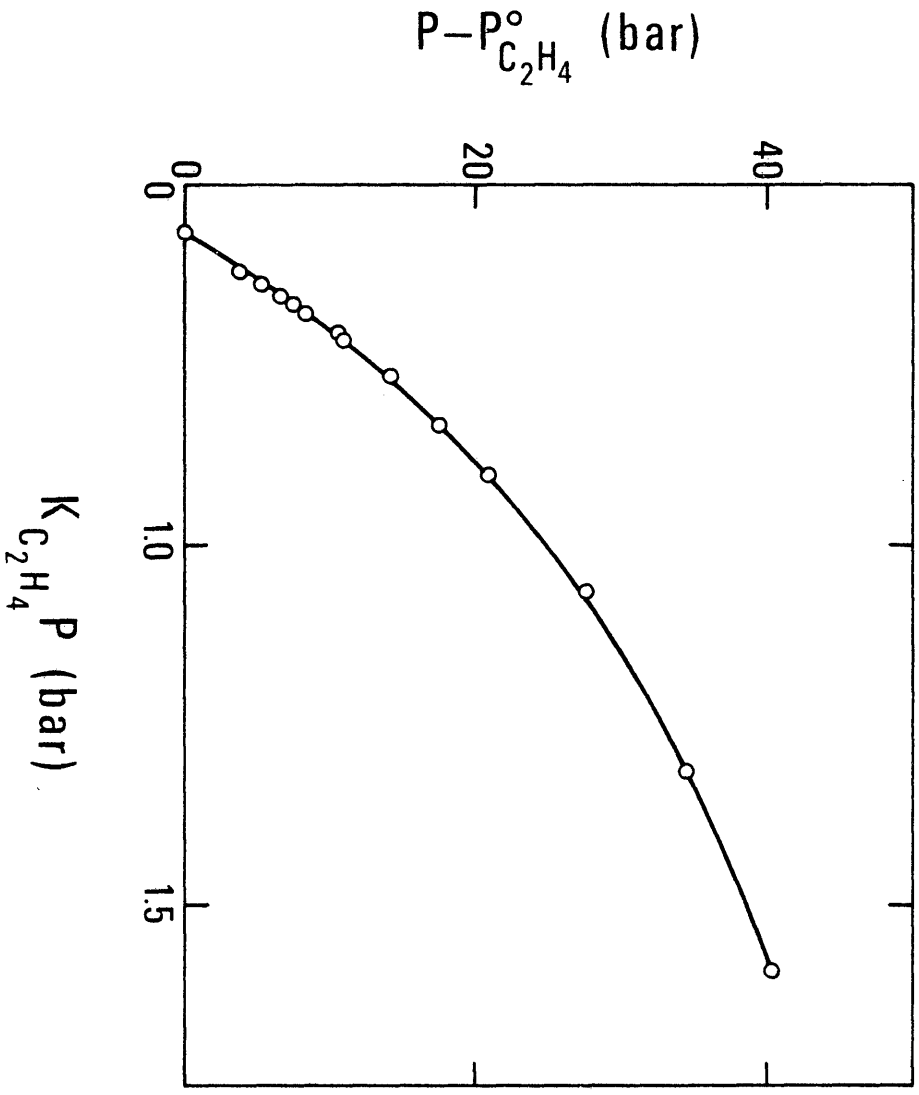

Figure 32. N_2+C_2H_4 System @ 160.00 K.

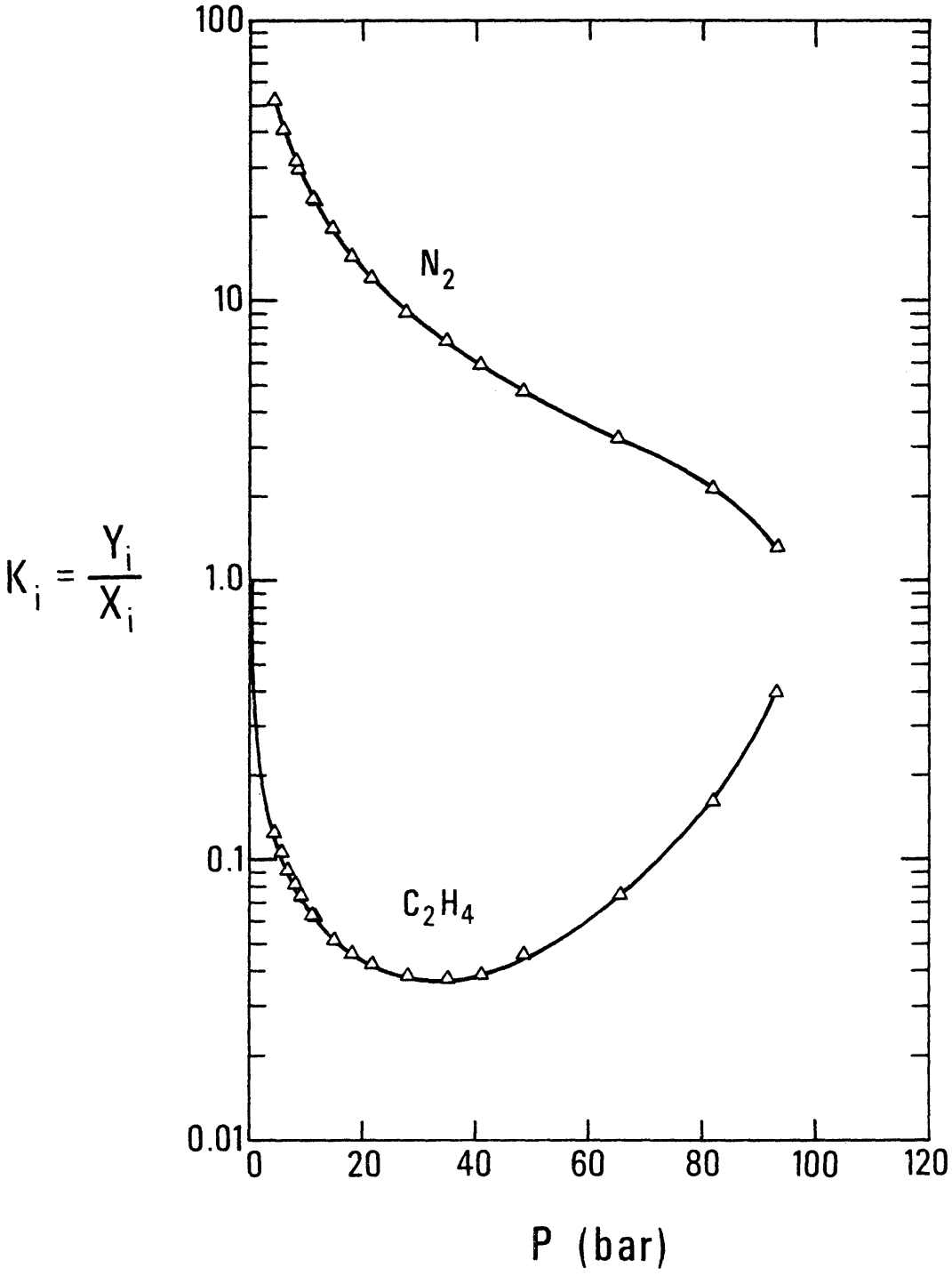

Figure 33. K Factor for N_2+C_2H_4 @ 160.00 K.

The smooth curvature of the P(T)-projection indicate good internal and external consistency since some of the data are of another investigation. A $P(X_{N_2})$-projection is shown in figure (36) for all the isotherms reported (Table 4-11). A smooth curve is obtained which further improves the chances of having consistent data especially for the transition region-isotherms (140 and 144.92 K) where no adequate consistency tests are available for the high pressure data of that region.

Figure (37) shows Henry's law constants (obtained from the $(P-P^0_{C_2H_4})$ versus X_{N_2} plots are different temperatures, (Table 4-12) versus temperature. Good consistency is exhibited as shown by the smoothness of the curves obtained. A similar plot of ln H_{N_2,C_2H_4} versus 1/T exhibits the same smoothness.

By inspection of the coexistence curve on figure (19), it can be seen that the two liquid compositions do not become identical at higher temperatures as observed in other systems with partial miscibility. Generally in such systems the two liquid compositions form a dome-like curve ending at the upper critical solution temperature (UCST). However, this system as well as the other similar systems $N_2 + C_nH_m$ (n = 2,3; m = 4,6,8) produce the flat shape shown in figure (39). Fannin, (1976) suggest that this may be a result of gravitational effects. Yu, et al. (1969), however concluded in their study of $N_2 + C_2H_6$ that the liquid-vapor critical temperatures are reached before the UCST (displacement of the UCST to higher pressures).

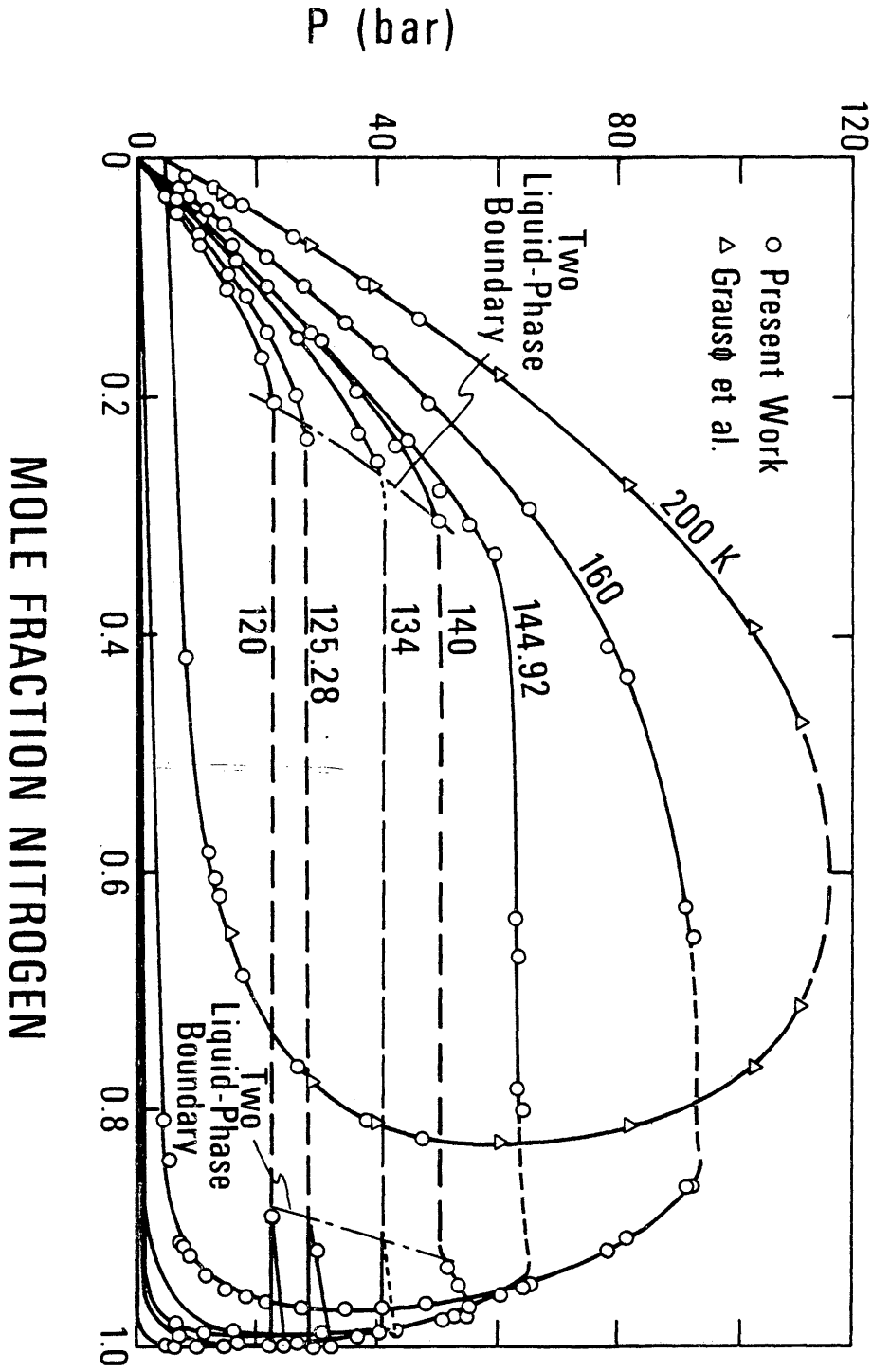

Figure 34. Liquid-Vapor Data for N_2+C_2H_4 Binary

TABLE 4-11
Critical Properties of N_2 + C_2H_4 Binary

T(K)	P_c (bar)	X_{N_2}	Source of Data
134.00	43.00	0.990	Present Work
140.00	55.00	0.970	" "
144.92	66.00	0.935	" "
160.00	94.00	0.850	" "
200.00	115.00	0.600	Grausø, et al. (1977)
260.00	80.00	0.250	" " "

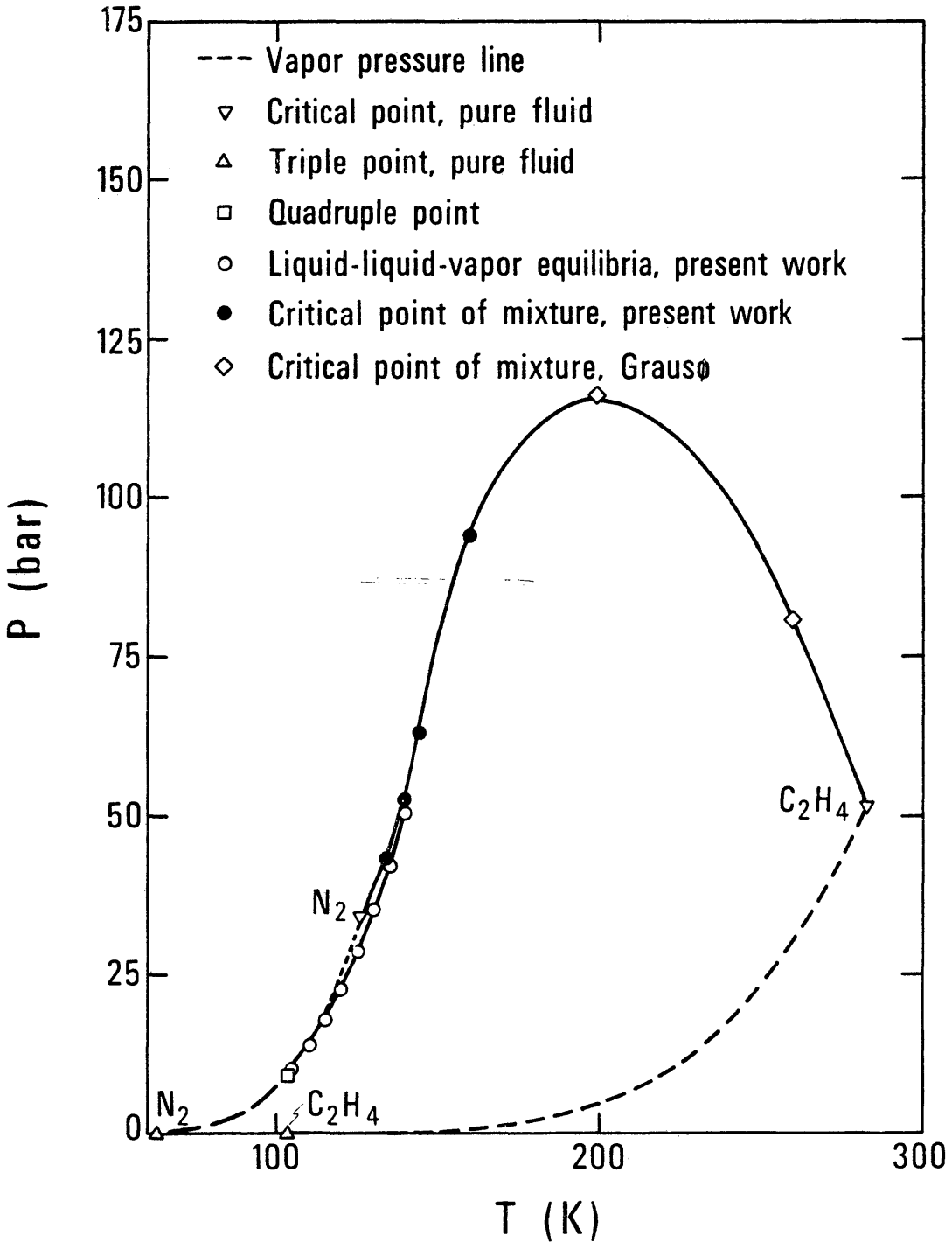

Figure 35. P(T) - Projection for N_2 + C_2H_4 System

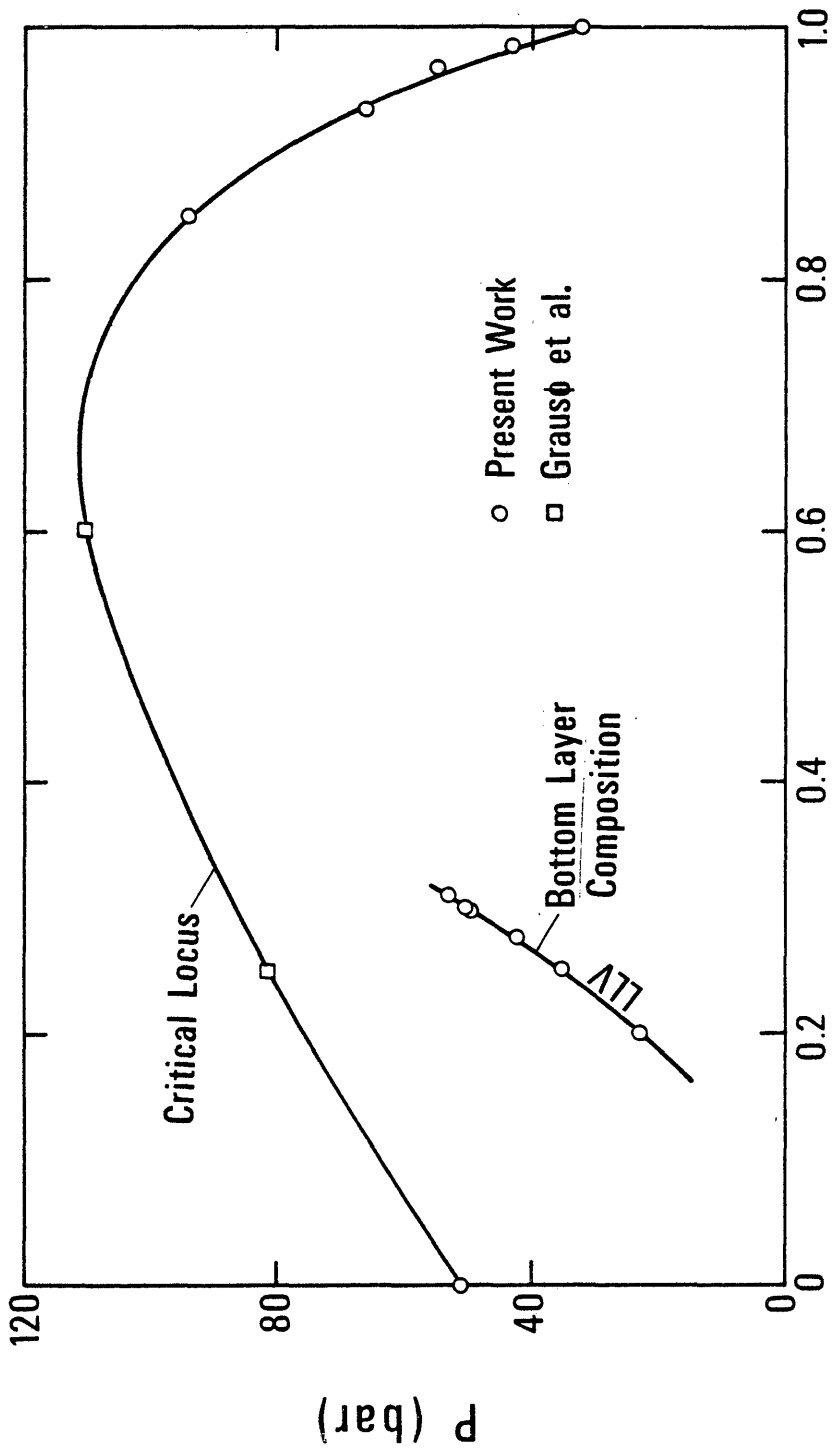

Figure 36. $P(X_{N_2})$ - Projection for $N_2 + C_2H_4$ System

T-2247

Table 4-12

Henry's Constant for $N_2 + C_2H_4$ System

T(K)	$\frac{1}{T} \times 10^3$	H_{N_2,C_2H_4} (bar)	$\ln H_{N_2,C_2H_4}$	Source of Data
120.00	8.333	143.5	4.966	Present Work
125.28	7.982	166.7	5.116	"
134.00	7.463	192.3	5.259	"
140.00	7.143	215.6	5.373	"
160.00	6.250	266.6	5.586	"
200.00	5.000	333.3	5.809	Grauso, et al.
260.00	3.846	320.6	5.770	"

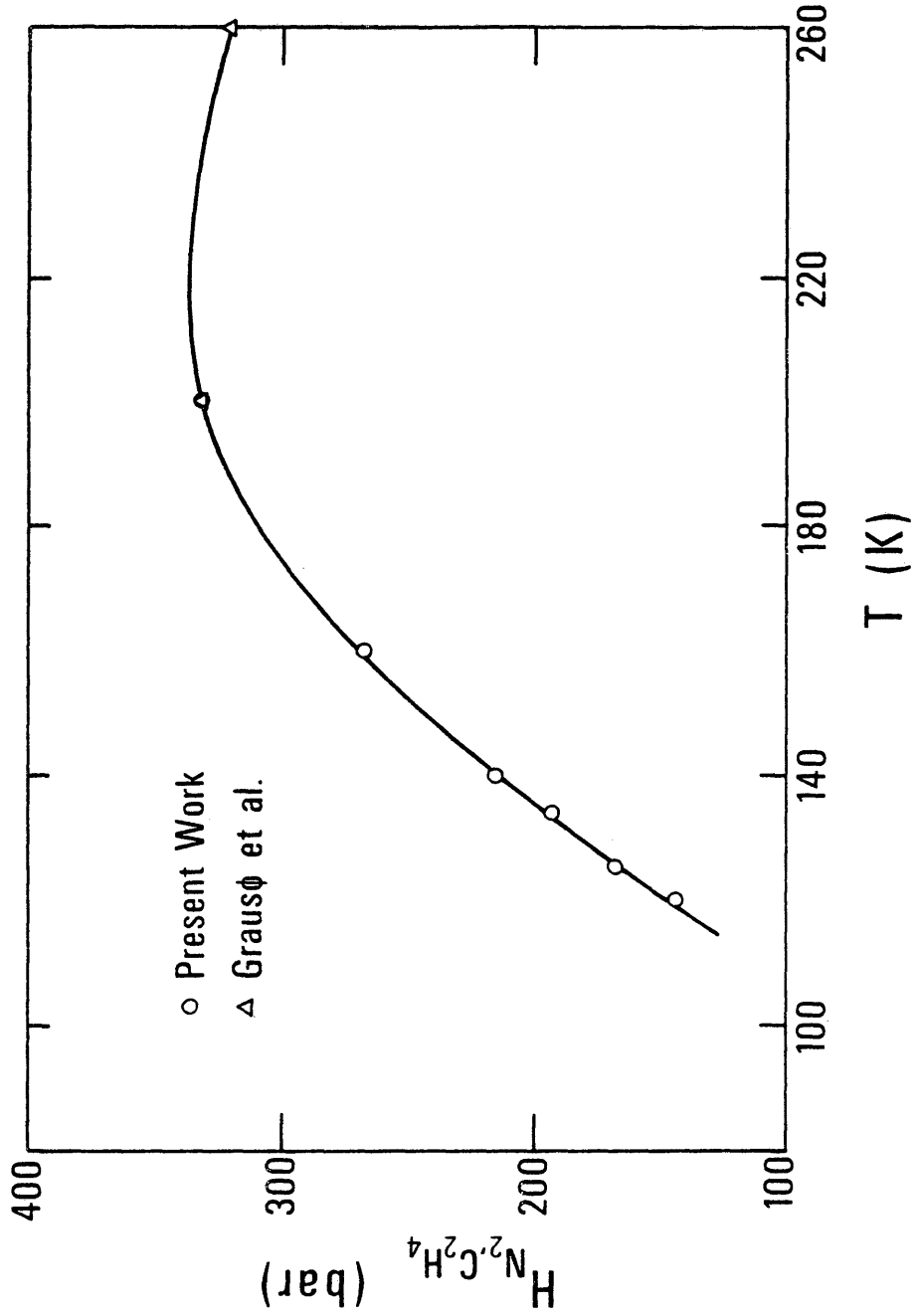

Figure 37. Henry's Constant for N_2 + C_2H_4

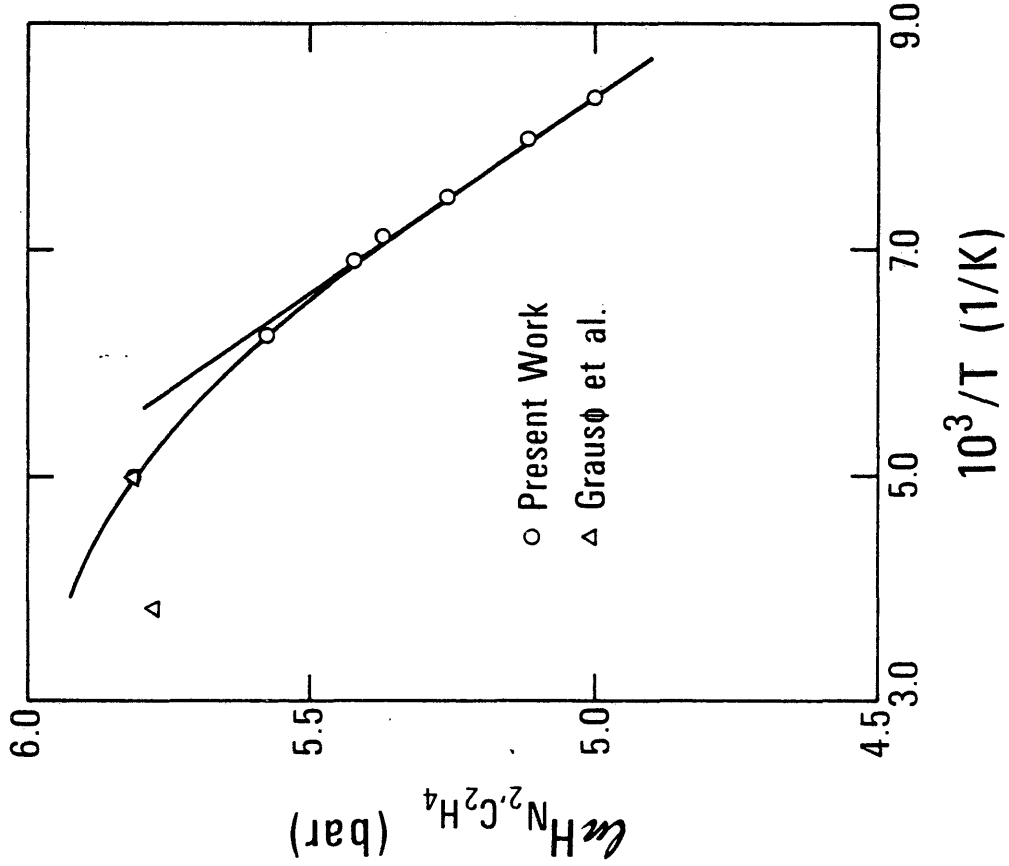

Figure 38. Henry's Constant for N_2 + C_2H_4 System

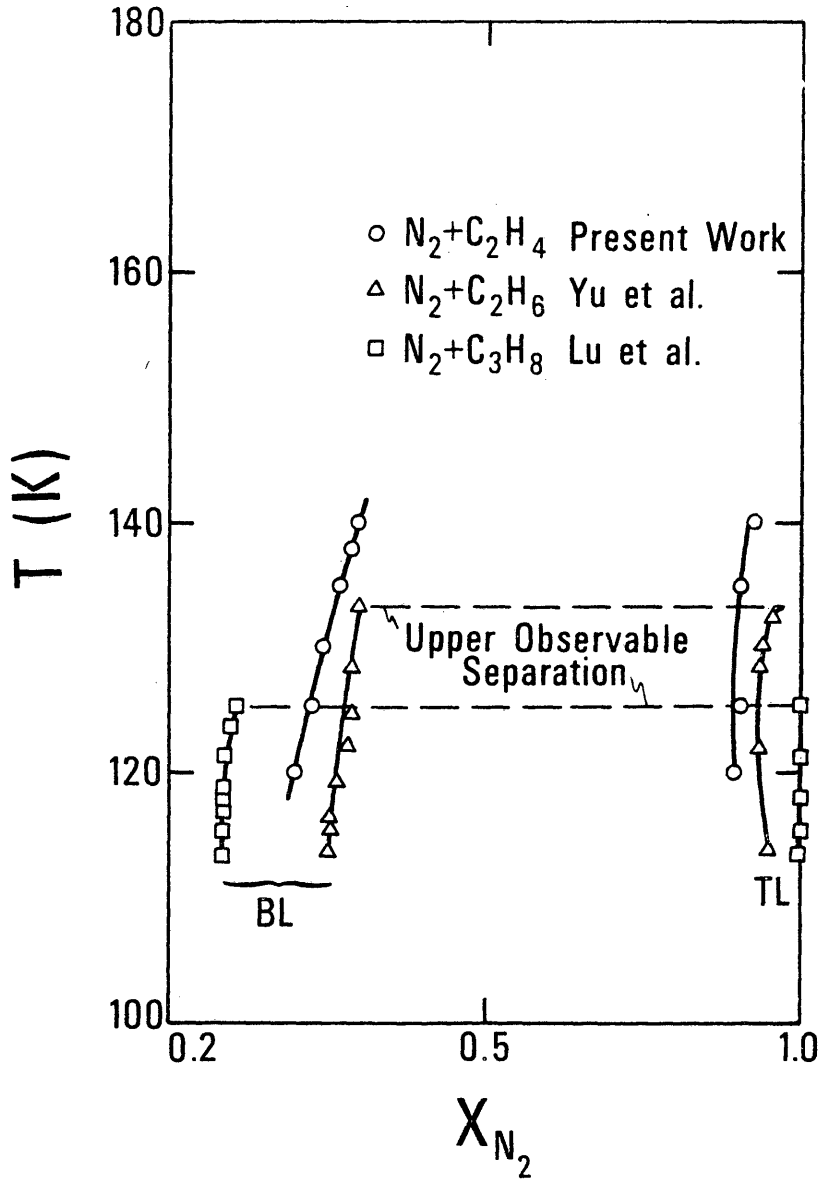

Figure 39. Coexistence Curve for N_2 + C_2H_4 , N_2+C_2H_6, and N_2+C_3H_8

Figure (19) also shows the quadruple point for this binary where two liquids, a gas and a solid,co-exixt.

Due to the combination of good external and internal consistency as indicated by the above cited tests, it is quite probable that good thermodynamic consistency exists for the data obtained for this system (N_2 + C_2H_4), especially for the isotherms far from the transition region.

CHAPTER 5

SEMI-THEORETICAL TREATMENT OF THE $N_2 + C_2H_4$ DATA AT THE SEPARATION CONDITIONS

The basic condition for equilibrium in thermodynamics is that the Gibbs free energy of the system must be at a minimum.

For systems with partial miscibility, this condition of minimum free energy exists when the liquid phase separates into two liquid phases. Figure (40) shows a schematic for ΔG of this condition in comparison with that of a miscible system (Eckert, 1968).

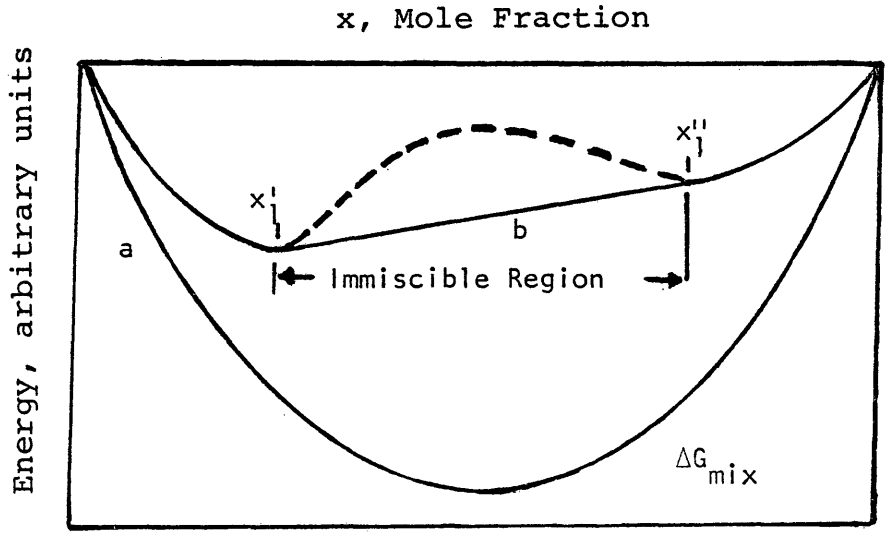

(a) Totally miscible system
(b) Partially Miscible system

Figure 40. Gibbs energy of binary mixtures

The molecular reasons for this immiscibility is that the energy and hence the enthalpy of the liquid mixture is generally lowest if the molecules are surrounded by their own kind. This preferential arrangement of molecules produces two liquid phases each rich in one of the two compenents in case of a binary mixture. This tendency to separate is opposed by the natural tendency of mixing which leads to higher entropy as expected by the second law of thermodynamics.

This balance between enthalpic effects and entropic effects is shifted in favor of the former at low temperature and consequently the separation phenomenon occurs. For most cases, this shift continues up to the upper critical solution temperature (UCST). Then the entropic effects grows stronger and the miscibility (mixing) increases producing a liquid-vapor phase equilibria instead of the three phases (liquid-liquid-vapor) observed in the separation region.

The measure of this balance is Gibbs free energy, which when expressed mathematically, the condition for partial miscibility (separation) in a binary mixture is: for any composition (Prausnitz, 1968).

$$\frac{\partial^2 \Delta G \text{ mix}}{\partial x^2} < 0$$

separation will occur.

Many systems have been reported to exhibit separation at lower temperatures (Eckert, et al., 1965). Of such systems, the $N_2 + C_nH_m$ (n = 2,3; m = 4,6,8) is of interest here since

it constitutes the family of binary mixtures including $N_2 + C_2H_4$ (our main concern).

In the following sections, an attempt will be made to quantify some of the parameters involved in the separation process for $N_2 + C_2H_4$ binary. Similarly, the concept can be then generalized to the rest of the binary mixtures in the family ($N_2 + C_nH_m$ (n = 2,3; m = 4,6,8)). This process involves the development of some theoretically-based equations to predict: (1) the separation pressure at any given temperature, and (2) the solubility of N_2 in the bottom liquid layer at the separation conditions. No attempt will be made for the prediction of the composition in the two other phases (the top liquid layer and the vapor phase) since they are almost pure N_2.

5.1 Separation Pressure Prediction

For a binary system with partial miscibility where the liquid phase separates into two phases, of different composition, the phase rule shows that this system is univariant and becomes fixed at constant temperature.

This univariant behavior was observed for $N_2 + C_nH_m$ (n = 2,3; m = 4,6,8) by several investigators. Ellington, et al. (1959) and Lu, et al. (1969) reported separation to occur at low temperatures (up to 133.3 K) in the $N_2 + C_2H_6$ system. Schneider, et al. (1969) reported that the same occurs in $N_2 + C_3H_8$. In this study $N_2 + C_2H_4$ system was studied and the separation was observed to occur at temperatures up to 140 K. Although

no studies were reported for $N_2 + C_3H_6$ at low temperatures, the separation is expected due to the similarity of its structure when compared with the above mentioned binaries, coupled with the similarities in behavior at higher temperature as shown in Figure (43). Since the $N_2 + C_2H_4$ system is univariant at low temperature, it therefore is expected that a unique relation between temperature pressure exists analogous to Clausius-Clapeyron equation. Such a relation between variations of temperatures and pressure in a univariant system has been discussed by Gibbs (Butler, 1936) and a general derivation was given which accomodates all types of univariant phase equilibria. Before we proceed with the presentation of the final equation given by Gibbs, let us go through the main steps which led to that equation.

If we let superscript g signify the vaper phase, superscript I signify the bottom liquid layer, and II signify the top liquid layer, then at equilibrium:

$$\mu^{I}_{1} = \mu^{II}_{1} = \mu^{g}_{1}$$

or

$$d\mu^{I}_{1} = d\mu^{II}_{1} = d\mu^{g}_{1} \qquad (5)$$

and

$$dP^{I} = dP^{II} = dP^{g} \qquad (6)$$

$$dT^{I} = dT^{II} = dT^{g} \qquad (7)$$

Also, by the Gibbs-Duhem equation, we obtain the following set of relations for the three coexisting phases:

$$
\begin{aligned}
S^I dT + X^I{}_1 d\mu_1 + X^I{}_2 d\mu_2 &= V^I dP \\
S^{II} dT + X^{II}{}_1 d\mu_1 + X^{II}{}_2 d\mu_2 &= V^{II} dP \qquad (8) \\
S^g dT + Y_1 d\mu_1 + Y_2 d\mu_2 &= V^g dP
\end{aligned}
$$

Where use was made of equations (5), (6), and (7) to eliminate superscripts on the μ, P, and T differentials.

Since $\sum X_i = 1$, then eliminating X_1^I, X_1^{II} and Y_1 equations (8) become:

$$
\begin{aligned}
S^I dT + X^I{}_2 (d\mu_2 - d\mu_1) + d\mu_1 &= V^I dP \\
S^{II} dT + X^{II}{}_2 (d\mu_2 - d\mu_1) + d\mu_1 &= V^{II} dP \\
S^g dT + Y_2 (d\mu_2 - d\mu_1) + d\mu_1 &= V^g dP
\end{aligned}
$$

To solve the above simultaneous equations using the notation of matrices and determinants we have:

$$
\begin{pmatrix} S^I & X^I{}_2 & 1 \\ S^{II} & X^{II}{}_2 & 1 \\ S^g & Y_2 & 1 \end{pmatrix} \begin{pmatrix} dT/dP \\ (d\mu_2 - d\mu_1)/dP \\ d\mu_1/dP \end{pmatrix} = \begin{pmatrix} V^I \\ V^{II} \\ V^g \end{pmatrix} \qquad (10)
$$

or by Cramers rule:

$$\frac{dP}{dT} = \frac{\begin{vmatrix} S^I & X^I_2 & 1 \\ S^{II} & X^{II}_2 & 1 \\ S^g & Y_2 & 1 \end{vmatrix}}{\begin{vmatrix} V^I & X^I_2 & 1 \\ V^{II} & X^{II}_2 & 1 \\ V^g & Y_2 & 1 \end{vmatrix}} \qquad (11)$$

This equation is a form of equation (129) given by Gibbs (Butler, 1936). Evaluating the determinants using the elements of the seond column, gives:

$$\frac{dP}{dT} = \frac{X^1_2 (S^g - S^{II}) + X^{II}_2 (S^I - S^g) + Y_2 (S^{II} - S^I)}{X^I_2 (V^g - V^{II}) + X^{II}_2 (V^I - V^g) + Y_2 (V^{II} - V^I)} \qquad (12)$$

Replacing dS_i by $\frac{dH_i}{T}$ then:

$$\frac{dP}{dT} = \frac{X^I_2 (H^g - H^{II}) + X^{II}_2 (H^I - H^g) + Y_2 (H^{II} - H^I)}{T\{X^I_2 (V^g - V^{II}) + X^{II}_2 (V^I - V^g) + Y_2(V^{II} - V^I)\}} \qquad (13)$$

This equation is similar to the Clausius-Clapeyron equation for a pure substance, and has the same functional dependence for $(\frac{dP}{dT})$ as that obtained for azeotropic systems. This led us to posulate a linear relation for lnP versus $\frac{1}{T}$, which proved correct, as shown in Figure (41).

Before we introduce any approximations to equation (13), lets simplify the equation by lumping all the enthalpy terms into one term, ΔH, and all the volume terms into ΔV. Equation (13) then becomes:

$$\frac{dP}{dT} = \frac{\Delta H}{T\Delta V} \qquad (14)$$

where:

$$\Delta H = X^{I}_{2} (H^{g} - H^{II}) + X^{II}_{2} (H^{I} - H^{g}) + Y_{2} (H^{II} - H^{I})$$

$$\Delta V = X^{I}_{2} (V^{g} - V^{II}) + X^{II}_{2} (V^{I} - V^{g}) + Y_{2} (V^{II} - V^{I})$$

Now, assuming that the vapor is ideal, $V^{I} << V^{g}$, and $V^{II} << V^{g}$, then $\Delta V = \frac{RT}{P}$, and hence from equation (14):

$$\frac{d\ln P}{dT} = \frac{\Delta H}{RT^{2}}$$

or: (15)

$$\frac{d\ln P}{d(1/T)} = \frac{\Delta H}{R}$$

Since ΔH is constant over the separation temperature range, then integration of equation (15) gives the linear relation:

$$\ln P = - \frac{\Delta H}{RT} + C$$

where: (Figure 41) 30

$$\frac{\Delta H}{R} = 666 \text{ K}$$

and

$$C = 8.676 \text{ bar}$$

then:

$$\ln P = - \frac{666}{T} + 8.676 \qquad (17)$$

Table 5-1 shows a comparison of the experimental values of the separation pressure at different temperatures to that predicted by Equation (17). An average absolute error of $\pm$ .08 bar is produced using Equation (17) which is well within the errors produced by the experimental technique, especially at higher pressures as shown in Figure (42).

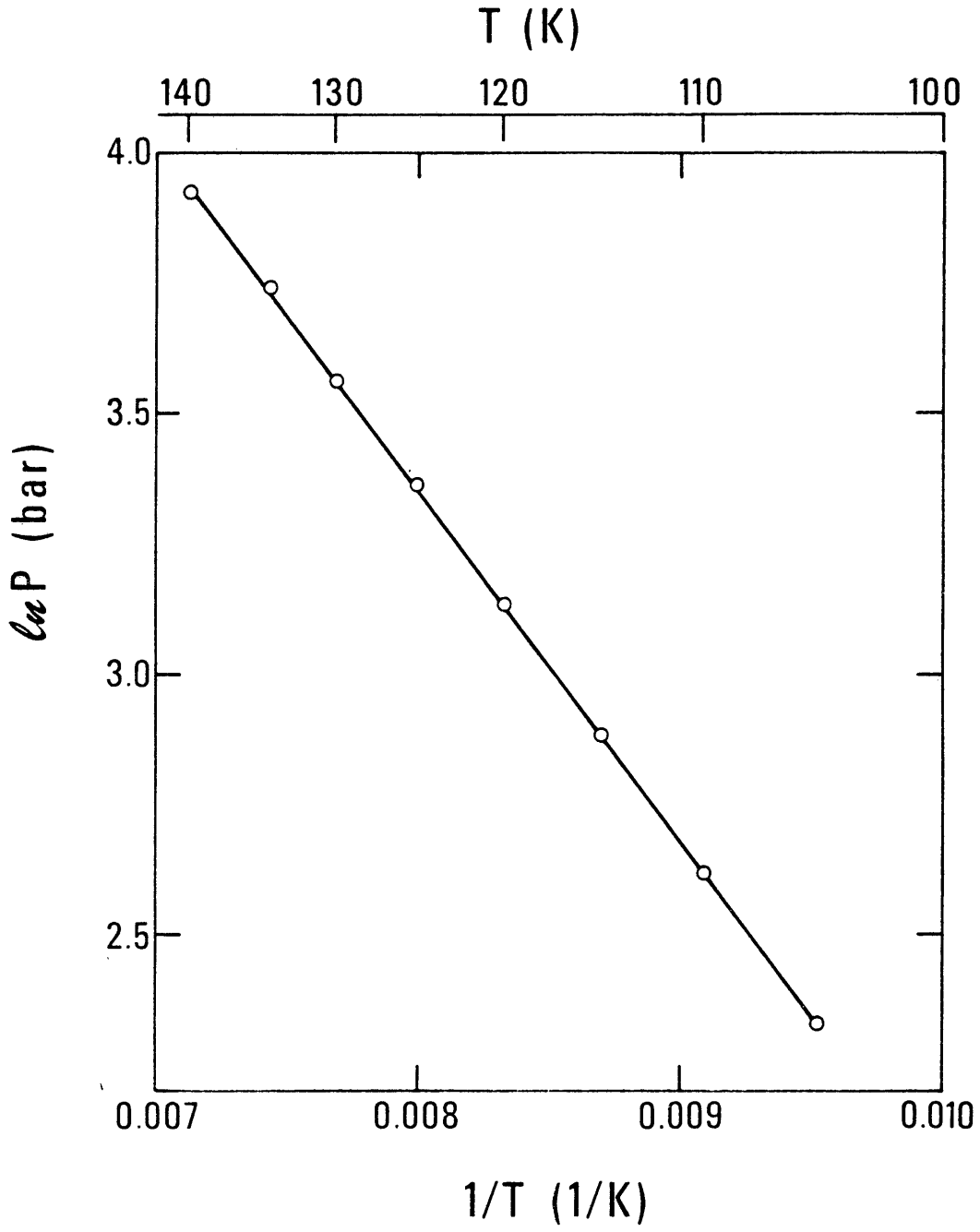

Figure 41. Separation Locus for N_2 + C_2H_4

T-2247

Table 5-1

Comparison of Experimental and Calcualted Separation Pressure for $N_2 + C_2H_4$ Binary

T(K)	P Experimental (bar)	P as Calculated from Eq. (17) (bar)	$\lvert P_{exp} - P_{cal} \rvert$ (bar)
105.00	10.25	10.31	0.06
110.00	13.71	13.70	0.01
115.00	17.90	17.91	0.01
120.00	22.85	22.78	0.07
125.28	28.80	28.79	0.01
130.00	35.10	34.92	0.18
135.00	42.10	42.21	0.11
140.00	50.26	50.34	0.08

Average $\lvert P_{exp} - P_{cal} \rvert$ = 0.078 bar

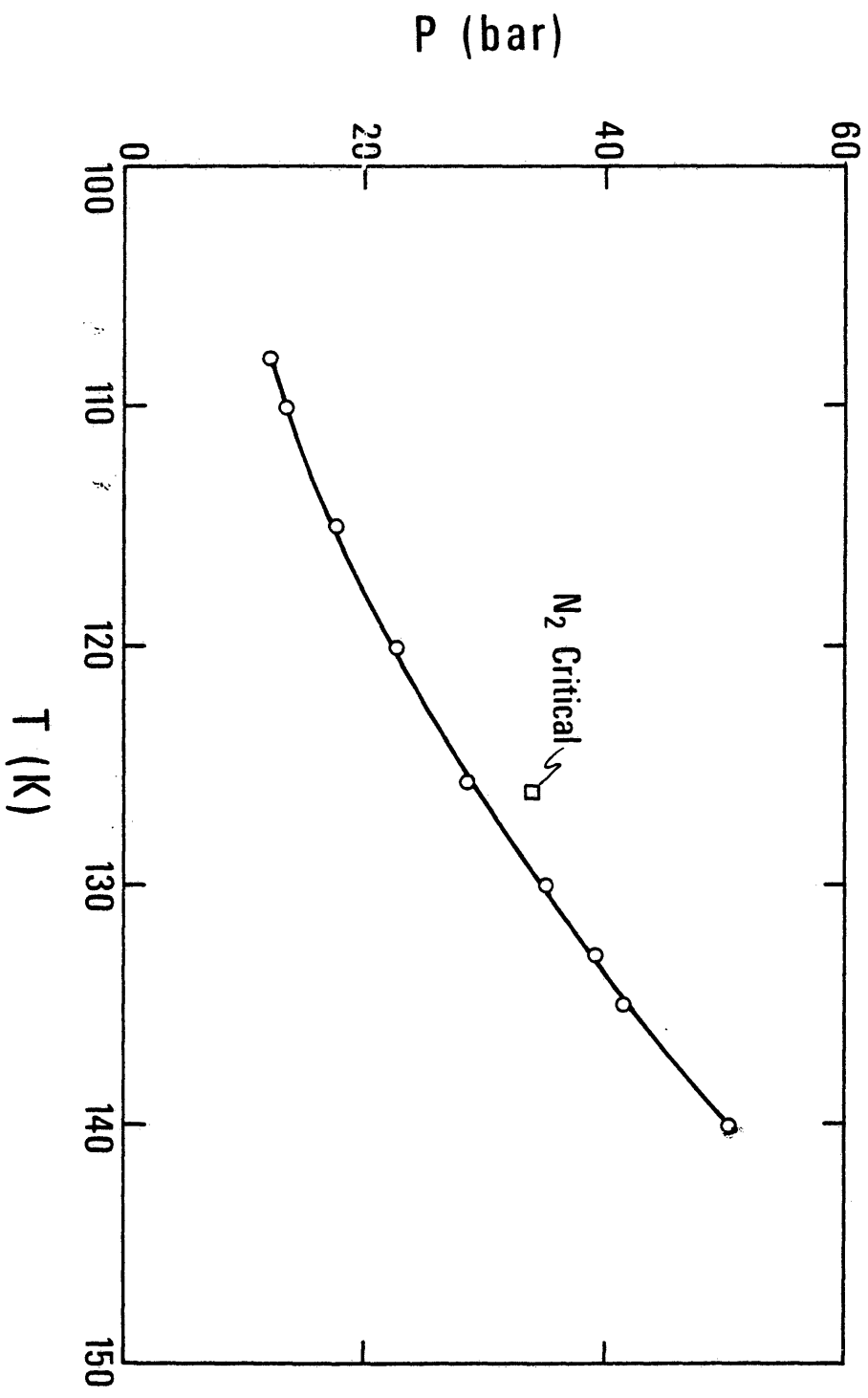

Figure 42. Separation Locus of N_2 + C_2H_4

5.2 Prediction of N_2 Solubility in the Bottom Liquid Layer

Although the system is strongly nonideal with the phase split as a manifestation of such behavior, still some simplifying assumptions would lead to some simple formulation of the temperature and pressure dependence of solubility.

At equilibrium: $$f_1^g = f_1^I$$

or: $$df_1^g = df_1^I$$

Expanding this equation to account for the changes in temperature, pressure, and composition:

$$\left(\frac{\partial \ln f_1}{\partial P}^g\right)_{T,Y} dp + \left(\frac{\partial \ln f_1}{\partial T}^g\right)_{P,Y} dT + \left(\frac{\partial \ln f_1}{\partial Y}^g\right)_{P,T} dy =$$

$$\left(\frac{\partial \ln f_1}{\partial P}^I\right)_{T,X} dp + \left(\frac{\partial \ln f_1}{\partial T}^I\right)_{P,X} dT + \left(\frac{\partial \ln f_1}{\partial X}^I\right)_{P,T} dX_1^I \qquad (18)$$

Assuming that the solvent (C_2H_4) is nonvolatile, which was verified by experiment, especially at $T<T_{C_{N_2}}$, then $dy=0$. Also, let us assume that the solutions formed (top and bottom liquid layers) are ideal, which in essence means that the strong nonideality exhibited by the phase split forced this separation, however, once the two liquid layers were formed, both can be assumed ideal (Smith and Van Ness, 1975).

For an ideal solution:

$$\left(\frac{\partial \ln f_1}{\partial X_1}\right)_{P,T} = \frac{1}{X_1}$$

and by definition(Lewis and Randall, 1961):

$$\left(\frac{\partial \ln f_1}{\partial P}\right)_{T,Y} = \frac{\bar{V}_1}{RT} \quad \text{and} \quad \left(\frac{\partial \ln f_1}{\partial T}\right)_{P,Y} = \frac{H^*_1 - \bar{H}}{RT^2}$$

however, since the solution is ideal in $\bar{V}_1 = V_1$ & $\bar{H}_1 = H_1$
Substituting in Equation (18), then:

$$\frac{V_1^g}{RT}\, dP + \frac{H^*_1 - H^g_1}{RT^2}\, dT = \frac{V^I_1}{RT}\, dP + \frac{H^*_1 - H^I_1}{RT^2}\, dT + \frac{dX^I_1}{X^I_1}$$

or:

$$\frac{dX^I_1}{X^I_1} = \frac{\Delta V_1^{g-I}}{RT}\, dP + \frac{\Delta H_1^{I-g}}{RT^2}\, dT \qquad (19)$$

Further assuming that $V_1^g >> V_1^I$, the vapor is ideal, and that ΔH_1 is constant with temperature, then Equation (19) can be integrated to give:

$$\ln X_1^I = \ln P - \frac{\Delta H_1}{RT} + C$$

since $\ln P = -\frac{\Delta H_1}{RT} + 8.676$ from Equation (16), then:

Table 5-2

N_2 Solubility in the Bottom Liquid Layer

T(K)	X_{N_2} Experimental	X_{N_2} Calculated*	$\lvert X_{exp} - X_{cal} \rvert$
120.00	0.2024	0.2015	9.2×10^{-4}
125.28	0.2282	0.2270	12.0×10^{-4}
130.00	0.2501	0.2505	5.0×10^{-4}
135.00	0.2761	0.2760	1.0×10^{-4}
140.00	0.3019	0.3020	1.0×10^{-4}

* From Equation (21)

$$\ln X_1^I = - \frac{\Delta H}{RT} + \frac{\Delta H_1}{RT} + 8.676 + C \qquad (20)$$

where: ΔH_1 = heat of condensation of N_2 @ Separation T & P (for the purpose of this calculation, we picked a value around 124 K and 30 bars)

Using the $\frac{\Delta H}{R}$ value (666 K) obtained in the last section and the information in Table 4-8, a semi-empirical equation for the prediction of N_2 solubility in the bottom liquid layer (X_1^I) can be obtained:

$$\ln X_1^I = - \frac{340}{T} + 1.23124 \qquad (21)$$

In comparison with Equation (20)

$$\frac{\Delta H_1}{R} = -326 \text{ K}$$
$$C = 7.44476$$

Comparison of experimental obtained values of X_1 (X_{N_2}) to those calculated by Equation (21) shows good agreement (with an average error of ± 0.0005) as shown in Table 5-2.

CHAPTER 6. PHASE BEHAVIOR IN N_2 + LIGHT HYDROCARBON SYSTEMS

The P (T) - projection of the critical curves for the N_2 + C_nH_m (n = 1,2,3; m = 4,6,8) systems are presented in figure (43) according to data available in the literature. Due to the different miscibility effects experienced by each binary, different critical locus behavior is exhibited, ranging from the continuous critical curve produced by N_2+C_1H_4 system to the interrupted critical locus of N_2+C_3H_8 (or C_3H_6), which consist of two branches. The first branch in this type of behavior starts from the critical point of the less volatile component (C_3) and proceeds to lower temperature and higher pressure transition region, whereas the second branch starts from the critical of the more volatile component (N_2) and ends at the so-called upper separation temperature (UST) on the three phase line (LLV) where two liquids and a vapor are in equilibrium. Schneider (1970) gives an excellent discussion on systems with similar behavior, and concludes that although all transitions do occur in a continuous manner, several variations for such transitions may occur.

For such systems with unusual critical behavior, three distinct areas of interest exist in each critical curve: (1) the LV critical locus which extends from the critical of the less volatile to the transition region, (2) the separation locus region where three phases coexist (LLV), and finally (3), the transition

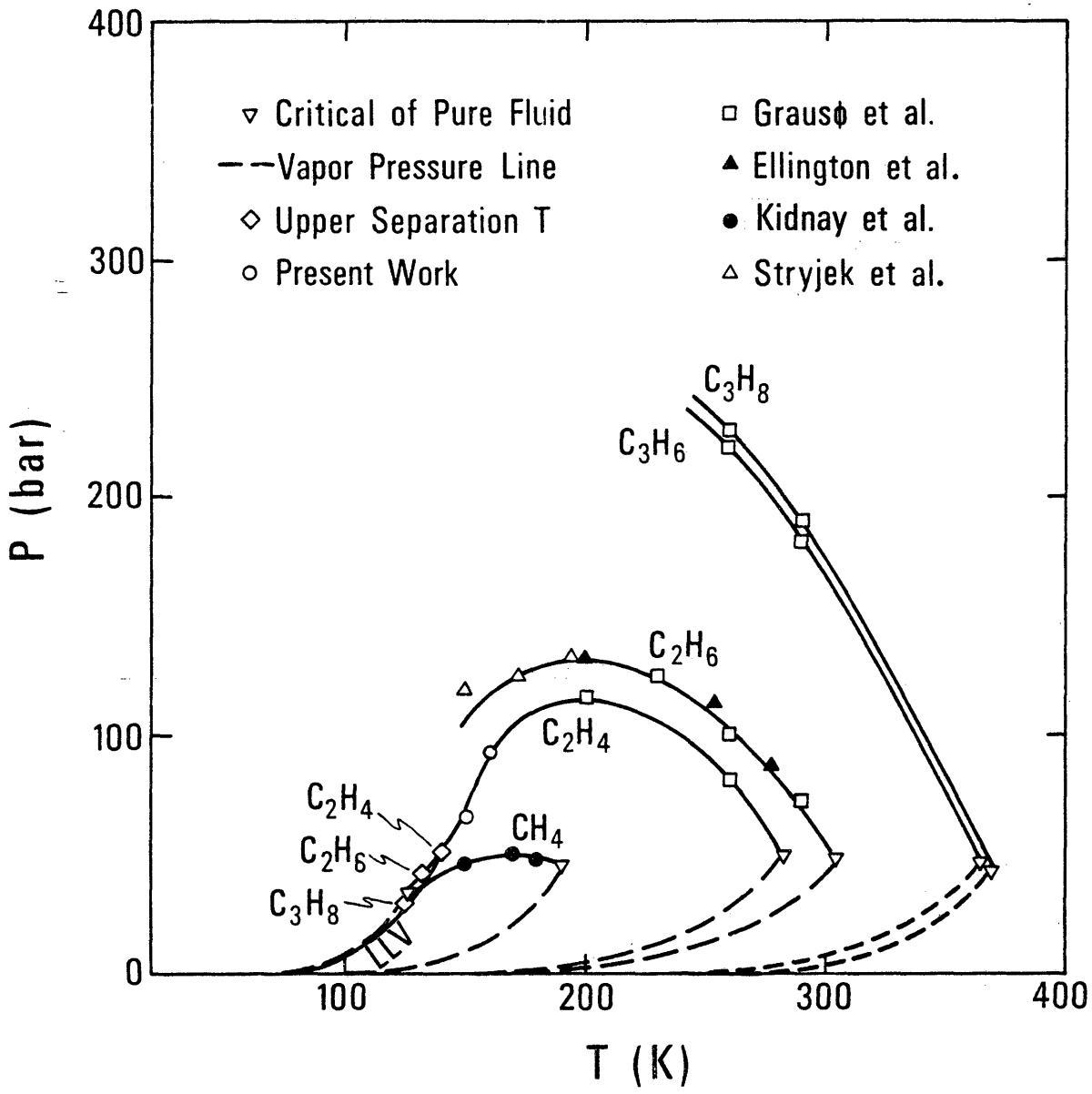

Figure 43. P(T)-Projection for the N_2+ Light Hydrocarbon Systems

region which consists of the area between the two above mentioned regions and where several transitional possibilities exist, i.e., vapor-liquid to liquid-liquid equilibria, vapor-liquid to gas-gas equilibria, or simply a continuous liquid-vapor critical locus as seen in the most miscible system (N_2 + CH_4). Although many investigators studied the LV critical locus and the separation locus region, especially for N_2 + C_2H_6 binary, no full description or conclusive explanations were given for the transition region.

Unfortunately, this study does not give such a description due to two serious limitations: (1) the lack of a visual equilibrium cell which is a vital tool in the study of phase behavior. (2) The lack of liquid-liquid equilibria data for the systems under investigation from which a superposition P(T) - projection for the liquid-vapor to liquid-liquid (or gas-gas) transition can be deduced. In this discussion, however, a partial overview for critical behavior for the C_nH_m (n = 1,2,3; m = 4,6,8) will be given, along with some explanation of why such behaviors occur.

By inspection of figure (43) different types of critical behavior are observed. Although the critical curves for N_2 + CH_4 and N_2 + C_2H_4 both pass through a pressure maximum in a continuous fashion between the critical points of the two pure fluids, the shape of the two maxima are different (the pressure maximum for the N_2 + C_2H_4 system is much more pronounced. This difference is well understood since the C_2H_4 system exhibits liquid phase

separation at lower temperatures whereas the CH_4 system does not. The critical curve for N_2 + C_2H_4 system, however, more data are needed, especially liquid-liquid equilibrium data, to give the final shape of the transition region between the vapor-liquid and the liquid-liquid equilibria.

Although several factors may effect the shape of the transition region of the critical curve, only what we consider the most important such as mutual solubility and gravitional effects will be discussed here:

(1) Solubility effects: figure (43) show the gradual displacement of the (projected) transition region with the mutual miscibility. It can be seen that the larger the molecular weight of the hydrocarbon is the less miscible with N_2, and consequently the higher the displacement of the transition region with pressure. CH_4 which displays the greatest mutual miscibility with N_2 produces a normal uninterrupted critical locus, whereas the C_3 systems shows very little miscibility as a result of strong separation effects, and consequently a very highly displaced transition region is produced. This type of higher pressure displacement in many cases leads to so-called "gas-gas" equilibria, where two highly compressed fluids of liquid-like density are in equilibrium, rather than the liquid-liquid equilibria expected for systems with partial miscibility. The C_2H_6 system is expected to be such a system (where the transition is made from liquid-vapor to liquid-liquid equilibria)

since it displays an intermediate mutual miscibility as compared with the above mentioned extremes. These observations are in good agreement with those cited for many systems (e.g., hydrocarbon + CO_2 system) by a number of investigators (Schneider, 1968, 1970). (2) Gravity effects: Fannin (1976) studied the gravitional effects on the coexistence curve for the CH_4 + CF_4 system where it was concluded that gravity effects may have had a significant effect on the thermodynamic behavior near the upper critical solution temperature (UCST). As a manifestation of such effects a flat top was produced in the coexistence curve, which represents the average mole fractions for which the critical composition exists somewhere in the cell when the UCST is reached. The N_2 + C_n H_m (n = 1,2,3; m = 4,6,8) systems exhibit this type of depression in the coexistence curve as shown in figure (39). However, no assertion can be made as to whether it is due to gravitional effects or otherwise. Yu, et al. (1967) in an attempt to explain this behavior (depression of the coexistence curve) stated that the N_2+C_2H_6 binary reached the normal liquid-vapor critical prior to reaching the UCST.

In conclusion more data are needed for the systems under investigation, especially at lower temperatures and higher pressures, before a complete description of the phase behavior can be obtained rather than speculative attempts.

CHAPTER 7. CONCLUSIONS

1. The experimental data presented in this study show a high degree of external and internal consistency which makes the thermodynamic consistency highly probable. Although this is true for most of the isotherms, a note of reservation should be added concerning the transition region isotherms since insufficient consistency tests are available.

2. From the study of phase behavior for the $N_2+C_nH_m$ ($n = 1,2,3; m = 4,6,8$), it was obvious that more experimental measurements are needed, especially in the phase transition region and the liquid-liquid equilibria region.

3. Although no experimental measurements were obtained for $N_2+C_3H_6$, similarity of behavior to the other systems investigated lead us to believe that the separation phenomena is highly probable in the lower temperature regions.

T-2247

NOMENCLATURE

f	fugacity
G	Gibbs free energy
H_{N2},C_2H_4	Henry's constant of N_2 in C_2H_4
H	enthalpy
K	equilibrium ratio, Y_i/X_i
	Number of moles
P	Total system pressure
R	Gas constant
T	Temperature
V	Volume
X	liquid-phase mole fraction
Y	Vapor-phase mole fraction
μ	Chemical potential
Subscripts	
1,2,i	Components, N_2,C_2H4
c	critical property
exp	experimental value
cal	calculated value
sep	separation property
Superscripts	
g	vapor phase
I	bottom liquid layer
II	top liquid layer
o	standard state
-	partial molar property

REFERENCES

Butler, J. A. V., 1936. A Commentary on the Scientific Writings of J. Willard Gibbs, I: Thermodynamics. In: F. G. Donnan and A. Hass (Editors), The General Thermodynamical System of Gibbs. Yale University Press, New Haven pp. 109-110.

Chang, S.P. and Lu, B.C.-Y., 1967, Vapor-liquid equilibria in the nitrogen-methane-ethane system. Chem. Eng. Progr. Symp. Ser., 63, (81):18.

Duncan, A.G., and Hiza, M.J., 1970, A multipurpose phase equilibrium apparatus to study mixtures of Cryogenic fluids: application to argon-methane, Advances in Cryogenic Engineering 15:42.

Eckert, C.A., and Prausnitz, J.M., 1965, Phase equilibria for strongly non-ideal liquid mixtures at low temperatures. AiChE J., 11:886.

Eckert, C.A., 1968, The order-disorder effect on solutions. Chem. Eng. Progr. Symp., 68 (88):1.

C& E News, 1979, Uncertainties plague ethylene industry. C & E News, 57 (22): 11.

Ellington, R.T., Eakin, B.E., Parent, J.D., et al, 1959, Vapor-liquid phase equilibria in the binary systems of methane, ethane and nitrogen, thermodynamic and transport properties of gases, liquids and solids, 180-94, Am. Soc. Mech. Engrs. Heat Transfer Div., McGraw-Hill, New York.

Fannin, A.A., 1976, Thermadynamics of Liquid Mixtures in the Region of An Upper Critical Solution Temperature: CH_4-CF_4. Ph.D. Thesis, University of California, Los Angles.

Goodwin, R.D., 1979, personal communication.

Grausø, L., Fredenslund, A., and Mollerup, J., 1977, Vapor-liquid equilibria data for the systems $C_2H_6+N_2$, $C_2H_4+N_2$, $C_3H_8+N_2$ and $C_3H_6+N_2$. Fluid phase equilibrium, 1:13.

Hiza, M.J., and Duncan, A.G., 1969, A simple gas recirculation pump for low flow and high pressure applications. Rev. Sci. Instr. 40:513

Hiza, M.J., Kidnay, A.J., and Miller, R.C., 1975, Equilibrium Properties of Fluid Mixtures, A bibliography of Data on Fluids of Cryogenic Interest. NSRDS Bibliographic Series, IFI/Plenum, New York.

Kidnay, A.J., Miller, R.C., Parrish, W.R., and Hiza, M.J., 1975, Liquid vapor phase equilibria in the N_2-C H system from 130 to 180 K. Cryogenics, 15 (6): 531.

Lewis, G.N., and Randall, M., Rev. Pitzer, K.S., and Brewer, L., 1961, Thermodynamics, (2nd Ed.), McGraw-Hill, New York, 219, 227-228 pp.

Lu, B.C.-Y., Chang, S.-D., Elshayal, I.M., Yu, P. and Poon, D.P.L., 1969, Low temperature phase equilibria of natural gas components. Proc. 1st Intern. Conf. Colorimetry and Thermodynamics, Warsaw, 775 pp.

Prausnitz, J.M., 1969, Molecular Thermodynamics of Fluid-Phase Equilibria. Prentice-Hall, Englewood, New Jersey, 235 pp.

Schneider, G., 1968, Phase equilibria in binary fluid systems of hydrocarbons with carbon dioxide, water, and methane, Chem. Eng. Progr. Symp. Ser., 64 (88):9.

_____, 1970, The thermodynamic description of phase transitions. Advances in Chem. Physics 17 (1):43.

_____, 1972, Phase behavior and critical phenomena in fluid mixtures under pressure. Ber. Bunsenges. Physik. Chem. 76 (314):325.

Simon, M., Fannin, A.A. and Knobler, C.M., 1972. Thermodynamic properties of the system CH_4-CF_4 in the neighborhood of the upper critical solution temperature. Ber. Bunsenges, Physik. Chem., 76(314):321.

Smith, J.M. and Van Ness, H.C., 1975, Introduction to Chemical Engineering Thermodynamics. McGraw-Hill, New York, 359 pp.

Street, W.B. and Jones, C.H., 1965, Liquid phase separation and liquid-vapor equilibrium in the system, Neon-Hydrogen, J. Chem. Phys. 42 (11):3989.

Stryjek, R., Chappelear, P.S. and Kobayashi, R., 1974, Low temperature vapor-liquid equilibra of nitrogen-ethane system. J. Chem. Eng. Data, 19:340.

Yu, P., Elshayal, I.M., and Lu, B.C.-Y., 1969, Liquid-liquid-vapor equilibria in the nitrogen-methane-ethane system. Canadian J. of Chem. Eng., 47: 495.

Wichterle, I., Salsburg, Z.W., Chappelear, P.S., and Kobayashi, R., 1971,"Unexpected" Vapor-liquid equilibria behavior in the critical region and some theoretical implications of critical exponents. Chem. Eng. Sci., 26 (7):1141.

APPENDIX

Gas Chromatograph Calibration

Four calibration mixtures of N_2 + C_2H_4 with different compositions ranging from 0.0967 to 0.7553 in C_2H_4 mole fraction were prepared by gravimetric methods. These calibration mixtures in addition to the pure components (N_2 and C_2H_4) were used in the preparation of the calibration curves. Samples from each mixture were analyzed in the gas chromatograph at a set known (from gravimetric measurements) the partial pressures (P_i) are consequently calculated as $P_i = PX_i$. The area (A_i) corresponding to each partial pressure was obtained from the electronic integrator. Earlier in the work, injection pressures of up to 16 psia were used; however, it was found later that the linear dependence of the response factor ($RF_i = \frac{A_i}{P_i}$) of nitrogen ends at P_{N_2} = 12 psia. Consequently, to eliminate this problem and to ensure minimum variation of RF_{N_2} with composition, the injection pressure was set to around 10 psia using a fused quartz precision pressure gauge.

The operating conditions of the gas chromatograph for the calibration as well as for the analysis of all the samples were:

Column used: five foot porapok R (0.21" I/D, 0.25" O/D, 80/100 mesh size)

Column temperature: 83 C

Current: 200 milliamps

Carrier gas: Helium at 20 psig.

Table A-1 shows the calibration data for $N_2 + C_2H_4$ obtained at the above mentioned conditions. A least square fit was used to correlate P_i to A_i. The straight line equation given for each component is:

$$P_{C_2H_4} = 0.0000206\ A_{C_2H_4} - 0.038311 \qquad (1)$$

$$P_{N_2} = 0.0000249\ A_{N_2} + 0.0124998 \qquad (2)$$

Comparison of the calculated values of X_i to the values determined gravimetrically are given in Table (A-1). The accuracy of the above equation was found to be $\pm$ 0.001 ($\pm$ .00087) in mole fraction. The reproducability of the measurements made for a large number of data samples (during the normal data collecting) was found to be $\pm$ 0.0005 in mole fraction.

Attempts were made to correlate P_i to A_i in the more commonly obtained equation form, $Y_i = mx_i$; however, results given by this type of fit produced more than twice the average error ($\pm$ 2.06 x 10^{-3}) given by the above equations (1) and (2). This need for an intercept in the calibration equations may be attributed to the slight shift in the current of the gas chromotograph. This also, may explain the larger error given for the pure component analysis where the normalization process is lacking (only one component present).

To make sure that no errors were made in the gravimetric measurements and that the analysis system is functioning properly,

Calibration Curve Data for Beckman GC-2A

$P_{C_2H_4}$ (psia)	$A_{C_2H_4}$	P_{N_2} (psia)	A_{N_2}	$Y_{C_2\ EXP}$	$Y_{C_2\ CAL}$	$Y_{N_2\ EXP}$	$Y_{N_2\ CAL}$	ERROR $(Y_{EXP}-Y_{CAL})$
7.7225	379450	6.6357	267460	0.53785	0.53827	0.46215	0.46173	-4.2×10^{-4}
7.9140	385185	6.80024	271865	0.53785	0.53797	0.46215	0.46203	-1.20×10^{-4}
4.2500	210130	11.02447	444060	0.27824	0.27932	0.72176	0.72068	-10.8×10^{-4}
4.1455	203700	10.7535	429480	0.27824	0.27972	0.72176	0.72029	-14.81×10^{-4}
11.6031	561590	3.75800	149590	0.75531	0.75522	0.24469	0.24478	0.91×10^{-4}
11.2629	545030	3.64878	144655	0.75531	0.75585	0.24469	0.244156	-5.37×10^{-4}
0.9270	47050	8.65821	349120	0.09671	0.09663	0.90329	0.90340	1.04×10^{-4}
0.9237	46600	8.62746	345750	0.09671	0.09657	0.90329	0.90342	1.32×10^{-4}
9.7383	477000	0.00	0.00	1.00	1.00501	0.00	0.00	-50.1×10^{-4}
10.8022	525280	0.00	0.00	1.00	0.99817	0.00	0.00	18.27×10^{-4}
0.00	0.00	8.41817	335950	0.00	0.00	1.00	0.99518	0.00
0.00	0.00	8.42206	336425	0.00	0.00		0.99613	0.00

the same calibration mixtures were analyzed in a different laboratory using a different analysis system; a Beckman GC 72-5 and a HP 3385A integrator.

An accuracy of $\pm$ .0005 ($\pm$ 4.35 x 10^{-4}) was obtained. This improvement in the accuracy can be attributed to the better consistency in the response factor ($RF = \frac{A_i}{P_i}$) for Beckman 72-5 GC as compared to the GC-2A model used in our calibration. The range of fluctuation observed in both calibrations was as follows:

Model	$RF_{C_2H_4}$ Range	% Fluctuation
Beckman GC 72-5	17373-17540	.96
Beckman GC-2A	48,945-49,808	1.70

The results of this calibration are given in Table A-2.

Table A-2

Calibration Curve Data for Beckman GC-72

$P_{C_2H_4}$ (psia)	$A_{C_2H_4}$	P_{N_2} (psia)	A_{N_2}	$Y_{C_2\ EXP}$	$Y_{C_2\ CAL}$	$Y_{N_2\ EXP}$	$Y_{N_2\ CAL}$	ERROR $(Y_{EXP} - Y_{CAL})$
8.94517	156900	2.89792	43210	0.755307	0.755197	0.24469	0.2448	1.10×10^{-4}
8.94517	156400	2.89792	43200	0.755307	0.75465	0.24469	0.24535	6.58×10^{-4}
1.14531	20100	10.69778	160100	0.096707	0.09598	0.90329	0.90302	-2.78×10^{-4}
1.14531	20000	10.69778	159900	0.096707	0.096659	0.90329	0.90334	4.72×10^{-4}
3.29522	57430	8.54787	127200	0.27824	0.27795	0.72176	0.72205	2.94×10^{-4}
3.29522	57250	8.54787	127100	0.27824	0.27747	0.72176	0.722525	7.65×10^{-4}
0.00	0.00	12.12004	180764	0.00	0.00045	1.00	0.99954	-4.54×10^{-4}
0.00	0.00	12.12004	180761	0.00	0.00045	1.00	0.99954	-4.54×10^{-4}